Modeling and Control of Advanced Technology Engines

by

Anna Stefanopoulou

A dissertation submitted in partial fulfillment
of the requirements for the degree of
Doctor of Philosophy
(Electrical Engineering:Systems)
in The University of Michigan
1996

Doctoral Committee:

Professor Jessy W. Grizzle, Co-Chair
Associate Professor James S. Freudenberg, Co-Chair
Professor Michael G. Parsons
Professor William B. Ribbens
Associate Professor Jeffrey L. Stein
Jeffrey A. Cook Principal Engineering Specialist, Ford Research Laboratory

ABSTRACT

Modeling and Control
of Advanced Technology Engines

by
Anna Stefanopoulou

Co-Chairs: Jessy W. Grizzle and James S. Freudenberg

Over the last two decades there has been a dramatic evolution in powertrain control systems, largely driven by government regulations aimed at improving fuel economy and reducing emissions. One way to potentially meet these performance requirements is to introduce additional design parameters via innovative mechanical configurations (new actuators). The design parameters, control variables in system terminology, provide additional degrees of freedom to optimize the performance of the engine over its wide range of operation.

In this dissertation, we study control design issues for two advanced technology engines: (i) a spark-ignition (SI) engine with secondary throttles placed in the intake ports of the cylinders, and (ii) an SI engine equipped with a variable cam timing (VCT) mechanism. Both engine configurations are multivariable and nonlinear, thus imposing challenging control problems associated with control authority, long sensor delays, and strongly coupled subsystems. We develop and validate dynamic engine models, study the subsystem interactions, identify performance tradeoffs, and apply classical and modern control techniques to improve engine performance. Moreover, we study the impact of modular controller architecture on the engine dynamic response, and demonstrate that even if the controller is eventually implemented in independent software modules, coordinating the design and analysis allows for a better assessment of the tradeoffs among the dynamic performance of different subsystems. Our results demonstrate the advantages of a systematic approach to developing advanced technology powertrain control systems.

Dedicated to George, Kaite, and Dolly.

ACKNOWLEDGEMENTS

My thanks go first to my advisors, Professors Jessy Grizzle and Jim Freudenberg. Their guidance and support made this work possible. I wish to thank Mr. Jeff Cook. I sincerely believe that this work would not exist without his inspiration. His constant encouragement, intuitive wisdom, and resolute leadership were instrumental in completing this work.

I owe special thanks to Professor Ribbens. He served on my dissertation, preliminary, and qualification examination committees, and raised issues for me to consider that ultimately led to a more thorough and complete dissertation. I would like to thank Professor Parsons for giving me the opportunity to come to the University of Michigan. His support during my first year of studies was invaluable. I would also like to thank Professor Stein for serving on my doctoral committee. The insightful comments of Professors Parsons and Stein exemplify the value of cross-disciplinary effort; my thesis would be less without their participation.

I also gratefully acknowledge the financial support of the National Science Foundation (Grant ECS-92-13551) and the Ford Motor Company.

I am indebted to the Ford Motor Company's Control Systems Department. There I was given the opportunity to work and gain immeasurable experience while pursuing my degree. My friends and colleagues Ken, Jing, Paul, Kip, Florian and Bill showed me the art of welding innovative ideas with engineering practice and mathematical reasoning. I would also like to thank Mrdjan, Steve, Ed and Chris for their valuable suggestions and friendly chats during the last months of my studies.

There were many days during the three years of my studies that I found myself working innumerous hours in the 4402 computer laboratory. This laboratory became my home, and my lab-mates Meera, Jon, Raga, Cecilia, Brian, Al, Craig, Erich, Manish, Tyrone, Steve R., Yi-Liang, and Steve H. became my family. I want to thank them for their willingness to help with any problem that arose, and I wish them the best.

There are a number of people without whose friendship my life in Ann Arbor wouldn't have been as meaningful and blissful. Chief among them are Ailan, Tayfun, Ruben, Stephane, and Jong Gwan. I owe a huge debt to all of them.

And, finally, my ultimate thanks go to my loving companion Paul, who stood by my side through all these years.

This thesis is dedicated to my father, George, who had decided that I will become an

engineer even before I was born, to my mother, Kaite, who encouraged all my ambitions, and to my sister, Dolly, who always argued that engineering is a world bleak and monochrome, and filled me with stories of magic, adventure and mystery.

TABLE OF CONTENTS

LIST OF TABLES

Table

LIST OF FIGURES

Figure

LIST OF APPENDICES

APPENDIX

CHAPTER 1

Introduction.

1.1 Background on Advanced Technology Engines.

Over the last two decades there has been a dramatic evolution in powertrain control systems, largely driven by government regulations : (i) stringent Federal and California emissions standards, (ii) increased fuel economy to comply with mandated Corporate Average Fuel Economy (CAFE), and (iii) minimum safety and reliability standards that are independent of age, environment, and varying fuel properties. These requirements create challenging control problems for two reasons:

- It is increasingly important to achieve control over transient behavior and meet performance objectives over the life of the vehicle. This requires the development of high performance and robust powertrain controllers.
- The performance objectives are often conflicting, or at best interrelated. One way to potentially meet these requirements is to introduce additional design parameters via innovative mechanical configurations (new actuators). The design parameters, control variables in system terminology, provide additional degrees of freedom to optimize the performance of the engine over its wide range of operation. The continuously variable transmission is an example of a recently implemented actuator that affects overall powertrain performance. Other actuators currently under consideration are electronic throttle, variable cam timing, camless valves, and direct injectors.

Historically, new actuators (exhaust gas recirculation valve, air bypass valve, fuel injectors) and sensors (exhaust gas oxygen sensor, mass air flow meter) have been introduced each time designers needed to meet additional engine performance requirements [15]. Performance standards and convenience pressed for the development of spark timing control. This additional control was used to advance or retard spark timing resulting in improved fuel economy and power. During the Eisenhower administration, federal emission legislation required emission control. This was accomplished by positive crankcase ventilation systems (PCV) used to minimize emissions from the crankcase, and secondary air systems used to oxidize hydrocarbons (HC) in feedgas emissions. Stricter emissions standards were met by

introducing external exhaust gas recirculation (EGR) to reduce oxides of nitrogen (NO_x) formation in feedgas emissions. Mandates in fuel economy led to the development of the idle speed regulation by the introduction of the air bypass valve. Development of the catalytic converter allowed further emission reduction, but required precise air-fuel ratio control, which was accomplished with the introduction of the exhaust gas oxygen sensor, and fuel injectors. The development and implementation of the corresponding control strategies were based on the relative independence of the different subsystems at low frequencies. Individual feedback loops were wrapped around sensors and actuators available for each subsystem (multiple single-input single output, SISO approach). In advanced technology automotive engines, the coupling between subsystems is strong, and imposes performance tradeoffs. Without knowledge of this interaction the powertrain control problem involves an extensive scheduling effort to define the new optimum operating points, and requires a laborious tuning process to calibrate the subsystem controllers to avoid unintentional excitations. Good control design in advanced technology automotive engines requires informed decisions of the performance tradeoffs early in the design process, and it is one of the subjects addressed by this dissertation.

In this dissertation we show that control design in advanced technology automotive engines necessitates a systematic modern control theoretical approach. In advanced technology automotive engines, the multiple SISO approach (decentralized controller architecture) reaches its limitations. In the following chapters we present a feasibility analysis of the engine control system for two innovative mechanical configurations of the spark ignition (SI) engine : (i) an SI engine equipped with secondary throttles placed in the intake ports of the cylinders, and (ii) an SI engine equipped with a variable cam timing (VCT) mechanism. Both mechanical designs affect the breathing process of the engine and are introduced to reduce emissions, increase fuel economy, and maintain drivability during rapid changes in the throttle position imposed by the driver (acceleration/ deceleration). Both actuators can be viewed as special cases of camless engine; the functionality of the secondary throttles is similar to the variable intake valve timing and lift, and the variable cam timing engine addresses the case of a variable intake and exhaust valve timing with fixed valve overlap. This study is an assessment of the achieved performance when compared to conventional engines, and an investigation of the effects of the new technology on the implementation of the complete powertrain control strategy. This work is based on the systematic approach of (i) deriving or identifying the dynamic model for the advanced technology engine design, (ii) validating the model using engine-dynamometer experimental data, (iii) studying the subsystem interconnections and making decisions on the performance tradeoffs in transient and steady-state engine operation, (iv) designing a controller that achieves a reasonable tradeoff in the performance requirements, and (v) investigating the controller complexity and the associated engine performance.

1.2 Engine Control.

Engine performance is primarily characterized by emission production, fuel efficiency and drivability. These in turn are affected by four fundamental engine variables: air charge, air-fuel ratio (A/F), exhaust gas recirculation (EGR) and spark timing. Automatic control of these variables has improved engine performance allowing optimum operation independent of aging, history, or environment [66], and has increased the convenience and safety level of the modern automobile [15]. A key contributor to the accomplishments in the area of engine control has been the availability of accurate and simple (control oriented) engine models. In the early 70's, control applications in the automotive industry paralleled achievements in engine and powertrain modeling. In this dissertation we model two innovative mechanical configurations of the SI engine, and use them for the analysis and synthesis of A/F and EGR controllers to achieve engine performance requirements. To serve as an introduction to this work, we review the most significant engine modeling efforts, and provide a brief description of the A/F and EGR control tasks and existing control designs.

1.2.1 Engine Modeling.

In this section we discuss the accomplishments in the area of engine modeling and its contributions to the analysis and development of engine control. The evolution of the engine models has three significant phases: (i) thermodynamic models, (ii) input-output models, specific to each application or engine configuration, and (iii) nonlinear models, physically based (generalized) for wide range of operation.

In the first of these phases, detailed thermodynamic methods were employed to understand the exact phenomena, to identify the variables that govern them, and ultimately to represent them with compact mathematical equations [3]. Numerical simulations allowed the designers to gain understanding of the engine behavior by performing numerical experiments, and testing the engine performance. The first non-thermodynamic models can be found in [32, 33, 34], where the authors developed crankangle event based models for compression ignition engine to perform stability analysis studies. Nonlinear dynamical models for SI engines have been developed in [65, 66], where spark, A/F, and EGR were optimized to minimize emissions while maintaining fuel economy. In these articles, the authors used control theoretical techniques to achieve performance improvements. Modern control methods were applied to linear engine models in [7] demonstrating the capabilities of control theoretical approaches in automotive applications. The need for precise transient A/F control emerged from the increasingly demanding emission requirements. Unknown fuel dynamics often misled control engineers to over-compensate for lean or rich A/F responses, so identification of fuel puddling and wall-wetting became a pressing problem. The first efforts led to the derivation of an input-output model of the fuel dynamics [75], and later to a more detailed characterization of transient A/F response [85, 1].

In the early 80's nonlinear dynamic models with wide range of operation (covering most

urban driving cycles) were developed [18, 17, 86, 58]. The work in [17] provides the most comprehensive model including actuator and sensors, and [86] incorporates exhaust emission and rotational dynamics. The effort in engine modeling has been expanded to include transmission and driveline characterization [60, 11]. In [13] the authors derive linearized models and study an important issue of engine control, namely, how multi-rate sampling affects engine control design. By the end of the 80's control engineers had developed a significant number of engine models, and a comprehensive list of them and discussion of their development can be found in [60] and in [62].

Currently, stringent requirements on emission, fuel economy, and safety require high performance and robust controllers. Complete, but generic, powertrain models are developed in [11, 23, 16, 35, 52], and are combined with modern control techniques in [10, 12, 76] to satisfy these requirements. Meeting the new performance requirements often requires accurate information and characterization of complicated phenomena [48], which is facilitated by the increased computational power in on-board control systems. In [61] the author addresses the challenging problem of reducing the development time needed to obtain accurate models, and provides a systematic approach to powertrain modeling and control effort.

1.2.2 Air-Fuel Ratio Control.

Vehicle feedgas emissions consist of carbon monoxides (CO), hydrocarbons (HC), and oxides of nitrogen (NO_x). In the early 1970s, three-way catalytic (TWC) converters were introduced to oxidize (HC and CO) and reduce (NO_x) pollutant species in the exhaust gases. The efficiency with which the undesirable exhaust gases are reduced to acceptable levels, or are converted to desirable gases, is a function of A/F. The sensitivity of the catalytic converter efficiency to A/F is shown in Figure 1.1. In this figure it can be seen that there is a very narrow range of A/F where high conversion efficiency for the primary three pollutants is attained. The A/F value were the highest efficiency is attained is the stoichiometric value (for standard fuels, $A/F = 14.64$). Due to this sensitivity, A/F control is an important task in controlling vehicle tailpipe emissions. In the 70's, A/F was based on regulation of fuel flow into the cylinders via carburaters [73], and later, with fuel injectors [69, 88]. After the development of the exhaust gas oxygen (EGO) sensor, electronic feedback fuel control was possible. Electronic feedback fuel control has since been used to keep A/F close to the stoichiometric value based on the A/F signal at the EGO sensor. Achieving precise A/F in both steady-state and transient engine operations is a challenging problem due to unpredictable inputs of the driver, the switching type EGO sensor, transport delays that limit accurate response during transients and the combined dynamics of the hot-wire anemometer used for the mass air flow sensing, the throttle body, the intake manifold, and fuel puddling dynamics.

For this reason, many studies have been conducted on A/F feedback control. These studies may be divided into two categories, the first of which addresses the scarcity and

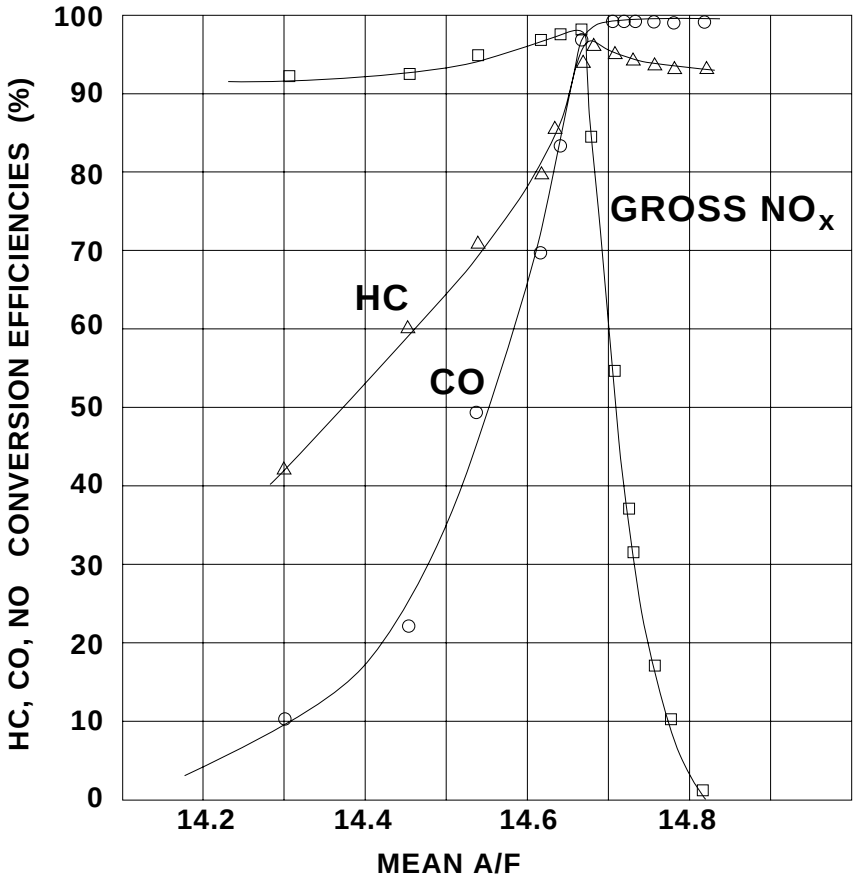

Figure 1.1: Typical three-way catalytic converter efficiency curves

nonlinearity of the conventional sensors. The emphasis in these studies is on the reconstruction of signals available for feedback, and the accurate and robust knowledge of the system states. The second category of studies addresses new engine configurations, i.e., modification of combustion parameters [3], and introduction of new actuators [8, 5] and sensors [64]. The new parameters in these engine configurations can improve A/F, but they often affect other engine variables. In this category of A/F control problems, the control designer has to identify and account for these interactions in order to meet the overall engine performance requirements. The work in this dissertation lies in the second category of A/F control studies. We control A/F for two different engine configurations after the introduction of new actuators. In the first problem, A/F excursions are minimized by the implementation of secondary throttles used to control air flow into the cylinders. The presence of the secondary throttles however can adversely affect drivability by making the engine seem sluggish. In the second problem, VCT is used to reduce feedgas emissions. This new control variable may cause disturbances in the A/F response of the engine. Both of these actuator configurations impose challenging multivariable problems that must be addressed by the control designer.

Previous work on the first category of A/F control studies consists of proportional-integral control and classical pole placement techniques, both in the discrete and continuous time domains [59, 46]. Furthermore, nonlinear analysis using describing functions has been used to study limit cycle behavior of the A/F response due to the switching type EGO sensor [63]. Multi-variable control with observers [57, 36] has been suggested as solutions to the problem of high performance and robust A/F control. Nonlinear sliding mode fuel injection controllers have been developed and tested in [10, 12, 54] providing an elegant alternative to the traditional gain scheduling of linear controllers, and show promising results even when using a switching EGO sensor. Individual A/F cylinder control using a single EGO sensor based on multi-rate sampling and periodic control techniques have given an answer to the alleviation of air charge maldistribution problems [28]. In related work, estimation of the air charge maldistribution in the cylinders is used in [47] along with a novel nonlinear observer technique. Use of nonlinear estimation also occurs in [36], were an extended Kalman filter is used for compensating the dynamics of fuel puddling. Adaptive compensation for the fuel dynamics has been successfully employed in [49] and [82]. In both studies the objective is the reconstruction of the A/F signal using a switching EGO sensor based on a fuzzy logic algorithm in [49], and a model-based approach in [82]. On-line identification techniques of the model used in [81, 39, 71] give promising results. In [71] the authors use a neural network that deals effectively with the long delay in the A/F process. On-line identification, observer design, and robust nonlinear control design techniques are areas of great importance to transient A/F control.

The second category of A/F control studies includes primarily engine control based on in-cylinder pressure measurements [64], and an electronically throttled engine [8, 39, 5]. The development of the electronic throttle control (ETC) or drive-by-wire (DBW) throttle system is an important research tool that provides a way of regulating the changes in air flow into the manifold caused by the primary throttle movement. These schemes show very good results in regulating A/F, and reducing emissions. In Chapter 2 we use this idea, and introduce secondary throttles in the inlet runners to allow coordination of air flow and fuel flow to achieve good A/F response during transients. The A/F performance improvement is shown to be achieved without slowing the engine torque response, and thus no tradeoff is made with drivability.

1.2.3 Exhaust Gas Recirculation.

Exhaust gas recirculation (EGR) was introduced in the early 1970s to suppress the formation of oxides of nitrogen (NO_x). The inert exhaust gases dilute the inducted air-fuel charge and lower the combustion temperature which reduces NO_x feedgas emissions.

Conventionally, exhaust gas recirculation is accomplished by controlling the exhaust gas that is supplied from the exhaust manifold to the intake manifold through a vacuum actuated valve. The EGR control algorithm is a simple PI or PID loop that adjusts the

amount of exhaust gas to the scheduled steady-state point which is a function of engine speed, coolant temperature and engine load (or another load related variable). EGR alters the breathing process dynamics and consequently the torque response. Careful steady-state and transient control design is necessary to maintain good engine torque response, and for this reason, EGR is typically turned off in transient engine operations, engine warm-up, and idling.

An innovative mechanical design approach to controlling EGR is the development of the variable cam timing (VCT) mechanism. By retarding the cam timing, combustion products which would otherwise be expelled during the exhaust stroke are retained in the cylinder during the subsequent intake stroke. This is a method of phasing the camshaft to control residual dilution and achieve the same results with the conventional external EGR system, thus providing an innovative solution to an old problem. The development of the VCT engine model and controller is addressed in Chapter 3 (engine model), Chapter 4 (control design), and Chapter 5 (implementation issues). With this work we show that dynamic VCT control is feasible.

1.3 Dynamic Interactions and Performance Tradeoffs.

To meet their stringent performance requirements, automotive engines have to be operated efficiently during both steady-state and transient operations. Past and current practice has been to optimize the additional design parameters that new actuators introduce only in steady-state using static engine mapping. The optimum operating points are defined by overlaying static maps of components that have to cooperate. Performance compromises in steady-state are alleviated with the introduction of feedforward terms that allow more freedom in achieving the design goals. However, the new Federal Test Procedure (FTP) for driving cycles consists of transient and high speed maneuvers, where the dynamic engine response is as important as the static engine behavior. These performance requirements press automotive engine designers to consider interactions between different processes at higher frequencies. Furthermore, the new actuators in the advanced technology automotive engines affect several subsystems, and cause severe performance tradeoffs. In this dissertation we show that the interaction between subsystems is a decisive factor in the control design of these highly multivariable engines. In the following chapters we identify the interactions that the secondary throttles and variable cam timing actuators introduce to the engine. These interactions are manifested through performance tradeoffs that the control engineer has to account for early in the design process. Briefly stated, *the secondary throttles and variable cam timing alter the engine breathing process which in turn affects fuel economy, emissions, and engine torque response over a wide range of operating conditions.* In designing controllers, we shall encounter three fundamental performance tradeoffs which are inherent to the advanced technology automotive engines.

(i) Fuel economy and emissions.

An approach for increasing fuel economy is to reduce energy losses. Engine operation (maintaining the same load) in high manifold pressure reduces the intake stroke pumping work required from the cylinders. High manifold pressure is associated with faster manifold filling dynamics, and therefore, changes in the throttle position are followed by rapid changes in the air charge. These changes introduce high bandwidth disturbances to the A/F response. Unless A/F control can successfully reject these disturbances, fuel economy (the initial design goal) will be followed by emission degradation.

(ii)NO_x feedgas emissions and catalytic converter efficiency.

Exhaust gas recirculation, used to suppress NO_x formation, alters the engine volumetric efficiency, and changes the breathing process dynamics. Exhaust gas recirculation and mass air flow into the cylinders are interconnected over a wide range of frequencies. High bandwidth control of feedgas NO_x rapidly alters the air charge and causes A/F excursions. In these cases, reduction in feedgas emissions is associated with reduction of the catalytic converter efficiency and may cause an increase in tail pipe emissions.

(iii) NO_x feedgas emissions and engine torque response.

NO_x feedgas reduction using exhaust gas recirculation affects the engine breathing process. Exhaust gas recirculation affects adversely the air charge and the mixture formation which is crucial to good engine torque response. The EGR control design must address the affects of the mixture dilution to the engine torque response both in steady-state and transient operations. Moreover, an open loop design is necessary since the conventional automobile is not equipped with an on-line torque sensor.

1.4 Overview.

Chapter 2 addresses the problem of controlling an engine equipped with secondary throttles. The new control variables affect the nonlinear breathing process and are introduced to allow joint management of air and fuel flow into the cylinders. A nonlinear feedforward map is developed as a solution to a control authority problem inherent to the two distinct operating regimes of the breathing process. A linear multivariable feedback is designed to limit air fuel excursions and track a torque command during transient operations. This novel approach provides an alternative to current drive-by-wire schemes and possesses major advantages for enhancing the safety level of the modern automobile.

Another innovative engine design is the variable cam timing engine. The effects of cam timing and secondary throttles in the breathing process are similar. The understanding gained from the control problem in Chapter 2 is applied to the modeling of the VCT engine. A mathematical representation for the variable cam timing engine is identified in Chapter 3. The variable cam timing engine allows the joint management of fuel flow and internal exhaust gas recirculation to minimize exhaust emissions, increase fuel economy and satisfy drivers' performance requirements over a wide range of operating conditions. The

mathematical representation is formulated by physically based differential equations; all parameters and key nonlinearities used are determined from regressed engine data. The models are experimentally validated by engine dynamometer testing.

In Chapter 4, a control scheme is developed to minimize feedgas NO_x and HC emissions and to maintain air fuel ratio at stoichiometry, while providing satisfactory torque response during rapid changes in throttle position. Control of the VCT engine is a challenging problem due to the strong interconnections between the cam phasing and A/F loop, and sensor limitations. Consequently we design a multivariable and a decentralized controller, and analyze how the multivariable controller achieves better performance than the decentralized controller. The impact of the control architecture (multivariable vs. decentralized) upon the dynamic response of the VCT engine is analyzed in Chapter 5. Finally, in Chapter 6 we summarize the results of this dissertation and discuss directions for future research.

1.5 Contributions of this Dissertation

The contributions of this dissertation are :

- An existing nonlinear dynamical engine model by Crossley and Cook [16] was modified to include the effects of secondary throttles placed before the intake ports of the cylinders on the performance of the SI engine. The model, based on physical engine characteristics, is a powerful tool in studying the effects of innovative actuation that can affect the breathing process of the SI engine.

- Identification of different control authority regions for regulating the steady-state air flow into the cylinders. This result, although well known in the thermodynamic community [37], has not been acknowledged by control engineers. Our ability to affect (or not affect) the air flow into the cylinders is an important consideration in engine control, because the air flow into the cylinders is a variable that affects the overall engine performance in the following manner: (i) drivability, by altering the air charge, (ii) fuel economy, by changing the pumping losses during the intake event, and (iii) emissions, by causing A/F excursions.

- Derivation of a new control-oriented engine model that represents an SI engine equipped with a variable cam timing mechanism over a wide range of operating conditions. The model includes the breathing process, torque and emission generation, and sensor/actuator dynamics. Based upon extensive laboratory measurements, a phenomenological engine model structure was elucidated. With respect to the basic model of [16], the VCT mechanism alters the mass air flow into the cylinders, the self-EGR, the torque response, and the emissions of the engine. The developed model reflects all these innovations. It has been validated with engine-dynamometer experimental data and used in the design and development of the VCT engine controller.

- A rigorous analysis of the consequences of the multivariable versus decentralized controller architecture on the dynamic response of the VCT engine. A multivariable and a decentralized controller were designed, and it was demonstrated that the multivariable controller can manage the performance tradeoffs better than the decentralized controller. Moreover, the multivariable controller structure was simplified, without detrimental consequences in the system dynamic response, providing a paradigm of how a control designer may carry out her/his task in light of the requirement for a modular controller architecture implementation.

CHAPTER 2

Engine with Secondary Throttles.

2.1 Introduction.

A challenging control problem is to keep the A/F close to stoichiometry during rapid changes in the throttle position. Rapid changes in the throttle position strongly influence the cylinder air charging process, mixture formation and transient performance of the engine. These rapid throttle movements reflect the driver's demand for changes in torque and vehicle acceleration.

A controller is developed in this chapter to keep the A/F close to stoichiometry so that the Three Way Catalyst (TWC) operates with high efficiency, and to track the driver's torque demand during rapid changes in throttle position. The torque set point to be achieved is a function of throttle position and engine speed. This function, when evaluated for all possible throttle positions and engine speeds, forms a nonlinear map; we will call this the "demand map".

The control of the A/F around stoichiometry is usually based on regulating the fuel flow to follow the air flow changes imposed by the driver. The associated feedback control systems do not have enough bandwidth to accommodate fast transients caused by the throttle movement due to the long delay in the induction-compression-combustion-exhaust cycle. The addition of a feedforward term for the fuel set-point does not completely alleviate this problem. Developments in the area of drive-by-wire (DBW) throttle systems [22, 8, 39, 5] indicate the need of an air control scheme in addition to the fuel control. This need motivates the following work that moves a step beyond the DBW scheme by developing a joint air-fuel management system which allows full control authority of the primary throttle position to the driver.

The control scheme presented here is based on the introduction of secondary throttles before the intake ports of the cylinders (Fig. 2.1). The new control variables (θ_c) regulate the air flow into the cylinders. These control variables in combination with the fuel injectors (F_c) achieve low A/F excursions and good tracking of torque demand by adjusting the air flow and the fuel flow into the cylinders. The control variables θ_c smooth out rapid changes of the charging process during throttle movements so that the fuel control path is able to

maintain stoichiometry.

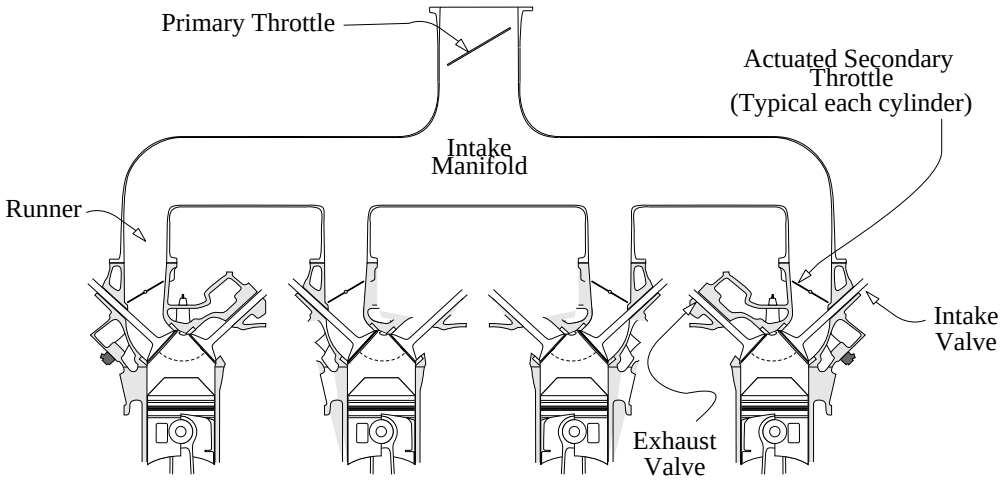

Figure 2.1: Schematic representation of 4-cylinder engine with secondary throttles.

The torque and A/F errors used by the controller are calculated by measuring the difference between actual and desired values. We assume direct measurement of the achieved torque[1]; we also use a linear EGO sensor for A/F measurement.

2.2 Engine Model.

This section gives an overview of the modifications of the nonlinear mathematical representation of the engine model developed in [16] and [23]. This model is a continuous-time nonlinear, low-frequency[2] phenomenological model with uniform pulse homogeneous charge, and lumped parameter approximation of breathing and rotational dynamics. The nonlinear mathematical representation of the engine model with secondary throttles is derived, based on physical engine characteristics, by modulating the mass air flow into the cylinders by a simple multiplication with a signal (θ_c). The signal (θ_c) takes values from 0 (closed) to 1 (wide open) and represents the effective area in the inlet runners. In this model all nonlinearities are regressed over engine-dynamometer data. The choice of parameters against which to regress the data is based upon physical principles explained in [37] for SI engines. Figure 2.2 shows the engine model with secondary throttles.

Breathing process dynamics

The manifold was analyzed as a single control volume with the throttle plate controlling

[1] We are assuming here that a reliable and accurate torque measurement is available, such as could be obtained from in-cylinder pressure sensor.

[2] In this model mass flow rate, manifold pressure, and torque are represented by their average values over an engine event.

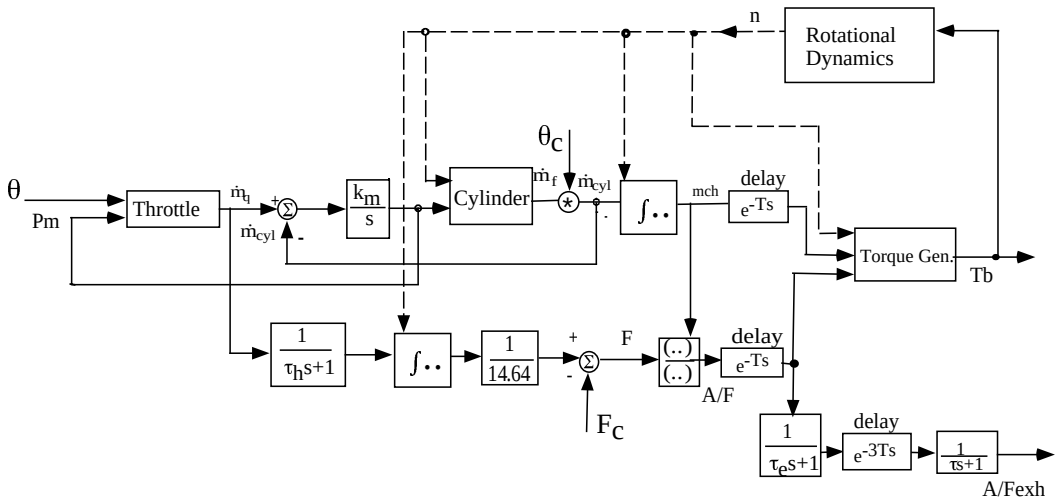

Figure 2.2: Engine model with secondary throttles.

mass air flow into the manifold, and the engine cylinders in combination with the secondary throttles controlling mass air flow out of the manifold. Based on the "Filling and Emptying Models" described in [37], manifold acts as a plenum, where the rate of change of the manifold pressure (P_m) is proportional to the mass air flow rate into the manifold ($\dot{m}_\theta$) minus the pumping mass air flow rate ($\dot{m}_{cyl}$) into the cylinders. The manifold dynamics are described by the following first order differential equation (see [60]) that relates the rate of change of the manifold pressure (P_m) to the flow rates into and out of the manifold ($\dot{m}_\theta$ and $\dot{m}_{cyl}$, respectively)

$$\frac{d}{dt}P_m = K_m(\dot{m}_\theta \Leftrightarrow \dot{m}_{cyl}), \text{ where } K_m = \frac{R \cdot T}{V_m} . \tag{2.1}$$

Based on the nominal manifold temperature (T), the manifold volume (V_m), and the specific gas constant $R = 287\ \frac{J}{Kg \cdot K}$, the constant K_m was calculated to be equal to $0.413\ \frac{bar}{g}$. This model is an engine event averaged representation of the intake manifold filling dynamics. The dynamic manifold pressure obtained by this model is not the instantaneous manifold pressure.

The mass air flow rate into the manifold ($\dot{m}_\theta$) through the primary throttle body is a function of throttle angle (θ), the upstream pressure (P_o), which we assume to be the atmospheric, i.e., $P_o = 1$ bar, and the downstream pressure, which is the manifold pressure (P_m). When the manifold pressure is less than half of atmospheric pressure, i.e., $P_m/P_o < 0.5$, the flow $\dot{m}_\theta$ through the throttle body is described as sonic flow and depends only on the primary throttle position. The function describing $\dot{m}_\theta$ in the two flow regimes is given

in [56] and [65] by :

$$\begin{aligned} \dot{m}_\theta &= f(\theta)g(P_m) \\ f(\theta) &= 2.821 \Leftrightarrow 0.05231\theta + 0.10299\theta^2 \Leftrightarrow 0.00063\theta^3 \\ g(P_m) &= \begin{cases} 1 & \text{if } P_m \leq P_o/2 \\ \frac{2}{P_O}\sqrt{P_m P_o \Leftrightarrow P_m^2} & \text{if } P_m > P_o/2 \end{cases} . \end{aligned} \tag{2.2}$$

The conventional engine pumping mass air flow rate ($\dot{m}_f$) is a function of manifold pressure (P_m) and engine speed (N) and is given in [16] by :

$$\dot{m}_f = \Leftrightarrow 0.366 + 0.008979 N P_m \Leftrightarrow 0.0337 N P_m^2 + 0.0001 N^2 P_m \quad . \tag{2.3}$$

The secondary throttles are restricting the air flow rate out of the manifold and into the cylinders, so the mass air flow rate into the cylinders ($\dot{m}_{cyl}$) is modeled by :

$$\dot{m}_{cyl} = \theta_c \cdot \dot{m}_f \quad . \tag{2.4}$$

Process delays

The discrete nature of the combustion process causes delays in the signal paths: between the mass charge formation and the torque generation there exists a delay equal to the compression stroke duration, and between the exhaust manifold and the exhaust gas oxygen (EGO) sensor there exists a delay which equals 3 times the intake event duration.

Exhaust process dynamics

The dynamics of the exhaust manifold and the linear EGO sensor are modeled by a first order differential equation with time constant equal to 0.15 sec and 0.20 sec, respectively.

Fuel path dynamics

The fuel puddling dynamics are important in accurate transient A/F control [8], [36], and [55]). In general, it is difficult to accurately model the fuel puddling dynamics [49] because the parameters of the model depend strongly on the fuel characteristics and the temperature of the engine during operation [82]. The model for the fuel puddling dynamics is given in [1] by

$$\begin{aligned} \dot{M}_{fp}(t) &= \Leftrightarrow \tfrac{1}{\tau_f} M_{fp}(t) + X\dot{M}_{fi}(t) \\ \dot{M}_f(t) &= (1 \Leftrightarrow X)\dot{M}_{fi}(t) + \tfrac{1}{\tau_f} M_{fp}(t) \\ \text{where,} \quad & \dot{M}_{fi} \ : \text{ injected fuel flow (Kg/sec) ,} \\ & \dot{M}_{fp} \ : \text{ fuel film mass flow (Kg/sec) ,} \\ & \dot{M}_f \ : \text{ cylinder port fuel mass flow (Kg/sec) ,} \\ \text{and} \quad & X \ : \text{ fraction of the injected fuel which is deposited on the manifold as fuel film.} \end{aligned} \tag{2.5}$$

The exact model of the fuel dynamics used for the engine with the secondary throttles was

developed in [1] :

$$
\begin{aligned}
&M_f = \tfrac{(1-X)\tau_f s+1}{\tau_f s+1} M_{fi}, where \\
&X = 0.3 + \tfrac{0.7}{90}\theta = 0.3 + \tfrac{0.7}{90}10 = 0.38, \\
&\theta = 10 : \text{angle in degrees of the primary throttle,} \\
&\text{and } \ \tau_f = 0.1 \text{ sec, resulting} \\
&M_f = \tfrac{0.62 \cdot s+1}{0.1 \cdot s+1} M_{fi}.
\end{aligned}
\tag{2.6}
$$

Precise transient A/F control during rapid changes in the throttle position by the driver requires feedforward compensation of the fuel command since the inherent delay in the A/F feedback loop prohibits rapid corrections through the feedback fuel command. The feedforward fuel command is regulated on the basis of the estimated cylinder air charge. The estimated cylinder air charge is calculated based on the mass air flow measurement at the mass air flow sensor (hot wire anemometer positioned upstream the throttle body), and integrated during the intake event. The estimated cylinder air charge is divided by 14.64 (nominal A/F) to provide the feedforward fuel flow command used in the A/F loop. The dynamics of the air flow meter are included in the model by a first order lag with a time constant equal to 0.13 sec.

Torque generation

The torque generated by an engine depends on the ignition of the cylinder charge, the mixture formation, and engine specific physical parameters. Analytical curve fitting techniques to dynamometer-engine experimental data are applied in [16] to estimate the steady-state brake torque generation given by:

$$
\begin{aligned}
T_b = \quad & \Leftrightarrow 181.3 + 379.36 m_a + 21.91 A/F \Leftrightarrow 0.85 A/F^2 + 0.26\sigma \Leftrightarrow 0.0028\sigma^2 \\
& 0.027N \Leftrightarrow 0.000107N^2 + 0.00048N\sigma + 2.55\sigma m_a \Leftrightarrow 0.05\sigma^2 m_a + 2.36\sigma m_e \\
&\text{where,} \\
& m_a \quad : \text{mass air charge (g/intake event) ,} \\
& A/F \quad : \text{air-to-fuel ratio ,} \\
& \sigma \quad : \text{degrees of spark advance before top dead center ,} \\
& N \quad : \text{engine speed (rad/sec) , and} \\
& m_e \quad : \text{exhaust gas recirculation (g/intake event).}
\end{aligned}
\tag{2.7}
$$

For simplicity in this study, we used the above equation with spark advance equal to 30 degrees ($\sigma = 30$), and exhaust gas recirculation equal to zero ($m_e = 0$).

Rotational dynamics

A very simplified model of the rotational dynamics is used for the engine with secondary throttles model. The rotational motion of the engine crankshaft is given in terms of the engine and the vehicle moment of inertia (J), angular acceleration ($\dot{\omega}$ in $\frac{rad}{sec^2}$), and the difference between the net torque generated by the engine (T_b in Nm) and the load torque

on the shaft (T_l in Nm).

$$\Sigma T = T_b \Leftrightarrow T_l = J\dot{\omega}. \tag{2.8}$$

The load torque in the shaft is calculated in [23] using experimental data. It can be represented as a function of the drag due to the engine friction (c_{de}), the aerodynamic drag (c_{dv}), and the selected gear ratio (gr) :

$$\begin{array}{ll} T_l & = (c_{de} + c_{dv} gr)\omega^2 \ , \\ c_{df} & = 0.00015, \ \text{ drag due to the engine friction } \ (\frac{Nm \cdot sec^2}{rad^2}), \\ c_{dv} & = 0.001, \ \text{ aerodynamic drag } \ (\frac{Nm \cdot sec^2}{rad^2}), \text{ and} \\ gr & = 0.197 \text{ (3rd gear).} \end{array} \tag{2.9}$$

The total inertia is a combination of the engine inertia (J_e), and the vehicle inertia reflected through the drivetrain, and is given by:

$$\begin{array}{ll} J & = J_e + m_v (r_w gr)^2 \ \frac{Nm \cdot sec^2}{rad} \text{ where,} \\ J_e & : \text{engine inertia,} \\ m_v & : \text{vehicle mass} \\ r_w & : \text{wheel radius} \\ gr & : \text{gear ratio} \end{array} \tag{2.10}$$

From vehicle data we selected $J_e = 0.14 \ \frac{Nm\,sec^2}{rad}$, $m_v = 920 \ kg$, and $r_w = 0.28 \ m$.

2.3 Nonlinear Breathing Process.

This section concentrates on the nonlinear dynamics of the engine breathing process. The study of the breathing process behavior is used to investigate and determine the operating regions where the secondary throttles (θ_c) have control authority in regulating the air charge into the cylinders. The air charge for every intake event is a function of the mass air flow rate into the cylinders and the engine speed, and it is directly related to the torque produced throughout the power stroke. Control over the transient and the steady state value of the mass air flow is necessary to meet the objectives of good torque tracking and maintaining the A/F at stoichiometry. The signal θ_c must influence the static and dynamic behavior of the manifold pressure, the air flow into the manifold through the primary throttle position, and the air flow into the cylinders through the secondary throttles.

For the basic model (without the secondary throttles) the steady state operating point occurs at the intersection of the two trajectories of the mass air flow rates. This point is the nominal point shown in Fig. 2.3. With the introduction of the secondary throttles it is possible to scale the engine pumping rate ($\dot{m}_f$) by different values depending upon the effective area of the passage that is regulated by opening and closing these new valves

$$\dot{m}_{cyl} = \theta_c \cdot \dot{m}_f \quad . \tag{2.11}$$

Figure 2.3 shows the new trajectories of the air flow rate into the cylinders and the resulting new equilibria (set points in Fig. reffig:intersections) for the breathing process. For sufficiently large $\theta_c < 1$, the steady state value of the mass air flow into the cylinder $\dot{m}_{cyl}$ is adjusted by causing the new equilibrium to shift from the sonic flow regime to the subsonic region. A closer investigation of the two regimes illustrates their significance in the new control scheme.

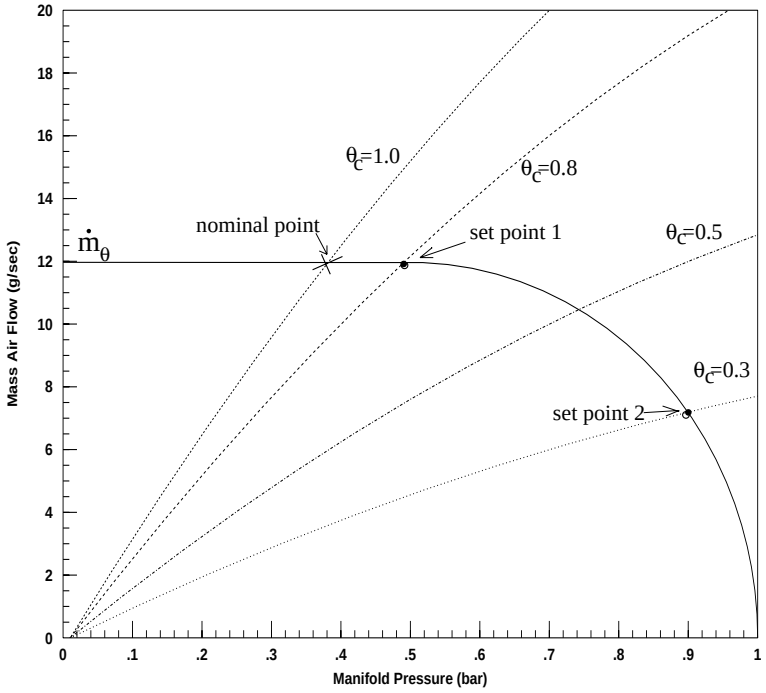

Figure 2.3: Trajectories of the air flow into the manifold ($\dot{m}_\theta$ for $\theta = 10$) and the air flow out of the manifold ($\dot{m}_{cyl}$) for several values of secondary throttles (θ_c).

When the flow through the primary throttle body is sonic and therefore does not depend on the manifold pressure, we operate in the flat region of $\dot{m}_\theta$ in Fig. 2.3. Small changes in θ_c cause no change in the steady state value of the mass air flow in and out of the manifold. For this reason, when the model of the breathing process is linearized, the secondary throttles have zero control authority on regulating the steady state mass air flow into the cylinders. This can be shown by the following transfer function between the control signal $\Delta\theta_c$ and the mass air flow into the cylinder $\Delta\dot{m}_{cyl}$ (see Fig. 2.4) :

$$\frac{\Delta\dot{m}_{cyl}}{\Delta\theta_c} = \frac{1}{1 + \frac{k_m k_1}{s}} = \frac{s}{s + k_m k_1} \quad . \tag{2.12}$$

The DC gain of the above transfer function is clearly zero. The usual technique of incorporating an integrator to regulate the steady state mass air flow into the cylinders cannot be used here, since the transfer function has a zero at the origin that cancels the integrator pole. It is also instructive to see this on a block diagram level. Figure 2.4 shows the linear

dynamics of the breathing process for sonic flow after the introduction of the secondary throttle. Note that the integrator loop, which is an intrinsic part of the manifold dynamics in sonic flow, rejects the signal θ_c in steady state. Thus, the control signal $\Delta\theta_c$ cannot adjust the air charge into the cylinder by "smoothing" the effect of rapid throttle changes. Consequently, the control command $\Delta\theta_c$ has zero control authority on the A/F and the steady state value of the engine torque.

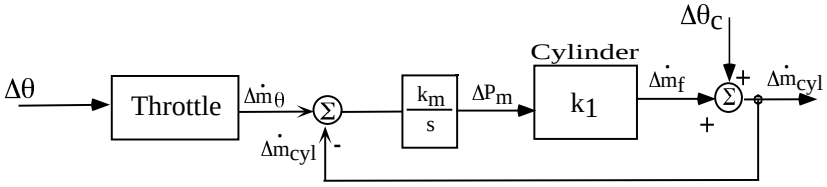

Figure 2.4: Block diagram of the linearized breathing process.

In the case where the flow is subsonic, i.e., $P_m/P_o > 0.5$, the air flow into the manifold depends on the primary throttle position and on the manifold pressure; thus, the linear model of the engine breathing process is different from the above, and the application of linear techniques such as LQG/LTR is possible. The slope of the function that describes $\dot{m}_\theta$ (see Fig. 2.3) indicates the control authority of its operating point. It is clear now that the control authority of the secondary throttles around the set-point 2 in Fig. 2.3 is preferable to that around the set-point 1. Around set-point 2, the secondary throttles can be used to "smooth" the abrupt changes of air flow by regulating the air flow rate into the cylinders at a slower rate.

In conclusion, a nonlinear feedforward design of the θ_c set-points that allows operation in the subsonic flow regime, where the secondary throttles have maximal control authority, is necessary. This map will provide the steady state position of the new control variables.

2.4 Feedforward Control Design.

The natural nominal position of the secondary throttles is wide open, i.e., $\theta_c = 1$. However, recall from Section 2.3 that under these conditions the secondary throttles often have zero control authority in adjusting the steady state value of the mass air flow into the cylinders. A solution that uses a control signal (θ_c), which consists of a nonlinear feedforward term ($\theta_{c_{fw}}$) plus a feedback term ($\theta_{c_{fb}}$) is proposed. The feedforward design ensures maximal control authority and smooth engine operation.

The nonlinear feedforward term ($\theta_{c_{fw}}$) is designed to satisfy the following three conditions: (i) it is a smooth and non-decreasing function of the primary throttle position (θ) and the engine speed (N), i.e., $\theta_{c_{fw}} = \theta_{c_{fw}}(\theta, N)$; (ii) the engine should deliver its maximum power output when operated at or close to wide open throttle (WOT), and (iii) maximal control authority should be available without sacrificing combustion stability and

performance. To achieve these objectives over a wide range of engine operating conditions we should consider the effects of combustion stability, thermodynamic performance indices and idle operating conditions. For example, it is unclear if the higher manifold pressure associated with the secondary throttles results in higher volumetric efficiency. Presently such an extended analysis has not been completed. Based only on a control authority analysis, the following map has been developed (see Fig. 2.5):

$$\theta_{c_{fw}} = \begin{cases} 0.55 & \text{if } 0^o < \theta < 12^o \\ 0.6445 \Leftrightarrow 0.0126 \cdot \theta + 1.3125 \cdot 10^{-4} \cdot \theta^2 + 2.1875 \cdot 10^{-5} \cdot \theta^3 & \text{if } 12^o \leq \theta < 20^o \\ 1 \Leftrightarrow (\frac{\theta - 60}{65})^2 & \text{if } 20^o \leq \theta < 60^o \\ 1 & \text{if } 60^o \leq \theta < 90^o \end{cases}$$

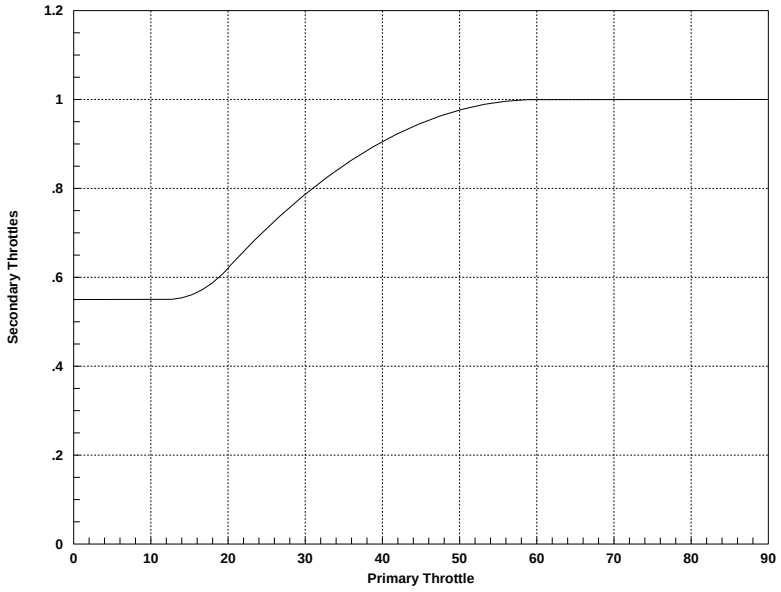

Figure 2.5: Static feedforward nonlinear term of the secondary throttles control signal (θ_c)

The reasoning behind this map is briefly explained. First, usual driving conditions in urban areas correspond to partly open primary throttle (θ) interrupted by rapid requests for acceleration and deceleration (which are the main causes of A/F excursion). At partly open throttle, the maximum power of the engine is not required and hence $\theta_{c_{fw}} < 1$ is acceptable. In addition, $\theta_{c_{fw}}$ has been adjusted to ensure that the breathing process is operating near set-point 2 in Fig. 2.3. When the primary throttle is at or near WOT, the secondary throttles must smoothly operate close to the wide open position to ensure that maximum engine output can be achieved. Under WOT conditions, $P_m/P_o \approx 1$. Therefore, the secondary throttles are operating in the maximal control authority region, however, they have freedom of movement only towards one direction. The secondary throttles can reduce the passage of the inlet runners and regulate the transient air flow rate into the cylinders during acceleration to cause lower A/F excursions. On the other hand, not much

can be done when the driver closes the primary throttle: the secondary throttles cannot open further ($0 < \theta_c \leq 1$) to "smooth" the abrupt decrease of the air flow into the manifold by providing additional air. Finally, when the primary throttle is nearly closed, there is a minimum position for the secondary throttles below which idle stability issues have to be addressed.

The above map has been used to investigate the contribution of the new control actuator to driveability improvement and emission reduction. Thermodynamic evaluation is needed to determine the interaction of the new control variables with the various engine performance indices. An initial assessment of the influence of the suggested feedforward scheme shows that the feedforward term is beneficial to the manifold dynamics. The engine operates at $P_m/P_o \approx 0.9$, i.e., manifold almost fully charged, which causes considerably faster manifold filling dynamics during part throttle driving. This can be seen by evaluating the time constant of the breathing dynamics at several operating points (see Fig. 2.3). Achieving fast quasi-steady conditions close to atmospheric pressure in the intake manifold can eliminate wide variation in the time constant of the fuel puddling dynamics. This might reduce the uncertainty inherent in the fuel flow transient behavior. A reduction of the pumping losses is also expected due to the low manifold vacuum, however the additional complication in the intake system of the engine might decrease the volumetric efficiency. Further investigation of all the above issues will determine the effect of the new control scheme on fuel economy. For control purposes, usage of the feedforward term shown in Fig. 2.5 makes linearization fruitful and allows linear feedback design.

2.5 Demand Map.

In the engine with the secondary throttles the input is the primary throttle position (driver's command). It is measured but not controlled. The torque set-point (T_{des}) is calculated from the primary throttle position (θ) and the engine speed (N) measurements. This requires a demand map, similar to the one used in DBW schemes [22], to determine the torque set-point for any throttle position and engine speed. This map is a nonlinear and well-defined map, i.e., torque has a unique value for specific throttle position and engine speed. To generate this map we run the simulation model of the engine with the secondary throttles for different throttle positions and gear ratios, and record the corresponding steady-state torque and engine speed response. The torque from the demand map will be used as the desired torque when the torque error is calculated to adjust the control signals.

2.6 Feedback Control Design.

In the following Sections we compare the A/F closed loop response of the engine with the secondary throttles (θ_c-scheme) with the conventional[3] A/F closed loop response (F_c-scheme), and with the A/F closed loop response of an engine equipped with electronic throttle (DBW-scheme). The comparison is based on simulation results using the nonlinear dynamic model described in Section 2.2. In this section we design three linear multivariable controllers for the three different schemes.

The main objective of the three control designs is to minimize the A/F excursion during rapid changes in pedal position. This is achieved with integral control, by augmenting the states of the system with the integrated state of A/F error. A secondary objective for the closed loop performance of the engine with the secondary throttles, and the engine with the electronic throttle is to maintain good torque response, during these transients. Good torque response amounts to (i) maintaining similarity of the rate of torque change in the first phase of the acceleration-deceleration with the conventional engine torque response, (ii) avoiding torque hesitation during the acceleration phase, and (iii) achieving in steady-state the desired torque response. This objective is accomplished with the introduction of the integrated state of torque error in the control design of the engine with the secondary throttles (θ_c-scheme), and the control design of the engine with the electronic throttle (DBW-scheme). With this objective we ensure that the θ_c and the DBW schemes have torque response similar to the conventional engine. This is an important objective and cannot be ignored, since the two schemes can "decouple" the driver from the engine (particularly the cylinders). The controller will try to filter the rapid changes in air charge (lowpass the disturbance) to minimize A/F excursions causing very slow engine torque response. Thus, designing the two schemes based on A/F regulation only, will cause unacceptable drivability. The three schemes can be summarized as :

F_c-scheme : During acceleration/deceleration, the driver changes the primary throttle position (θ), and fuel command is used to minimize A/F excursions caused by the rapid changes in the throttle position. The fuel regulation is based on A/F, torque, and throttle position measurements. The A/F is measured using a linear EGO sensor. These measurements improve the conventional fuel regulation, which is a PI feedback controller based on the A/F measurement, and a feedforward compensator based on the mass air flow (MAF) or manifold pressure (MAP) measurement.

θ_c-scheme : As above, the driver controls the primary throttle position (θ), and the controller regulates secondary throttle position (θ_c) and fuel command (F_c) to mini-

[3]This scheme is called conventional because we use only the fuel command to control A/F at stoichiometry during rapid changes in throttle position. In the other two schemes ("non-conventional") we coordinate fuel and air flow into the cylinders to maintain stoichiometry. Although we call the F_c-scheme as conventional A/F control, neither the control strategy nor the measurements used are conventional.

mize A/F excursions and maintain good torque response. In this scheme we use the same measurements as above, i.e., A/F, torque, and throttle position measurements.

DBW-scheme : In this scheme, the driver controls the pedal position, and the controller regulates the throttle position (θ_e), and the fuel command (F_c) to precisely control A/F and track the torque demand (T_{des}). The measurements used in this scheme are identical to the ones used in the previous schemes.

The control structure of the three different schemes is schematicaly shown in Fig. 2.6.

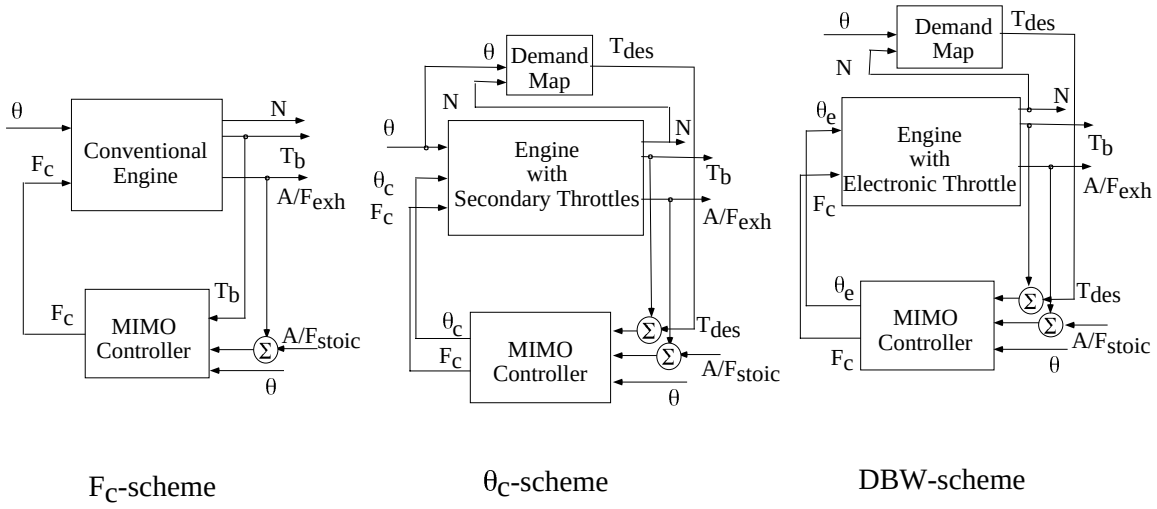

Figure 2.6: Schematic representation of the three control schemes.

The multivariable control law used for all the three designs is based in LQG design methodology. Robustness of the three control designs to actuator uncertainty is an important issue of the feasibility of the different control configurations. The engine model used in the design of the multivariable controller does not include neither θ_c actuator dynamics nor electronic throttle actuator dynamics. Furthermore, there is a great level of uncertainty in the fuel puddling dynamics. For this reason, we adjust the observer gain in all three designs so that the LQG controller can asymptotically approach the robustness properties of the LQR design.

The operating point about which we choose to linearize the engine model lies in the acceleration curve of the engine and third gear was used in the powertrain rotational dynamics. The nominal primary throttle position used was $\theta = 20^o$, and the nominal set-point for the secondary throttles was 61% open, resulting in manifold pressure $P_m = 0.96$ bar. The air flow into the cylinders was 15.4 g/sec at 3000 RPM producing 31.5 Nm of torque. The same amount of torque is produced by the conventional engine at a primary throttle position of $\theta = 11.8^o$, with a manifold pressure of 0.51 bar. Note that this operating point falls into the low control authority region explained in Section 2.3.

2.6.1 Feedback Control Design using Secondary Throttles.

The engine model with the secondary throttles is linearized at throttle position equal to 20 degrees, secondary throttles equal to 61% open, engine speed equal at 3000 rpm. The state variables of the linearized model are manifold pressure, A/F at the EGO sensor, mass air flow, angular velocity, fuel puddle, and states associated with second order Padé approximation of the delays in the processes and signals. The state space representation of the linearized model of the engine with the secondary throttles is given by :

$$\dot{x}(t) = Ax(t) + Bu(t) + B_r r(t)$$
$$y(t) = Cx(t)$$

$$\text{where} \quad u = \begin{bmatrix} \theta_c \text{ (sec. throttles)} \\ F_c \text{ (fuel command)} \end{bmatrix}, \quad r = \theta \text{ (primary throttle)},$$
$$\text{and } y = \begin{bmatrix} T_b & \text{(torque meas.)} \\ A/F_{exh} & \text{(meas. at the EGO sensor)} \end{bmatrix},$$

and

$$A = \begin{bmatrix} -0.079 & 139.786 & 0 & 0 & 0 & -1.013 & 0 & 0 & 0 & 0 & 0 \\ 0.019 & -100 & 10.7952 & 0 & 0 & 0 & 0 & 0 & 0 & 0 & 0 \\ -0.0289 & 0 & -74.61 & 0 & 0 & 0 & 0 & 0 & 0 & 0 & 0 \\ 0 & 0 & 0 & -6.667 & 0 & 2 & 0 & 0 & 0 & 0 & 0 \\ -0.0001 & 0 & -0.485 & 0 & -7.692 & 0 & 0 & 0 & 0 & 0 & 0 \\ 0 & 0 & 0.01 & 0 & -1.587 & -0.001 & 0 & 0 & 0 & 0 & -2.529 \\ 0 & 0 & 0 & 0 & 0 & 0 & 61.40 & 288.55 & 0 & 0 & 0 \\ 0 & 0 & 0 & 0 & 0 & 0 & -0.0333 & 0.20 & 5.067 & 0 & 0 \\ 0 & 0 & 0 & 333.33 & 0 & 0 & 0 & -33.33 & -566.667 & 0 & 0 \\ 0. & 0. & 0. & 0. & 0. & 0. & 0. & 0. & 2. & -5. & 0. \\ 0 & 0 & 0 & 0 & 3.846 & 0 & 0 & 0 & 0 & 0 & -10. \end{bmatrix},$$

$$B = \begin{bmatrix} 0 & 0 \\ 25.9675 & 0 \\ -10.2811 & 0 \\ 0 & 0 \\ 0 & 0 \\ 2.361e+03 & -8.254e+04 \\ 0. & 0. \\ 0. & 0. \\ 0. & 0. \\ 0. & 0. \\ 0. & 2. \end{bmatrix}, \quad B_r = \begin{bmatrix} 0 \\ 0.4908 \\ 0.3622 \\ 0 \\ 0.0038 \\ 44.6284 \\ 0 \\ 0 \\ 0 \\ 0 \end{bmatrix},$$

$$C = \begin{bmatrix} -0.0231 & 410.86 & 0 & 0 & 0 & -2.978 & 0 & 0 & 0 & 0 & 0 \\ 0 & 0 & 0 & 0 & 0 & 0 & 0 & 0 & 0 & 2.5 & 0 \end{bmatrix}.$$

During changes in throttle position, it is important to maintain A/F at stoichiometry and maintain zero tracking error in the torque response. This is accomplished by augmenting

the state vector with the integral of the error in the A/F response ($\dot{q}_2 = A/F_{stoic} \Leftrightarrow A/F_{exh}$), and the integral of the error in the torque response ($\dot{q}_1 = T_{b_{des}} \Leftrightarrow T_{b_m}$):

$$\dot{q} = y \Leftrightarrow \begin{bmatrix} T_{b_{des}} \\ A/F_{stoic} \end{bmatrix} \quad . \tag{2.13}$$

We augment the input and state vector as follows :

$$\hat{r} = \begin{bmatrix} \theta \\ T_{b_{des}} \\ A/F_{stoic} \end{bmatrix} \quad \text{, and } \hat{x} = \begin{bmatrix} x \\ q \end{bmatrix}. \tag{2.14}$$

The resulting augmented system is :

$$\underbrace{\begin{bmatrix} \dot{x} \\ \dot{q} \end{bmatrix}}_{\dot{\hat{x}}} = \underbrace{\begin{bmatrix} A & 0 \\ C & 0 \end{bmatrix}}_{\hat{A}} \underbrace{\begin{bmatrix} x \\ q \end{bmatrix}}_{\hat{x}} + \underbrace{\begin{bmatrix} B \\ 0 \end{bmatrix}}_{\hat{B}} u + \underbrace{\begin{bmatrix} B_r & 0 \\ 0 & \Leftrightarrow I \end{bmatrix}}_{\hat{B}_r} \hat{r}, \, . \tag{2.15}$$

The controller feedback gain

$$u = \Leftrightarrow K \hat{x} = \begin{bmatrix} \Leftrightarrow K_1 & \Leftrightarrow K_2 \end{bmatrix} \begin{bmatrix} x \\ q \end{bmatrix}$$

is found by solving the LQR problem. The weighting matrices R_{xx} and R_{uu} in the minimization of the cost function

$$J = \int_0^\infty \left(x' R_{xx} x + u' R_{uu} u \right) dt$$

were tuned so that the closed loop objectives (defined in Section 2.6) are satisfied. The resulting K_1 and K_2 feedback gains are :

$$K_1 = \begin{bmatrix} 0.0004 & 0.0411 & 0.0060 & 0.0156 & -0.0173 & 0.0000 & 0.0000 & 0.0000 & 0.0004 & 0.0190 & -0.0352 \\ 0.0000 & 0.0023 & -0.0122 & -0.0247 & 1.8198 & -0.0004 & -0.0001 & -0.0001 & -0.0014 & -0.0810 & 2.5977 \end{bmatrix}$$

$$K_2 = \begin{bmatrix} 0.0099 & 0.0450 \\ 0.0014 & -0.3130 \end{bmatrix} \quad . \tag{2.16}$$

For the complete LQG/LTR controller design we need to estimate the states (x) using an Kalman filter. The real symmetric positive semi-definite matrix representing the intensities of the state noises Q_{xx}, and the real symmetric positive definite matrix representing the intensities of the measurement noises Q_{yy} were assumed diagonal. Loop transfer recovery

in the input was employed and the resulting observer gain is given by :

$$L = \begin{bmatrix} 0.2582 & -0.6951 \\ 0.0001 & -0.0001 \\ -0.0001 & 0.0003 \\ -0.4108 & 0.3324 \\ 0.0016 & 0.0000 \\ -6.3386 & 0.2615 \\ -56.4934 & 79.6739 \\ 6.4796 & -18.2527 \\ -0.5916 & 1.2789 \\ -0.0322 & 0.4568 \\ 0.0018 & -0.0001 \end{bmatrix} . \tag{2.17}$$

The combined observer and controller state-space representation is described by the following equations:

$$\begin{aligned} \dot{x}_e &= Ax_e + Bu + B_r r_1 + L(y \Leftrightarrow y_e) \\ y_e &= Cx_e \\ u &= \Leftrightarrow K_1 x_e \Leftrightarrow K_2 q \\ \dot{q} &= y \Leftrightarrow \begin{bmatrix} r_2 \\ r_3 \end{bmatrix} \quad , \text{ where } x_e \text{ is the estimated state,} \end{aligned} \tag{2.18}$$

and finally,

$$\begin{aligned} \frac{d}{dt}\begin{bmatrix} x_e \\ q \end{bmatrix} &= \begin{bmatrix} A \Leftrightarrow LC \Leftrightarrow BK_1 & \Leftrightarrow BK_2 \\ 0 & 0 \end{bmatrix}\begin{bmatrix} x_e \\ q \end{bmatrix} + \begin{bmatrix} L \\ I \end{bmatrix} y + \begin{bmatrix} B_r & 0 \\ 0 & \Leftrightarrow I \end{bmatrix} \hat{r} \\ u &= \begin{bmatrix} \Leftrightarrow K_1 & \Leftrightarrow K_2 \end{bmatrix}\begin{bmatrix} x_e \\ q \end{bmatrix} . \end{aligned} \tag{2.19}$$

2.6.2 Fuel Feedback Control Design.

The control structure of the conventional fuel control configuration is shown in Section 2.6. We used the engine model described in Section 2.2 without the secondary throttles. The model is linearized at throttle position equal to 11.8 degrees, and engine speed equal at 3000 rpm. The state space representation of the linearized model is given by:

$$\begin{aligned} \dot{x}(t) &= Ax(t) + Bu(t) + B_r r(t) \\ y(t) &= cx(t) \end{aligned}$$

where $u = F_c$ (fuel command), $r = \theta$ (primary throttle) , and
$y = A/F_{exh}$ (meas. at the EGO sensor),

$$A = \begin{bmatrix} -0.079 & 139.785 & 0 & 0 & 0 & -1.013 & 0 & 0 & 0 & 0 \\ 0.0173 & -100 & 26.852 & 0 & 0 & 0 & 0 & 0 & 0 & 0 \\ -0.0280 & 0 & -10.908 & 0 & 0 & 0 & 0 & 0 & 0 & 0 \\ 0 & 0 & 0 & -6.67 & 0 & 2 & 0 & 0 & 0 & 0 \\ -0.0001 & 0 & -0.0019 & 0 & -7.692 & 0 & 0 & 0 & 0 & 0 \\ 0 & 0 & 0.024 & 0 & -1.5874 & -0.001 & 0 & 0 & -2.53 & 0 \\ 0. & 0. & 0. & 0. & 0. & 0. & 100. & 900. & 0. & 0. \\ 0 & 0 & 0 & -222.2 & 0 & 0 & -33.3 & -233.3 & 0 & 0 \\ 0. & 0. & 0. & 0. & 0. & 0. & 0. & 2. & -5. & 0. \\ 0 & 0 & 0 & 0 & 3.84 & 0 & 0 & 0 & 0 & -10 \end{bmatrix},$$

$$B = \begin{bmatrix} 0 \\ 0 \\ 0 \\ 0 \\ 0 \\ -8254.3 \\ 0 \\ 0 \\ 0 \\ 2 \end{bmatrix}, \quad B_r = \begin{bmatrix} 0.0000 \\ 0.0000 \\ 0.8710 \\ 0.0000 \\ 0.0060 \\ 0.0000 \\ 0.0000 \\ 0.0000 \\ 0.0000 \\ 0.0000 \end{bmatrix},$$

$$c = \begin{bmatrix} 0 & 0 & 0 & 0 & 0 & 0 & 0 & 0 & 2.5000 & 0 \end{bmatrix}.$$

The control objective in the conventional engine (A/F control is based on regulating the fuel flow) is to maintain A/F at stoichiometry during changes in pedal position. For this reason, we used integral control, and the augmented the input and state vector are given by :

$$\hat{r} = \begin{bmatrix} \theta \\ A/F_{stoic} \end{bmatrix} \text{ , and } \hat{x} = \begin{bmatrix} x \\ q \end{bmatrix}. \tag{2.20}$$

The resulting augmented system is :

$$\underbrace{\begin{bmatrix} \dot{x} \\ \dot{q} \end{bmatrix}}_{\dot{\hat{x}}} = \underbrace{\begin{bmatrix} A & 0 \\ c & 0 \end{bmatrix}}_{\hat{A}} \underbrace{\begin{bmatrix} x \\ q \end{bmatrix}}_{\hat{x}} + \underbrace{\begin{bmatrix} B \\ 0 \end{bmatrix}}_{\hat{B}} u + \underbrace{\begin{bmatrix} B_r & 0 \\ 0 & \Leftrightarrow 1 \end{bmatrix}}_{\hat{B}_r} \hat{r}, \tag{2.21}$$

We set the LQR problem and adjusted the R_{xx} and R_{uu} of the cost function to minimize the A/F excursions. The resulting controller feedback gains are given by :

$$\begin{aligned} K_1 &= \begin{bmatrix} 0 & 0 & -0.027 & -0.035 & 1.877 & -0.0006 & 0.0016 & 0.0045 & -0.195 & 2.801 \end{bmatrix} \\ k_2 &= -0.9487 \, . \end{aligned} \tag{2.22}$$

We assumed that torque measurements are available to better estimate the states. In the observer design we accounted for the fuel puddling dynamics by adjusting the Kalman filter

gain using loop transfer recovery in the input. The resulting observer gain is :

$$L = \begin{bmatrix} 0.3080 & -0.8831 \\ 0.0001 & 0.0004 \\ -0.0001 & 0.0022 \\ -0.5737 & 0.3602 \\ 0.0059 & 0.0000 \\ -20.1610 & 0.0494 \\ 4.7225 & -12.2339 \\ -0.0597 & 1.4371 \\ 0.0019 & 0.5101 \\ 0.0066 & 0.0000 \end{bmatrix}. \tag{2.23}$$

The combined observer and controller state-space representation is described by the following equations:

$$\begin{aligned} \dot{x}_e &= Ax_e + Bu + B_r r_1 + L(y \Leftrightarrow y_e) \\ y &= \begin{bmatrix} T_b \\ A/F_{exh} \end{bmatrix} = Cx_e \\ u &= \Leftrightarrow K_1 x_e \Leftrightarrow k_2 q \\ \dot{q} &= A/F_{exh} \Leftrightarrow r_2 = [0,1] \cdot y \Leftrightarrow r_2 \quad \text{where } x_e \text{ is the estimated state,} \end{aligned} \tag{2.24}$$

and finally,

$$\begin{aligned} \frac{d}{dt}\begin{bmatrix} x_e \\ q \end{bmatrix} &= \begin{bmatrix} A \Leftrightarrow LC \Leftrightarrow BK_1 & \Leftrightarrow Bk_2 \\ 0 & 0 \end{bmatrix}\begin{bmatrix} x_e \\ q \end{bmatrix} + \begin{bmatrix} L \\ 0 \quad 1 \end{bmatrix} y + \begin{bmatrix} B_r & 0 \\ 0 & \Leftrightarrow 1 \end{bmatrix} \hat{r} \\ u &= \begin{bmatrix} \Leftrightarrow K_1 & \Leftrightarrow k_2 \end{bmatrix}\begin{bmatrix} x_e \\ q \end{bmatrix}. \end{aligned} \tag{2.25}$$

2.6.3 Feedback Control Design using Electronic Throttle.

In an engine equiped with a electronic throttle, the driver controls the accelerator pedal position, but the actual throttle position that regulates the air flow into the manifold is electronically controlled. The engine model described in Section 2.2 is modified to include the new control command, and linearized at throttle position equal to 11.8 degrees, engine speed equal at 3000 rpm. The state space representation of the linearized model is given by :

$$\begin{aligned} \dot{x}(t) &= Ax(t) + Bu(t) \\ y(t) &= Cx(t) \end{aligned} \tag{2.26}$$

$$\text{where } u = \begin{bmatrix} \theta_e \text{ (electr. thr. command)} \\ F_c \text{ (fuel command)} \end{bmatrix}, y = \begin{bmatrix} T_b & \text{(torque measurement)} \\ A/F_{exh} & \text{(meas. at the EGO sensor)} \end{bmatrix},$$

and

$$A = \begin{bmatrix} -100 & 26.852 & 0 & 0 & 0 & 0 & 0 & 0 & 0.017 & 0 \\ 0 & -10.908 & 0 & 0 & 0 & 0 & 0 & 0 & -0.028 & 0 \\ 0 & 0 & -6.667 & 0 & 2 & 0 & 0 & 0 & 0 & 0 \\ 0 & -0.002 & 0 & -7.692 & 0 & 0 & 0 & 0 & -0.0001 & 0 \\ 0 & 244.19 & 0 & -1.587e+05 & 0 & 0 & 0 & 1.575 & 0 & 0 \\ 0 & 0 & 0 & 0 & 0 & 100 & 900 & 0 & 0 & 0 \\ 0 & 0 & -222.22 & 0 & 0 & -33.33 & -233.33 & 0 & 0 & 0 \\ 0. & 0. & 0. & 0. & 0. & 0. & 2. & -5. & 0. & 0. \\ 139.786 & 0 & 0 & 0 & -1.013 & 0 & 0 & 0 & -0.076 & 0 \\ 0 & 0 & 0 & 3.846 & 0 & 0 & 0 & 0 & 0 & -10 \end{bmatrix},$$

$$B = \begin{bmatrix} 0.0000 & 0.0000 \\ 0.8710 & 0.0000 \\ 0.0000 & 0.0000 \\ 0.0060 & 0.0000 \\ 0.0000 & -82543 \\ 0. & 0 \\ 0. & 0. \\ 0. & 0. \\ 0. & 0. \\ 0. & 2. \end{bmatrix}, C = \begin{bmatrix} 410.86 & 0 & 0 & 0 & -2.978 & 0 & 0 & 0 & 0.023 & 0 \\ 0 & 0 & 0 & 0 & 0 & 0 & 0 & 2.5 & 0 & 0 \end{bmatrix}.$$

Changes in the accelerator pedal position imposed by the driver represent changes in the demanded torque. In the case of electronically throttled engine, the driver is disconnected from the engine, and does not cause "disturbances" in the A/F loop. However, we have to maintain good engine torque response to satisfy drivability requirements. This is accomplished by augmenting the states with the integral of the error in the torque response. In this control scheme, A/F control is limited only by sensor/actuator limitations and uncertainties in the modeling. The integrated states, the input vector, and the augmented state vector are given by:

$$\dot{q} = y \Leftrightarrow \begin{bmatrix} T_{b_{des}} \\ A/F_{stoic} \end{bmatrix}, \quad r = \begin{bmatrix} T_{b_{des}} \\ A/F_{stoic} \end{bmatrix}, \quad \text{and } \hat{x} = \begin{bmatrix} x \\ q \end{bmatrix}. \tag{2.27}$$

The resulting augmented system is :

$$\underbrace{\begin{bmatrix} \dot{x} \\ \dot{q} \end{bmatrix}}_{\dot{\hat{x}}} = \underbrace{\begin{bmatrix} A & 0 \\ C & 0 \end{bmatrix}}_{\hat{A}} \underbrace{\begin{bmatrix} x \\ q \end{bmatrix}}_{\hat{x}} + \underbrace{\begin{bmatrix} B \\ 0 \end{bmatrix}}_{\hat{B}} u + \underbrace{\begin{bmatrix} 0 \\ \Leftrightarrow I \end{bmatrix}}_{\hat{B}_r} r, \tag{2.28}$$

The control design followed is similar to the earlier design in Section 2.6.1. The controller feedback gains are given by :

$$K_1 = \begin{bmatrix} 0.4046 & 0.9368 & 0.1478 & -0.0005 & 0.00 & -0.0016 & -0.0047 & 0.1574 & -0.0233 & -0.0009 \\ 2.7691 & -0.8089 & -0.5292 & 1.9192 & -0.0290 & 0.0199 & 0.0551 & -2.277 & -0.0005 & 3.0441 \end{bmatrix}$$

$$K_2 = \begin{bmatrix} 0.1000 & 0.3135 \\ 0.0031 & -9.9951 \end{bmatrix}, \tag{2.29}$$

and the observer gain L is given by :

$$L = \begin{bmatrix} 0.0000 & 0.0004 \\ -0.0001 & 0.0020 \\ -0.4094 & 0.3463 \\ 0.0016 & 0.0000 \\ -6.3390 & 0.3095 \\ 7.3912 & -11.4118 \\ -0.5880 & 1.3235 \\ -0.0300 & 0.4716 \\ 0.2397 & -0.8408 \\ 0.0018 & -0.0001 \end{bmatrix}. \tag{2.30}$$

The combined observer and controller state-space representation is given by :

$$\begin{aligned} \dot{x}_e &= Ax_e + Bu + L(y \Leftrightarrow y_e) \\ y_e &= Cx_e \\ u &= \Leftrightarrow K_1 x_e \Leftrightarrow K_2 q \\ \dot{q} &= y \Leftrightarrow \begin{bmatrix} r_1 \\ r_2 \end{bmatrix} \quad \text{where } x_e \text{ is the estimated state,} \end{aligned} \tag{2.31}$$

and finally,

$$\begin{aligned} \frac{d}{dt}\begin{bmatrix} x_e \\ q \end{bmatrix} &= \begin{bmatrix} A \Leftrightarrow LC & \Leftrightarrow BK_1 & \Leftrightarrow BK_2 \\ 0 & & 0 \end{bmatrix}\begin{bmatrix} x_e \\ q \end{bmatrix} + \begin{bmatrix} L \\ I \end{bmatrix} y + \begin{bmatrix} 0 \\ \Leftrightarrow I \end{bmatrix} r \\ u &= \begin{bmatrix} \Leftrightarrow K_1 & \Leftrightarrow K_2 \end{bmatrix}\begin{bmatrix} x_e \\ q \end{bmatrix}. \end{aligned} \tag{2.32}$$

2.7 Simulation Example.

The purpose of this example is to illustrate some of the properties of the closed loop system using the secondary throttles, and compare them with the conventional fuel control scheme, and the electronic throttle control scheme. Figure 2.7 is a simulation of the nominal response of the θ_c-scheme and the F_c-scheme for a 10% step change in primary throttle position, which corresponds to 16% step change in torque demand. The θ_c-scheme has $\pm 0.14\%$ A/F excursion and essentially zero A/F and torque error after 50 intake events. A dynamic model of the catalytic converter is needed to evaluate the effects of these A/F excursions to tailpipe emissions. The dynamic catalytic converter response depends on the amplitude and the frequency of the A/F excursions, and a control oriented model of this behavior is not available. The integrated error of A/F during a rapid throttle movement can be used, however, as a measurement of engine emissions during that period. The integrated error of A/F for the F_c-scheme is 0.0402 and for the θ_c-scheme is 0.0051, which indicates a possible reduction of engine emissions. Also, the engine reaches the specified torque faster than in the F_c-scheme, improving drivability significantly. Note that the conventional fuel pulsewidth duration control does not affect the torque performance of the engine.

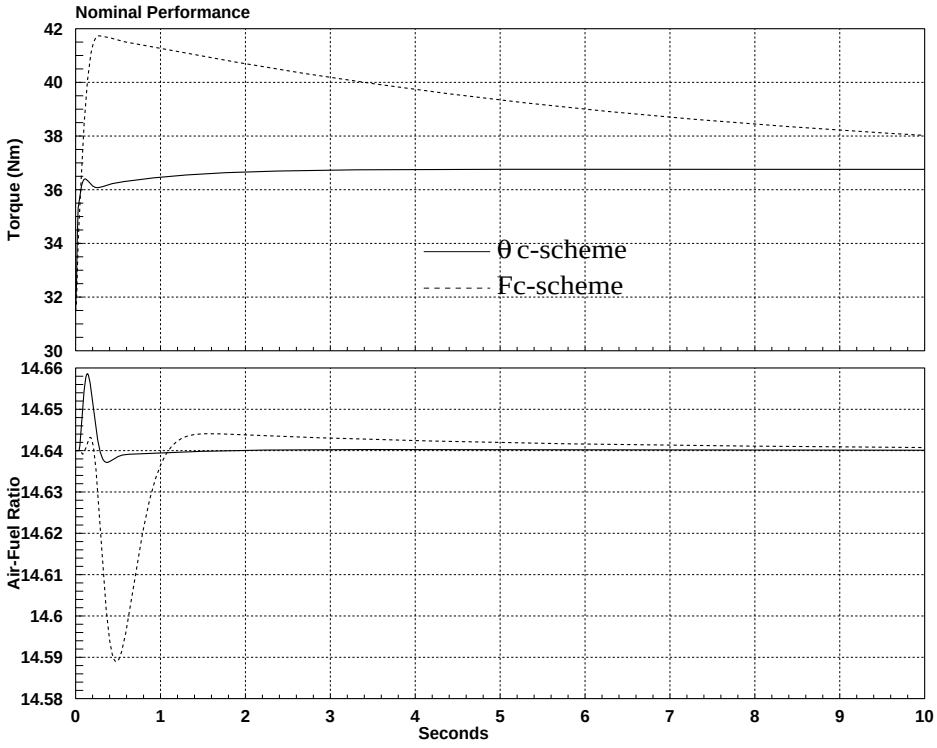

Figure 2.7: Simulation of the θ_c-scheme and F_c-scheme.

The simulation in Fig. 2.8 demonstrates the torque tracking performance of the proposed scheme in comparison with the DBW-scheme. The emissions performance is equivalent in the two systems. Both responses are well within the high-efficiency window of the catalyst, though the absence of the lean spike in the A/F in tip-in conditions in the DBW-scheme is immediately noticeable. In DBW throttle systems the engine is decoupled from the disturbances caused by the rapid throttle movements which are imposed by the driver. The closed loop system has the feature of isolating the high bandwidth torque demands by breaking the linkage between the driver and the primary throttles, facilitating smooth A/F control during transient engine operation. To achieve the same good A/F results we will need to form a smoother torque response in the engine.

The performance of the θ_c-scheme was also tested under uncertainty in the fuel puddling dynamics due to its importance in accurate transient A/F control. Figure 2.9 shows the torque and A/F response of the above control schemes using a time constant of 0.2 sec in the puddling dynamics (see Section 2.2). The simulation results show a limited performance degradation of the closed loops, however the θ_c-scheme maintains the improvement of the torque response better than the other two methods. We have the same comparative results between the F_c-scheme and the θ_c-scheme: integrated A/F error in F_c-scheme is 0.0547, and in θ_c-scheme is 0.0084. The A/F response of the DBW-scheme slightly degrades and the A/F integrated error is 0.0085. Therefore, the θ_c-scheme maintains emissions results

comparable to the DBW-scheme.

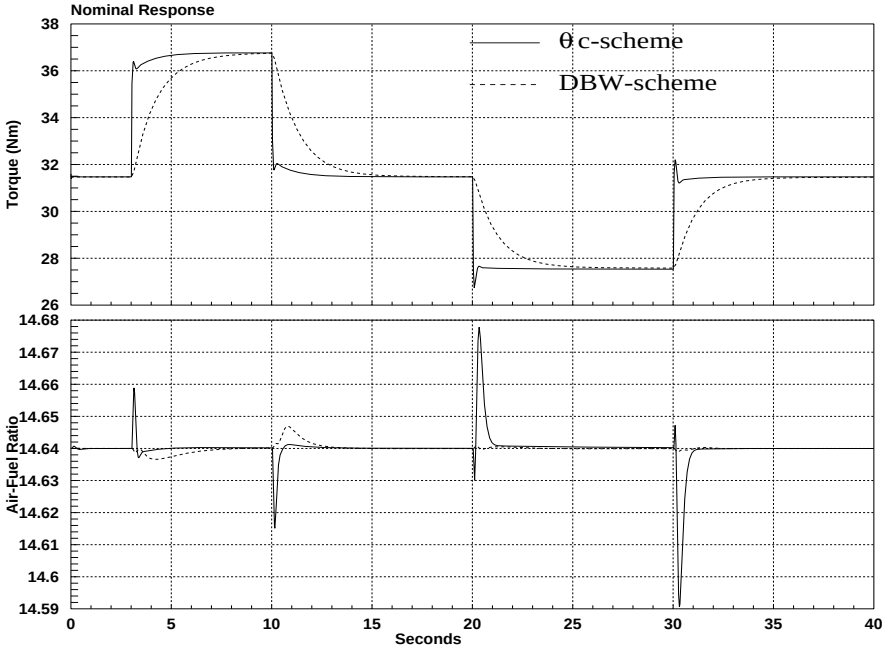

Figure 2.8: Closed loop response of the θ_c-scheme and DBW-scheme for a square wave in the demanded torque.

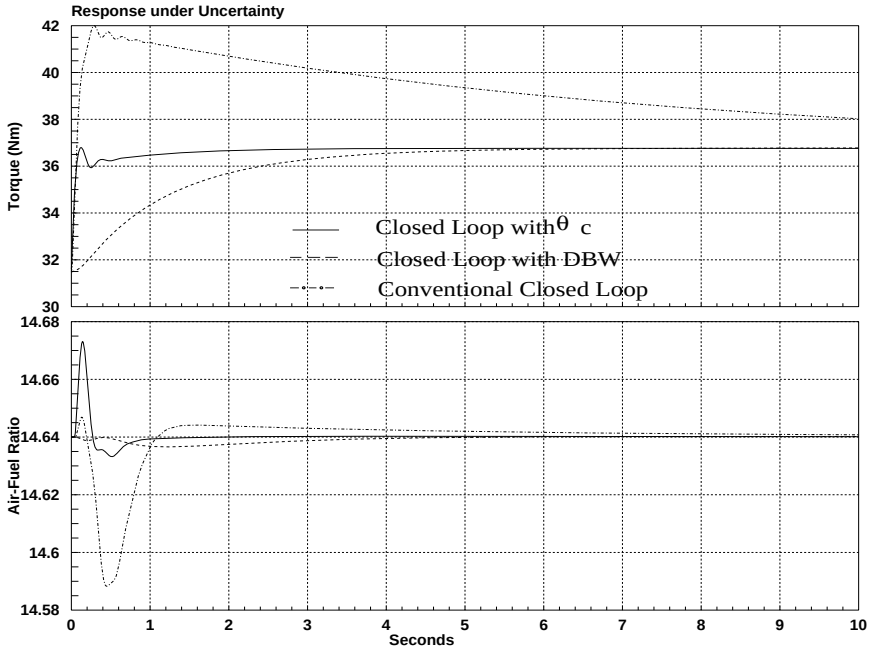

Figure 2.9: Closed loop performance under uncertainty in the fuel puddling dynamics.

2.8 Conclusions.

In this chapter, we investigated a control scheme for transient A/F and torque control during rapid changes in the throttle position. The air and fuel management scheme based on the secondary throttles seems promising in enhancing the engine performance. This work is very important in understanding the breathing process dynamics and its nonlinear behavior. The developed control scheme addresses the principles of controlling the breathing process which is a fundamental process to emissions, fuel economy, and torque response. The secondary throttles can be replaced by electronically controlled intake valves. Variable intake valve timing and lift is a special case of a camless engine, and the modeling and control design of the engine with the secondary throttles contributes to the development of dynamically controlled camless engines. Another special case of the camless engine is an engine with variable camshaft timing that allows control of the intake and exhaust valve timing with fixed overlap. This topic will be pursued in the following chapters.

CHAPTER 3

Modeling of Variable Cam Timing Engine.

3.1 Introduction to the VCT Engine Control Problem.

Variable cam timing schemes have been studied extensively and have been found to reduce emissions [45, 79] increase fuel economy [21, 41, 26] and improve full load performance [40]. The primary emphasis of this work is on reducing emissions while satisfying drivability requirements at part load and medium engine speed. Variable cam timing can inhibit the production of oxides of nitrogen (NO_x) and reduce the amount of unburned hydrocarbons (HC) emitted to the exhaust system [45]. By retarding the cam timing, combustion products which would otherwise be expelled during the exhaust stroke are retained in the cylinder during the subsequent intake stroke. The contribution of this diluent to the mixture in the cylinder reduces the combustion temperature and suppresses NO_x formation. In addition, this process often reduces HC emissions since the internally recirculated exhaust gas subjected to the additional combustion cycle is generally from the crevice volumes at the piston/cylinder wall interface and is rich in unburned HC. The effect is to reduce the base HC and NO_x emission levels of the engine with respect to a conventional powerplant, resulting in lower tailpipe emissions at equivalent catalytic converter efficiencies. Of course, VCT obviates the requirement for external exhaust gas recirculation (EGR) systems commonly used for NO_x reduction. Furthermore, by retarding the cam phasing, the amount of fresh air into the cylinder is reduced. This results in the need for a higher manifold pressure in order to maintain the same load. Operation in high manifold pressure is advantageous since it is associated with reduced intake stroke pumping work [31, 83], and therefore, increased fuel economy. One type of VCT engine utilizes a hydraulically actuated mechanism to rotate the camshaft relative to the crankshaft and advance the valve timing with respect to the engine induction and exhaust strokes. This is illustrated in the valve lift profiles shown in Fig. 3.1.

The goal in the following chapters is twofold: (i) reduce feedgas NO_x and HC emissions, and (ii) provide satisfactory torque response to meet vehicle and customer performance requirements during changes in throttle position. Rapid throttle movements reflect the driver's demand for changes in torque and vehicle acceleration, and strongly influence the

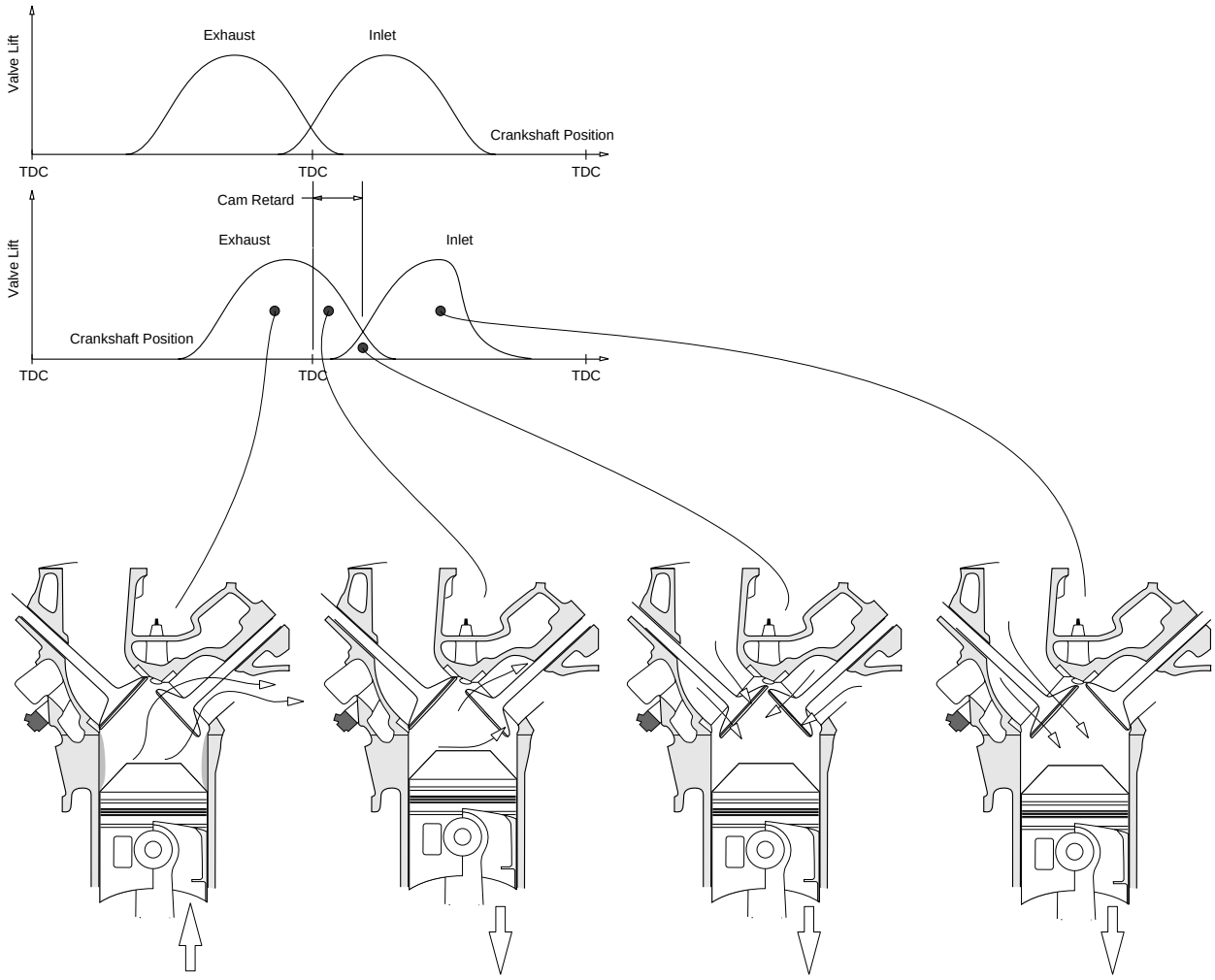

Figure 3.1: Valve lift profiles of a conventional and a variable cam timing engine. By retarding the cam phasing the exhaust valve stays open during the intake event for a longer time period. This causes the induction and reburn of the last part of the exhaust gases which is rich in unburned HC. The resulting diluent, also, lowers the combustion temperature and suppresses feedgas NO_x emissions. The amount of reduction will vary with engine speed and load.

cylinder air charging process, mixture formation and transient performance of the engine. For both tailpipe HC and NO_x emissions, the primary control objectives are to (i) reduce the NO_x and HC feedgas by changing the cam timing of the engine, and (ii) maintain the A/F at stoichiometry at all times since this corresponds to the point of maximum efficiency of the catalytic converter. The additional complexity is that rapid throttle movements imposed by the driver are now accompanied by changes in cam phasing in order to minimize the amount of NO_x and HC in the feedgas. These changes affect the cylinder air charge, and can cause large A/F excursions which makes the task of A/F control even more challenging.

3.2 Dynamic Engine Model.

The development of a control-oriented model involves the understanding of the region of interest and the input-output relationship that need to be identified (see Fig. 3.2). Details about the region of interest can be found in Appendix A.

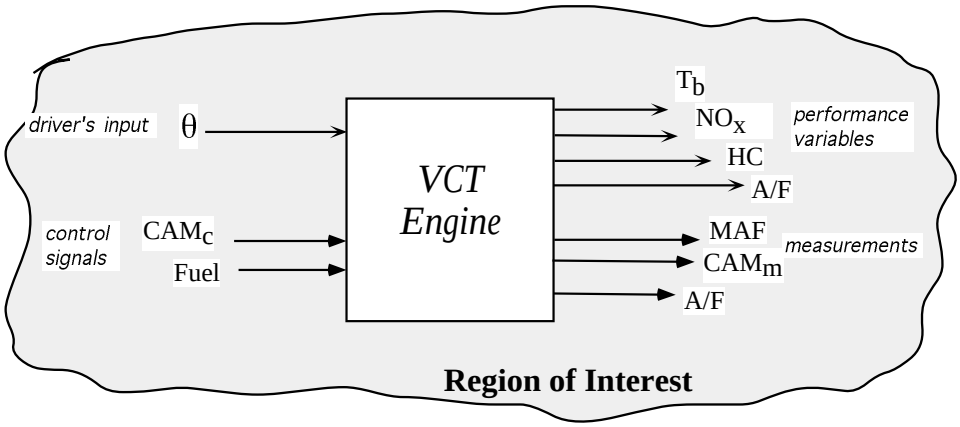

Figure 3.2: Schematic representation of the unknown input-output relationship of the VCT engine over the region of interest.

The VCT engine model is derived based on physical principles and described by measurable parameters. It is a continuous, nonlinear, low-frequency[1], phenomenological representation of an eight cylinder experimental VCT engine, based on [16], with appropriate modifications for variable cam timing.

The dynamic elements of the engine model are described by physically based equations, whereas the pseudo-static elements are described by empirically based expressions as in [16]. The structure of the VCT engine model was identified by engine-dynamometer experiments; the VCT mechanism was found to alter the mass air flow into the cylinders, the self EGR, the engine torque response, and exhaust emissions. The mass air flow through the throttle body, engine pumping rate, brake torque generation and feedgas NO_x and HC emissions

[1] This model represents dynamics averaged over an engine event.

generation are complex functions, depend on many engine parameters, and are difficult to model analytically, so they are included as nonlinear static empirical relations. Their parameters are determined from regressed dynamometer-engine steady-state data using the least squares approach. Physically based differential and difference equations are used to describe the dynamic elements of the engine, such as inlet manifold dynamics and the delayed processes in the signal paths. The identification of these parameters is based on the dynamic response of the experimental engine mounted in thedynamometer to small step inputs. Furthermore, the model includes actuator and sensor dynamics, and some important computational delays. The following subsections describe each of the engine components, and, at the end of this chapter, the identified model is validated against actual engine-dynamometer data.

3.2.1 Breathing Process.

The model of the breathing process is a very important part of the engine modeling task because it affects most engine performance indices: fuel economy, emissions, drivability. The dynamic equation for the manifold is based on the principles of conservation of mass, thermodynamic energy and momentum which are satisfied by assuming uniform pressure and temperature in the plenum between the throttle body and the intake valves. To use the state equation, the air into the intake manifold is assumed to be homogeneous. The model of the breathing process is based on an averaged representation over an engine event and does not allow the study of high frequency phenomena as acoustic and inertia effects that occur during the intake stroke [48].

Based on the previous assumptions the manifold acts as a plenum, and its dynamics can be described by the following first order differential equation (as in [16]) that relates the rate of change of the manifold pressure (P_m) to the mass air flow rates into and out of the manifold ($\dot{m}_\theta$ and $\dot{m}_{cyl}$, respectively)

$$\frac{d}{dt}P_m = K_m(\dot{m}_\theta \Leftrightarrow \dot{m}_{cyl}), \text{ where } K_m = \frac{R \cdot T}{V_m} \quad . \tag{3.1}$$

The constant $K_m = 0.12\frac{bar}{g}$ has been identified from dynamic experimental data. Its physically based value can be derived from $K_m = \frac{R \cdot T}{V_m}$, where $R = 287\ \frac{J}{Kg \cdot K}$ the specific gas constant, $T = 288\ K$ the nominal temperature, and $V = 7\ lt = 0.007\ m^3$ the manifold volume, resulting in $K_m = 11808 \cdot 10^5\ \frac{J}{Kg \cdot m^3} = 0.118\frac{bar}{g}$.

For the derivation of the mass air flow through the throttle body, we assumed one-dimensional, steady, compressible flow of an ideal gas as developed in [56]. The mass air flow rate into the manifold ($\dot{m}_\theta$) through the primary throttle body is a function of throttle angle (θ), the upstream pressure (P_o), which we assume to be atmospheric, i.e., $P_o = 1$ bar, and the downstream pressure, which is the manifold pressure (P_m). The function describing

$\dot{m}_\theta$ (shown in Fig. 3.3 for different values of θ) is described by

$$\dot{m}_\theta = g_1(P_m) \cdot g_2(\theta)$$
$$g_1(P_m) = \begin{cases} 1 & \text{if } P_m \leq P_O/2 \\ \frac{2}{P_O}\sqrt{P_m P_O \Leftrightarrow P_m^2} & \text{if } P_m > P_O/2 \end{cases} \tag{3.2}$$
$$g_2(\theta) = F(1, \theta, \theta^2, \theta^3)$$

where $g_2(\theta)$ is a third order polynomial of throttle angle. The exact equation $g_2(\theta)$ can be found in Appendix B.1.

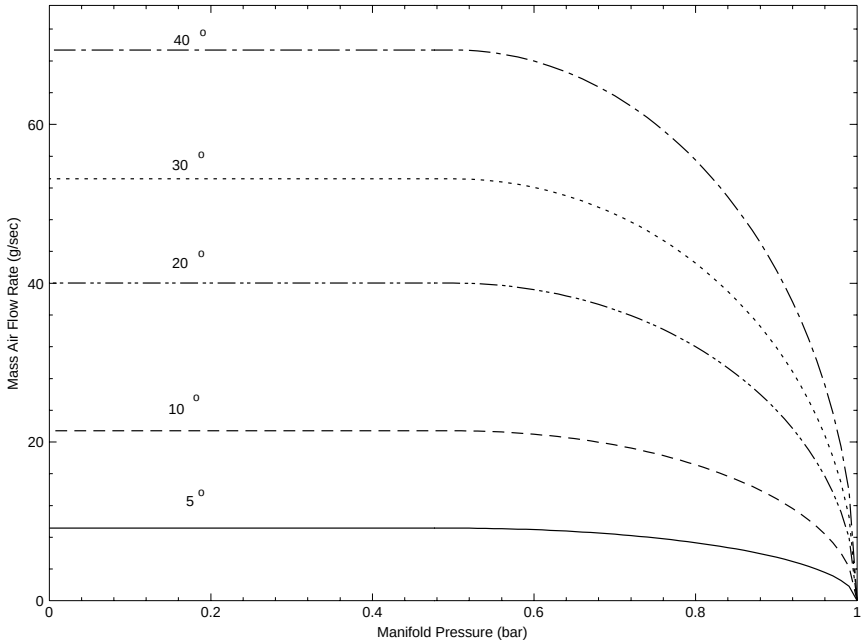

Figure 3.3: Mass air flow rate through the throttle body as a function of manifold pressure for different throttle angles. Note the two distinct operating regimes of sonic and subsonic flow.

The pulsating mass air flow out of the manifold and into the cylinders (during the intake event) is a complicated function of engine characteristics including pressure losses in the intake valve, as well as losses from the wall friction, and inertia [60]. It can be represented, however, by an empirical relationship assuming quasi-steady operating conditions, and averaging the mass air flow into the cylinders over an engine event (180 degrees of crankshaft revolution). The empirical relationship can be developed by treating the engine as a pump and assuming constant intake temperature and exhaust gas pressure. The engine pumping mass air flow rate ($\dot{m}_{cyl}$) is a function of the cam phasing (CAM), the manifold pressure (P_m), and the engine speed (N). The resulting polynomial is of degree three, and a third order polynomial in each individual variable:

$$\dot{m}_{cyl} = F(1, CAM, CAM^2, CAM^3, P_m, P_m^2, P_m^3, N, N^2, N^3) \quad . \tag{3.3}$$

The exact identified polynomial can be found in Appendix B.2. Figure 3.4 shows the

variation of mass air flow rate with manifold pressure (P_m) for different values of cam phasing (CAM) at constant engine speed (1000 RPM).

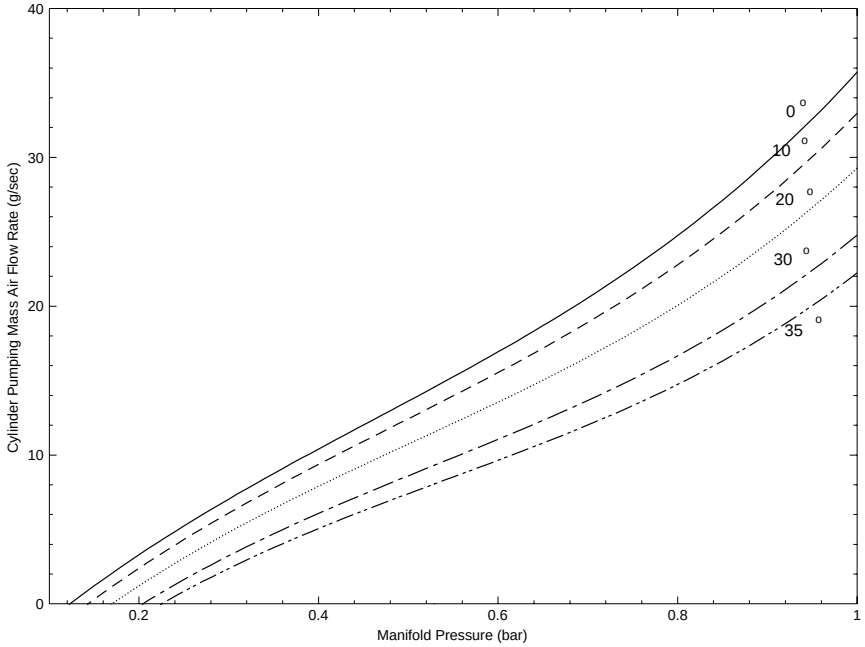

Figure 3.4: Engine pumping mass air flow rate as a function of manifold pressure for five different cam timing values.

The equilibrium of the breathing process occurs when $\dot{m}_\theta = \dot{m}_{cyl}$, and the steady-state manifold pressure and mass air flow into the cylinders is obtained at the intersection of $\dot{m}_\theta$ with $\dot{m}_{cyl}$. Figure 3.5 shows different operating conditions and the corresponding equilibrium points for several throttle positions, engine speeds and cam timings. Note that cam timing affects the steady state mass air flow the same way as the secondary throttles (see Fig. 2.3).

3.2.2 Torque Generation.

The generation of engine torque is a complex process that depends on geometric cylinder and valve features, thermodynamic properties of the unburned and burned gases, the mass and energy equation and the combustion process. The brake torque model derived in this dissertation is an empirical relationship of independent and measurable parameters by assuming fuel, air, and the residual gas uniformly mixed, and quasi-steady operation averaging the individual cylinder torque generation over one engine event. Therefore, engine torque (T_b) can be mapped as a function of the air charge (m_a), the air fuel ratio (A/F), and the engine speed (N). Spark timing is scheduled at minimum spark advance to achieve best torque (MBT). The modeled torque equation is a polynomial of degree three, and a

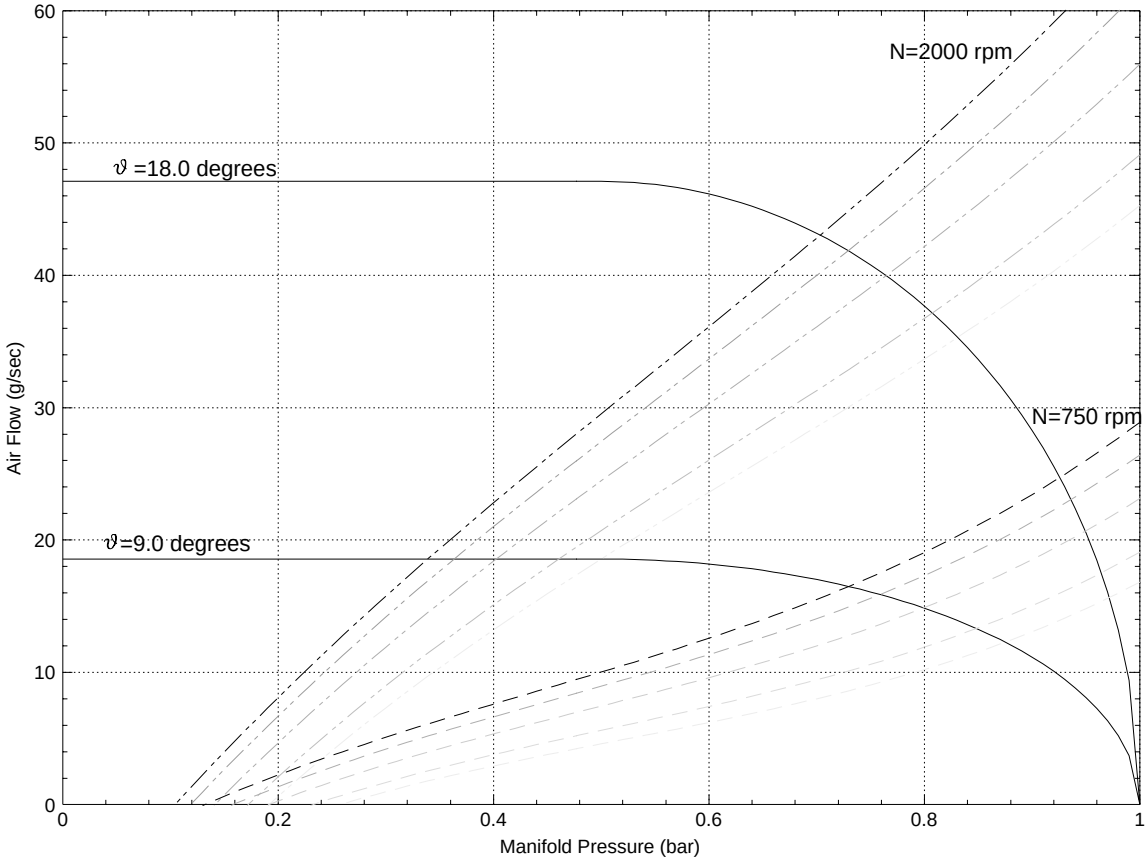

Figure 3.5: Mass air flow rate into ($\dot{m}_\theta$) and out ($\dot{m}_{cyl}$) of the manifold as a function of manifold pressure for two different engine speeds and five cam timing values ($0^o, 10^o, 20^o, 30^o$,and 35^o).

third order polynomial in each individual variable :

$$T_b = F(1, m_a, {m_a}^2, {m_a}^3, A/F, A/F^2, A/F^3, N, N^2, N^3) \quad . \tag{3.4}$$

The exact equation of brake torque is contained in Appendix B.3. The variation of torque with A/F for different values of cylinder air charge (grams per intake event) at constant engine speed (1500 RPM) is shown in Fig. 3.6.

3.2.3 Feedgas NO_x and HC emissions.

We call NO_x emissions the group of nitric oxides NO and nitric dioxides NO_2 produced inside the engine cylinder. In SI engines, experiments and chemical equilibrium considerations indicate that at typical flame temperatures NO_2/NO ratios are negligible small. The principle source of NO is the oxidation of atmospheric (molecular) nitrogen since gasoline contains negligible amounts of nitrogen. Nitric oxide forms in high-temperature burned gases. The higher the burned gas temperature the higher the rate of NO formation. Residual gas plus recycled exhaust reduce the combustion temperature, and consequently reduce the NO formation. The most important engine variables affecting NO_x are the burned gas

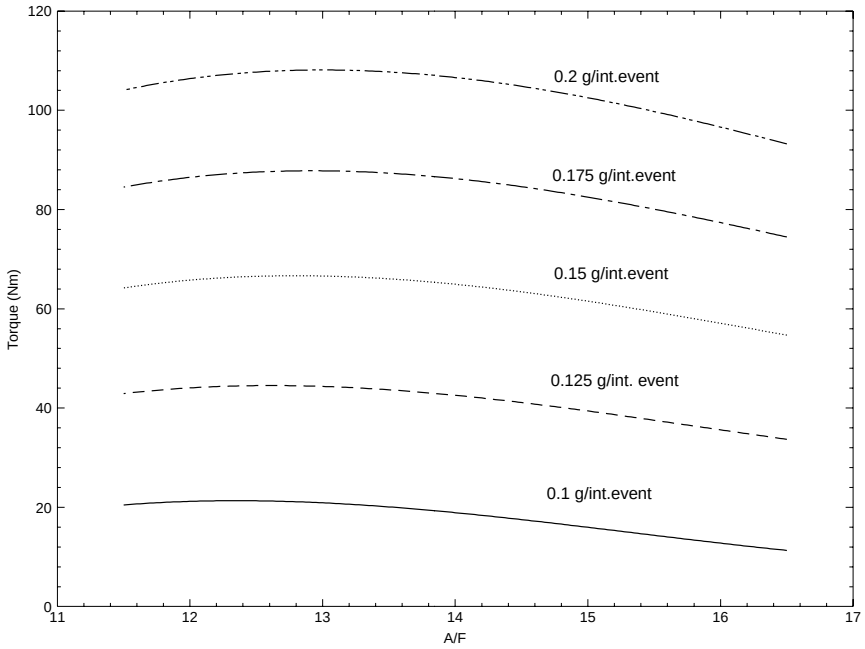

Figure 3.6: Engine torque as function of A/F for different values of air charge at constant engine speed (1500 RPM).

fraction of the unburned mixture, the A/F and the spark timing. For simplicity, the spark timing is scheduled at MBT. Regression of data from the dynamometer and the emission analyzer result in an empirical relationship for the feedgas NO_x emissions. The quasi-static NO_x can be described by a polynomial of engine speed (N), cam phasing (CAM), air fuel ratio (A/F), and manifold pressure (P_m). The four variable regression applied in the NO_x emission data results in an eighth degree polynomial. The modeled NO_x equation is a second, first, third and second order polynomial of engine speed (N), cam phasing (CAM), air fuel ratio (A/F), and manifold pressure (P_m), respectively :

$$NO_x = F_1(1, N, N^2) \cdot F_2(1, CAM) \cdot F_3(1, A/F, A/F^2, A/F^3) \cdot F_4(1, P_m, P_m^2) \quad . \tag{3.5}$$

The exact coefficients from the regression analysis can be found in Appendix B.4. Figure 3.7 shows the NO_x dependency on A/F and CAM phasing. Studies about the prediction of dynamic NO_x emissions based on the static engine mapping [80] show that the dynamic NO_x is also a function of the dynamic cylinder wall temperature. This dependency is not included in this study and might result in higher predicted NO_x emissions than the actual during an acceleration-deceleration maneuver.

Feedgas HC emissions are the result of incomplete combustion of the hydrocarbons in the fuel. HC formation is based on four complex mechanisms even under the assumption of fuel, air, and residual gas uniform mixture. The mechanism of flame quenching at the combustion chamber walls results in a layer of unburned HC attaching to the cylinder wall that is consequently scraped off by the piston off the cylinder walls [37], and exits the

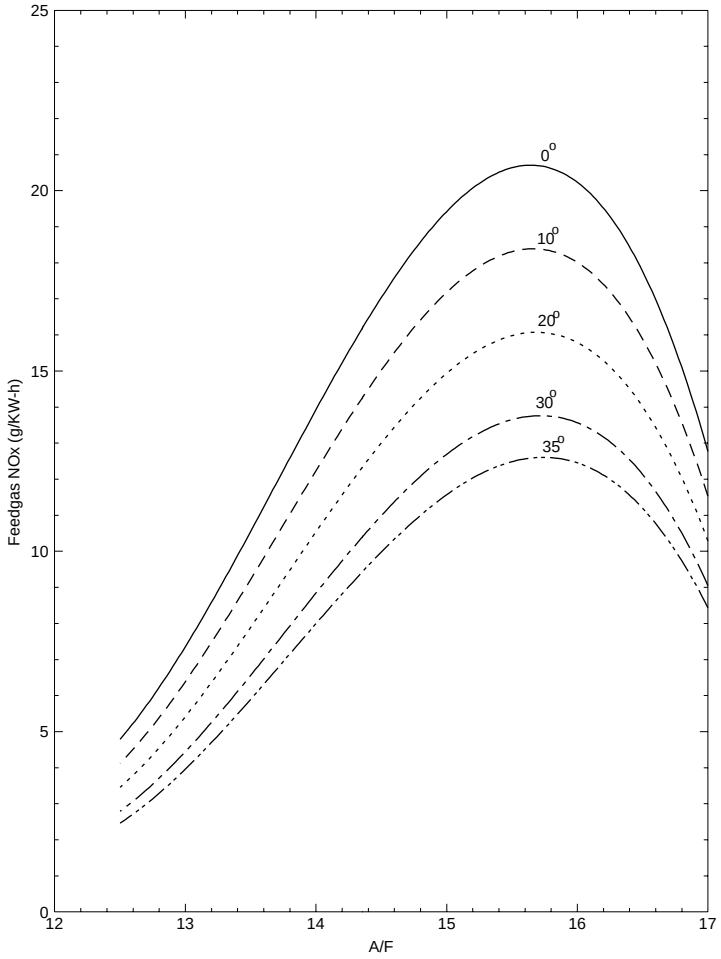

Figure 3.7: Feedgas NO_x emission plotted versus A/F for different CAM timing values at constant manifold pressure ($P_m = 0.4$ bar), and engine speed ($N = 2000$ RPM).

cylinder during the last phase of the exhaust stroke. By retarding the cam phasing we keep this last part of the exhaust gases in the cylinder and reburn it.

The feedgas HC emissions can be modeled by an empirical function of independent engine variables. The emitted amount of HC increases sharply as manifold pressure P_m decreases. For this reason the modeled HC emission equation is a polynomial of the engine speed (N), cam phasing (CAM), air fuel ratio (A/F), and inverse manifold pressure ($\frac{1}{P_m}$). Observing the data trend led us to include a term of modulated cam phasing ($\frac{CAM}{P_m{}^{\frac{1}{16}}}$), which significantly improves the statistical measures of the regression analysis. The derived equation describing HC emissions is given by :

$$HC = F_1(1, N, N^2) \cdot F_2(1, A/F, A/F^2) \cdot F_3(1, \frac{1}{P_m}) + F_4(1, CAM, \frac{CAM}{P_m{}^{\frac{1}{16}}}) \quad . \tag{3.6}$$

Figure 3.8 shows the variation of HC emissions with A/F and cam phasing at constant manifold pressure ($P_m = 0.4$ bar), and engine speed ($N = 2000$ RPM).

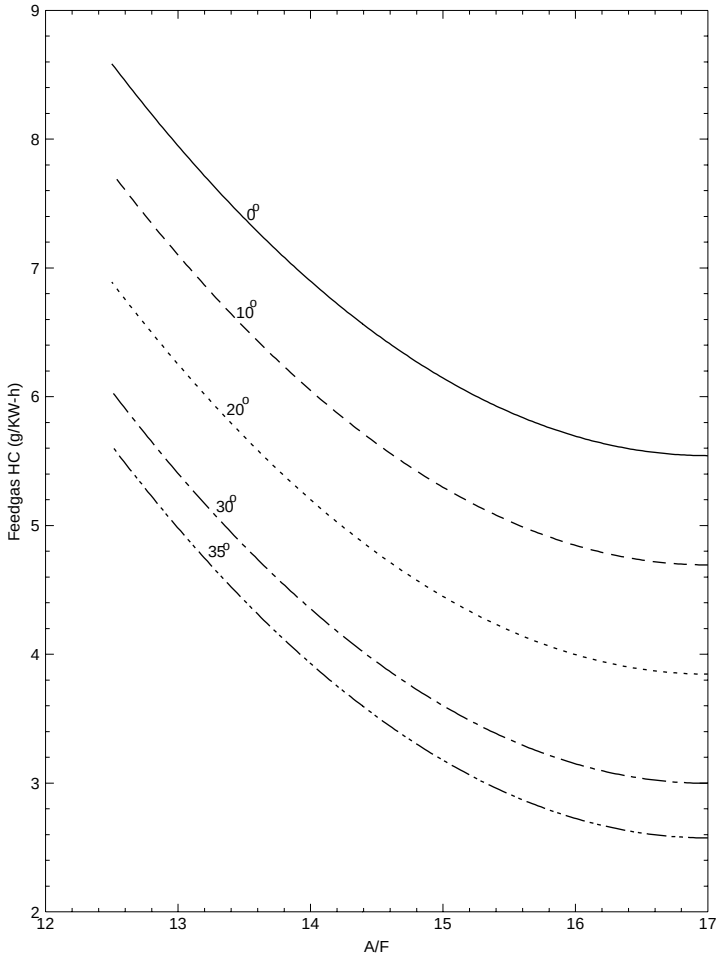

Figure 3.8: Feedgas HC emission versus A/F for different CAM timings at constant manifold pressure ($P_m = 0.4$ bar), and engine speed ($N = 2000$ RPM) .

The exact function that represents the HC emissions can be found in Appendix B.5. In [30] it is shown that dynamic feedgas HC emissions can be accurately predicted by the regression anlysis of the static measurements.

3.2.4 Process Delays.

The fundamental sampling rate for an n cylinder engine at engine speed N (revolutions per minute) is $\frac{1}{\Delta T} = \frac{N \cdot n}{120}$, where ΔT (seconds) is the fundamental sampling time interval. The discrete nature of the engine causes delays in the signal paths. For the engine studied, a delay of $4\Delta T$ seconds is assumed between the induction of the air and fuel mixture into the cylinders, and the corresponding torque response. The delay of $4\Delta T$ seconds corresponds to the induction-to-power stroke physical delay. We should note here that even though we cannot measure torque, its modeled value is used as a performance variable together with NO_x and HC emissions in the control design. The NO_x and HC emissions are steady

state measurements (average values) and cannot be measured in a dynamic manner. Their identified static nonlinear maps, however, will be included in the VCT model in the same dynamic manner as the torque generation function.

A delay of $9\Delta T$ seconds is also identified between the mass charge formation and the time when its corresponding exhaust gas reaches the EGO sensor. This delay corresponds to a $4\Delta T$ seconds delay of the induction-to-power stroke process, a $4\Delta T$ seconds delay of the power-to-exhaust stroke process, and a ΔT seconds delay of the transport process in the exhaust manifold. To achieve good combustion properties, the fuel is injected on closed intake valves, i.e., during the exhaust stroke prior to the intake event. Including the computational delay involved in the fuel pulse width calculation, a total delay of $2\Delta T$ seconds is estimated between the commanded fuel pulse width and the formation of its corresponding charge.

3.2.5 Actuators and Sensors.

The dynamics of the VCT actuator have been identified using parametric identification methods from the Matlab system identification toolbox and are described by the following transfer function :

$$\frac{CAM_{actual}}{CAM_{commanded}} = \frac{\Leftrightarrow 0.706s + 705.8}{s^2 + 16.13s + 705.8} \quad . \tag{3.7}$$

Also, a reduced order model has been developed for the same actuator for control purposes, and is given by

$$\frac{CAM_{actual}}{CAM_{commanded}} = \frac{\Leftrightarrow 0.013s + 26.959}{s + 26.959} \quad . \tag{3.8}$$

The dynamics of the EGO sensor are modeled as a first order lag followed by a preload (relay or switching-type) nonlinearity. The preload nonlinearity in the EGO sensor is viewed as a coarse form of quantization which can be adjusted in a later design phase. The time constant of the EGO sensor is typically 70 msec.

A hot wire anemometer is used to measure the mass air flow rate through the throttle body. A first order lag with time constant equal to 27 msec is used to describe the air meter dynamics. Finally, cam phasing measurements are received with a delay of ΔT seconds.

3.3 Region of Validity.

The block diagram of the identified control-oriented VCT engine simulation model is shown in Fig. 3.9. The data collected for the identification of the VCT engine model lie between 750 rpm and 2000 rpm, which covers most of the operating region in the current FTP cycle for this engine. The data collected represent engine operation for throttle positions less than 25 degrees; operation beyond this region requires extrapolation and should be used cautiously.

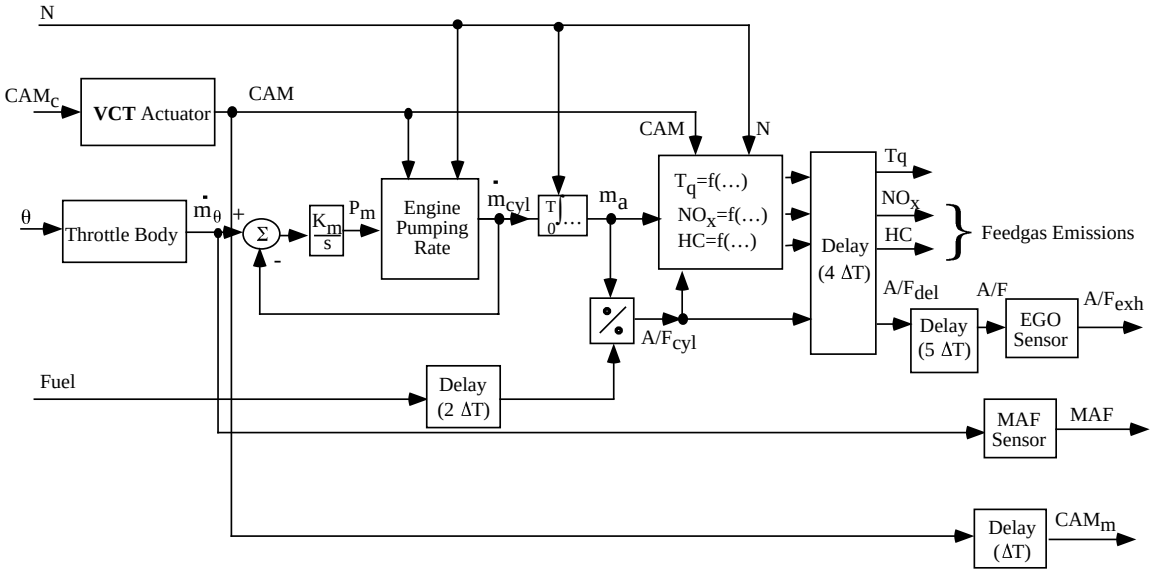

Figure 3.9: Block diagram of the identified control-oriented VCT engine model.

The derived model does not include fuel puddling dynamics, which is one of the important causes of A/F excursions during transient operation. This issue can be addressed by evaluating the sensitivity of the designed control scheme to the uncertain dynamics.

The VCT engine model also does not include the rotational dynamics of the dynamometer. Engine speed is a slowly varying state with respect to breathing and A/F dynamics, and therefore constant engine speed is assumed for the control design phase. The implemented controller, however, must be scheduled with respect to engine speed.

3.4 Model Validation.

The test work here involves the comparison of the identified model response with actual engine data to small step inputs. The set of data used for the validation is different from the set of data used for the model development. Figure 3.10 shows the response of manifold pressure (P_m), measured mass air flow (MAF), and the generated torque (T_b) to a step change in throttle position. Figure 3.11 shows the response of the actual cam position (CAM), manifold pressure (P_m) and generated torque (T_b) to a step change in cam position. Note that since this dynamic experiment lies in the sonic regime, the steady-state torque response is independent of the cam phasing. However the large torque drop during the cam phasing transition might be crucial to drivability requirements. It is important to note here that the large torque drop predicted by the model captured accurately the actual engine response to a misfire that occurred during the rapid change in the cam phasing. The test-cell technician who helped with the experiments felt that the identified model outperformed the measurements in predicting the torque response during rapid changes in cam timing.

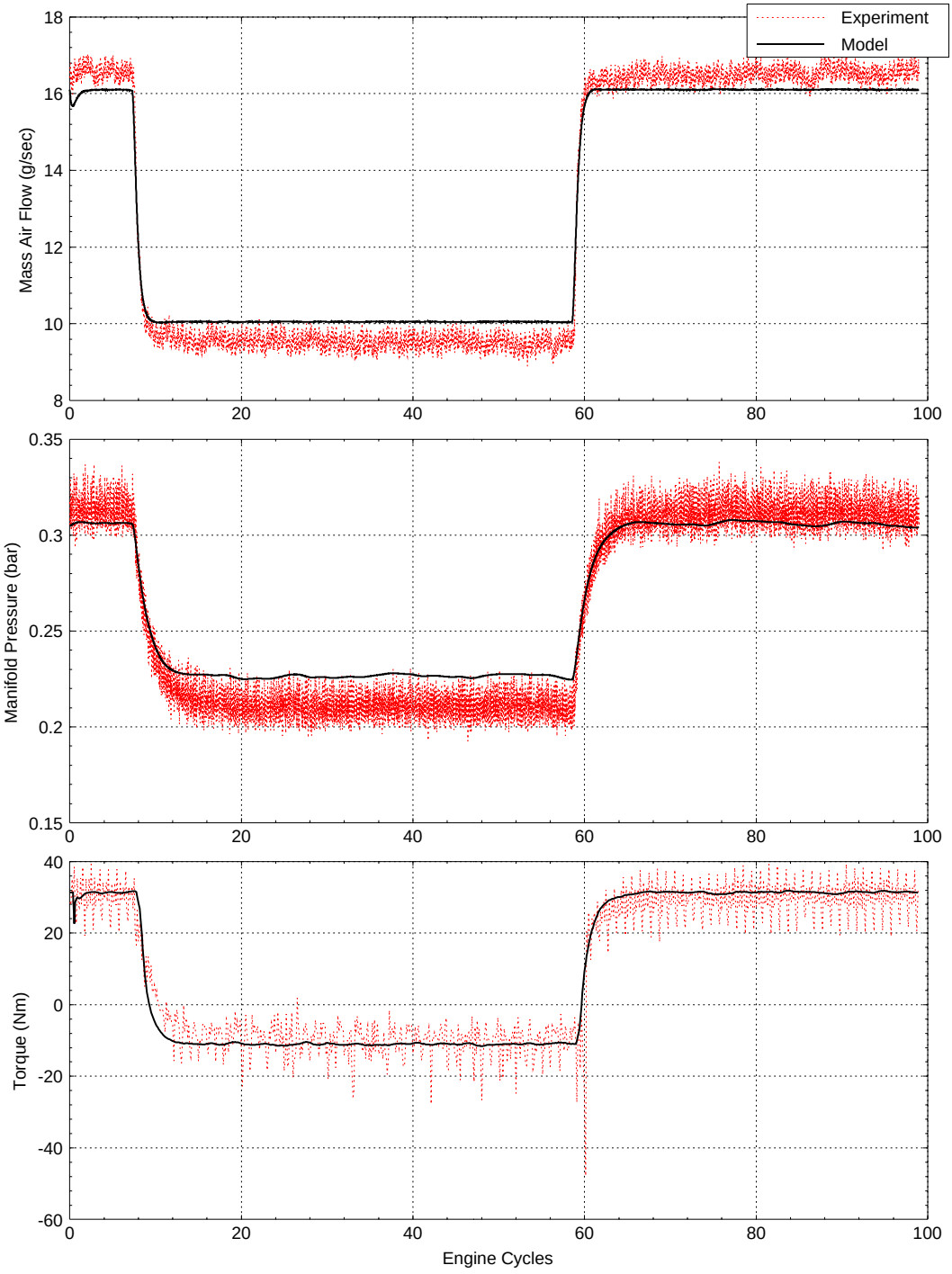

Figure 3.10: Model and engine actual dynamic response to throttle step command.

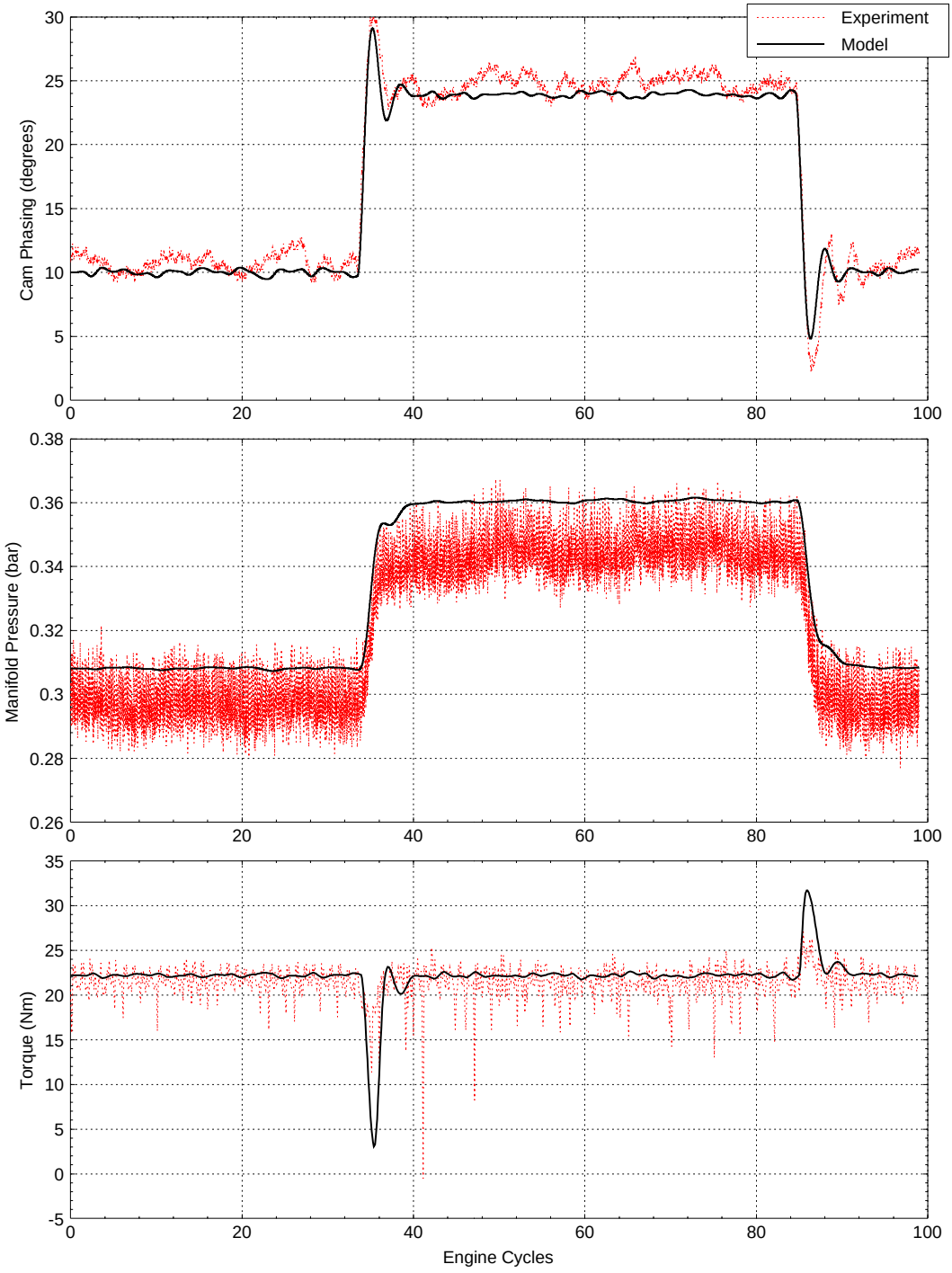

Figure 3.11: Model and engine actual dynamic response to cam phasing step command

CHAPTER 4

Control of Variable Cam Timing Engine.

4.1 Feedback Controller Structure.

The control oriented model developed has two actuators: the fuel injector pulse widths (F_c) and the cam position (CAM_c). The measured outputs are: air fuel ratio (A/F_{exh}) at the EGO sensor, the mass air flow (MAF), throttle position (θ_m), and cam phasing (CAM_m). The goal of the control design is to keep emissions as low as possible, by maintaining air fuel ratio (A/F) close to stoichiometry, and minimizing feedgas NO_x and HC emissions, while providing good driveability during rapid throttle movements.

Performance variables are tailpipe emissions, and the engine torque response during throttle changes. Tailpipe emissions depend on (i) the NO_x and HC feedgas emissions that the catalytic converter has to process, and (ii) the A/F signal that regulates the catalytic converter efficiency. Conventional automobiles are not equipped with sensors that can provide feedgas emissions and torque measurement. The control scheme studied will address the static torque and feedgas emissions performance requirements through nonlinear scheduling of the steady-state cam phasing. The structure of the feedback controller is shown in Fig. 4.1.

4.2 Performance Tradeoffs.

The purpose of this section is to explain the dynamics of the spark ignition engine equipped with a variable cam timing (VCT) mechanism, and how these affect the control design specifications. The dynamic and static interactions between the cam phasing and several subsystems of the engine are very important in the early phase of the control design process, because they lead to performance tradeoffs. Achievement of satisfactory overall engine performance requires judicious decisions about these performance tradeoffs. The following subsections describe the interaction between cam timing and engine torque response, and the interaction between the cam phasing and the A/F signal. The effects of these interactions on the engine performance, and how these are translated to control design specifications are explained.

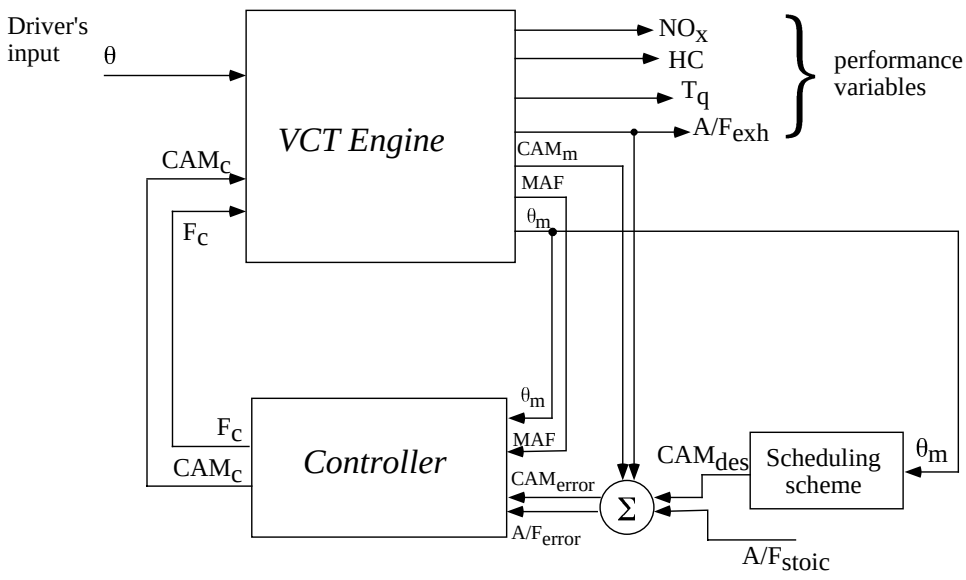

Figure 4.1: Diagrammatic representation of the feedback controller structure.

4.2.1 Engine Torque Response versus Feedgas Emissions.

Here we are considering the basic customer performance requirement: the torque response of the engine. Variable cam timing can alter the steady-state and the transient engine torque response, and the control scheme must carefully schedule the cam phasing. On the other hand, satisfying low NO_x and HC emissions is straightforward, as can be seen in Figs. 3.7 and 3.8, by using the maximum cam phasing whenever possible. The steady-state cam phasing that minimizes emissions is scheduled as follows: (1) near idle it is scheduled for idle stability which requires cam phasing equal to zero; (2) at mid-throttle it is scheduled for emissions which favors fully retarded cam phasing; and (3) at wide open throttle (WOT) it is scheduled for maximum torque which requires cam phasing to be advanced back to 0 degrees. Figure 4.2(a) shows the engine load response for the above cam phasing scheduling scheme and constant engine speed.

However, the above scheduling scheme cannot be implemented because it introduces torque discontinuities, which might entail drivability problems, and possibly introduces large A/F excursions, which, in turn, might affect adversely the tailpipe emissions. The designed cam scheduling scheme in Fig. 4.2(b) ensures reduction of feedgas emissions under the constraint of smooth steady-state torque response. Figure 4.3 shows the resulting steady-state cam phasing for engine speed equal to 2000 RPM.

This scheme satisfies smooth static torque requirements and low feedgas emissions. However, the transition of the cam phasing between set-points during rapid throttle changes is a crucial parameter in achieving good driveability. There is a dynamic interaction between the cam phasing and the torque response. Reduction of the feedgas emissions and good dynamic torque response cannot be achieved independently because good torque response

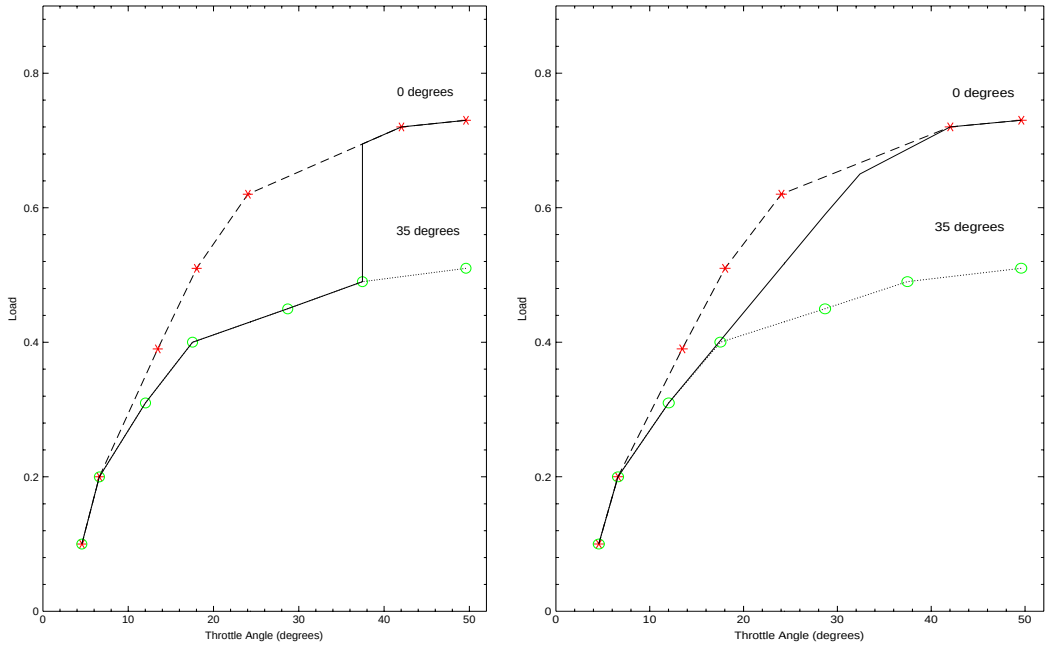

(a) (b)

Figure 4.2: Load response of an engine with variable cam timing mechanism and mechanical throttle for different scheduling schemes of cam phasing: (a) ideal schedule; (b) realizable scheme.

favors slow cam phasing to the new set points, but this might degrade the feedgas emissions which require fast cam transients. The following simulations illustrate a compromise between the torque response and emissions, and will be used to define the cam phasing control loop bandwidth.

Figures 4.4 and 4.5 illustrate cam phasing and torque response to step changes in throttle position at 750, and 2000 rpm. In all simulations, stoichiometric A/F and MBT spark timing were used. Therefore the torque response in Figs. 4.4 and 4.5 is only a function of air charge and internal exhaust gas recirculation (or cam phasing). The cam phasing controller dynamics are described by a low-pass filter between the desired and the commanded cam phasing. Figure 4.4 shows the cam phasing and torque response at 750 rpm for controllers with time constants between 0.5 and 1.5 engine cycles. Good torque response is a critical requirement at low engine speeds, and a time constant of 1 engine cycle was considered sufficient at this operating point. Figure 4.5 shows the cam phasing and torque response at 2000 rpm for various cam phasing controller dynamics. Here, the interaction between torque and cam phasing loop is considerably weaker than the interaction at lower engine speeds, and a time constant of 1 engine cycle is once again adequate for the cam phasing controller. Therefore, the bandwidth of the cam phasing controller has to be scheduled based on engine speed to correspond to one engine cycle in order to achieve good torque response over the entire operating regime.

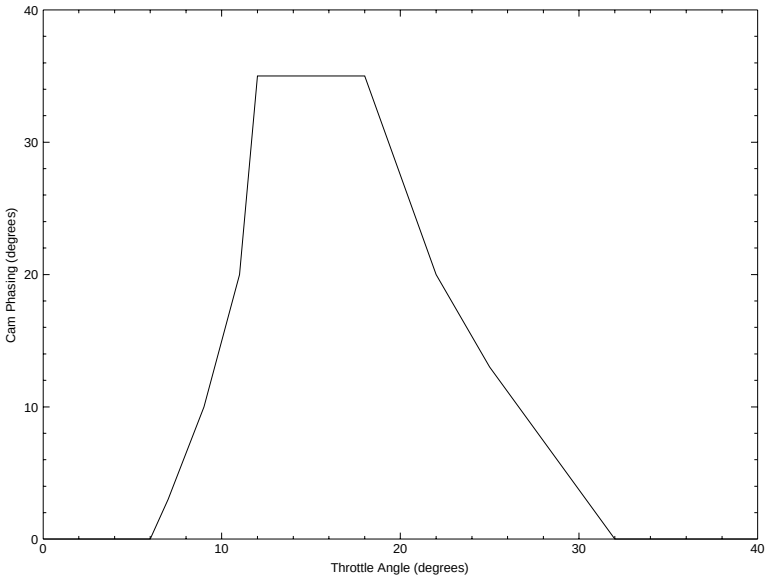

Figure 4.3: Steady state cam phasing

4.2.2 Nonlinear Breathing Process and Feedforward Fuel Control

In the VCT engine, changes in the throttle position are now followed by changes in the cam phasing based on the scheduling scheme shown in Fig. 4.3. The desired cam phasing reduces feedgas emissions by regulating the diluent in the cylinders. The contribution of this diluent to the mixture in the cylinder affects the breathing process, and consequently the mass charge in the cylinders, which in turn affects the air fuel ratio (A/F) in the cylinder mixture. This makes the A/F response highly coupled with the cam phasing activity.

It is important here to mention that variable cam timing does not affect the steady-state of the breathing process in the sonic regime. Note that in the breathing process, the cam phasing variable has the same topology as the secondary throttles from Section 2.3. In the subsonic regime, changes in cam phasing affect the dynamic and steady-state A/F response. Cam phasing is regulating feedgas emissions during changes in throttle position, but through its interaction with A/F, it affects the catalytic converter efficiency.

The structure of the electronic fuel control always consists of a feedback and a feedforward term. The feedback term regulates the fuel command based on the significantly delayed A/F signal from the EGO sensor, which inhibits good control. Due to these limitations, the feedforward term is important in adjusting the fuel command based on the measured mass air flow (MAF) and the measured cam position (CAM_m). The feedforward term is also necessary when the engine is cold and the A/F measurement is not available. The feedforward and feedback term in the fuel command result in a two degrees of freedom control topology, which gives more freedom in achieving the design goals during rapid throttle steps.

The feedforward term ($F_{c_{fw}}$) is based on the recent work in [27], and is modified to

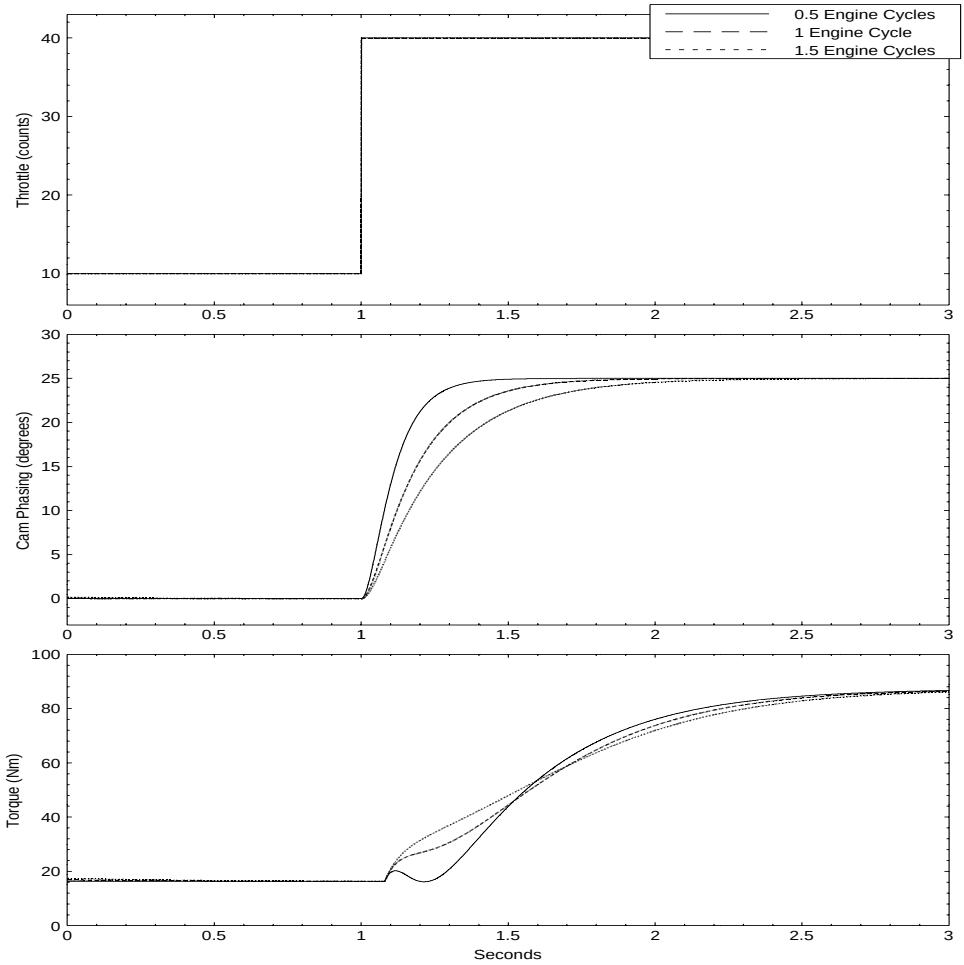

Figure 4.4: Torque response (at 750 rpm) using different low-pass filters in the cam phasing dynamics.

include the effects of variable cam timing on the cylinder air charge. The task involves the estimation of the cylinder pumping mass air flow rate ($\widehat{\dot{m}_{cyl}}$) from the measured cam phasing (CAM_m), the estimated manifold pressure ($\widehat{P_m}$), and the engine speed

$$\widehat{\dot{m}_{cyl}} = P(CAM_m, \widehat{P_m}, N) \tag{4.1}$$

The estimated manifold pressure ($\widehat{P_m}$) is calculated as (see also Equation 3.1)

$$\frac{d}{dt}\widehat{P_m} = K_m(\tau \frac{d}{dt} MAF + MAF \Leftrightarrow \widehat{\dot{m}_{cyl}}) \tag{4.2}$$

where we have used the dynamics of the mass air flow meter : $\tau \frac{d}{dt} MAF + MAF = \dot{m}_\theta$. To eliminate the derivative on the air flow measurement, we use the variable

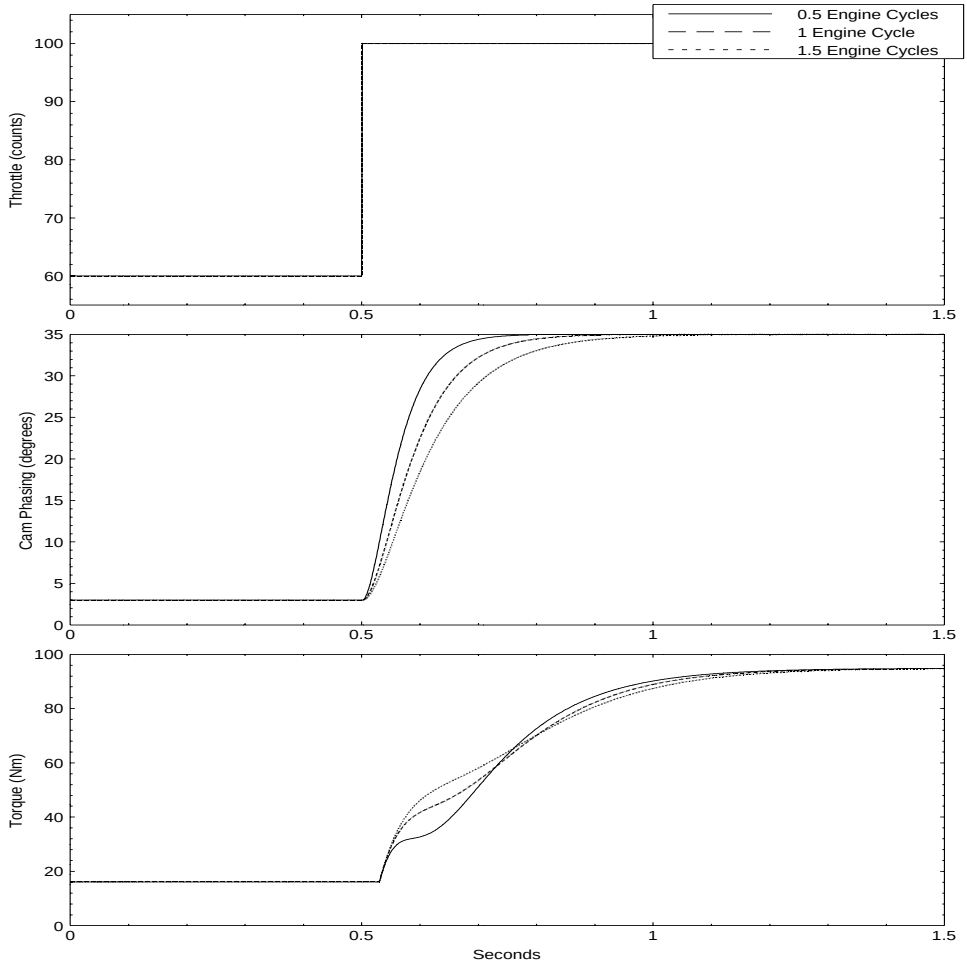

Figure 4.5: Torque response (at 2000 rpm) using different low-pass filters in the cam phasing dynamics.

$\chi = \widehat{P_m} \Leftrightarrow K_m \cdot \tau \cdot MAF$. This yields the estimated cylinder mass air flow rate :

$$\begin{aligned} \tfrac{d}{dt}\chi &= K_m(MAF \Leftrightarrow \widehat{\dot{m}_{cyl}}) \\ \widehat{P_m} &= \chi + K_m \cdot \tau \cdot MAF \\ \widehat{\dot{m}_{cyl}} &= P(CAM_m, \widehat{P_m}, N) \end{aligned} \tag{4.3}$$

For the estimation of the mass air charge into the cylinders ($\widehat{m_a}$) we assumed uniform flow during the intake event (ΔT, for the calculation of ΔT see 3.2.4) :

$$\widehat{m_a} = \widehat{\dot{m}_{cyl}} \cdot \Delta T = \widehat{\dot{m}_{cyl}} \cdot \frac{15}{N} \text{ where } N : \text{engine speed in rpm} \tag{4.4}$$

The feedforward fuel command ($F_{c_{fw}}$) is given by :

$$F_{c_{fw}} = \frac{\widehat{m_a}}{14.64}\,. \tag{4.5}$$

4.2.3 Catalytic Converter Efficiency versus Feedgas Emissions.

The feedforward term ensures decoupling of the cam phasing and the A/F in steady-state, but allows high frequency interaction. Reducing feedgas NO_x and HC emissions favors instantaneous change of the cam phasing to the scheduled set-point. Such cam phasing activity would cause a high frequency disturbance to the A/F loop. Unfortunately the long delay (810 degrees) in the A/F measurement associated with the combustion-exhaust stroke and the transport delay in the exhaust manifold imposes a bandwidth limitation on the A/F loop. If the disturbance to the A/F loop caused by the cam activity is at high frequency (i.e., beyond the achievable bandwidth of the A/F controller), then the disturbance cannot be rejected. In this case, it is a common technique to slow down the cam phasing signal, i.e., to de-tune the subsystem that causes the high frequency disturbance. This alternative, although consistent with current design practice, entails loss of the potential benefits of the VCT engine.

The dynamic performance tradeoff is between (a) the feedgas emissions that the catalytic converter must process and (b) the efficiency of the catalytic converter (which is a function of A/F excursions from stoichiometry). Due to the interaction between the cam timing loop and the A/F loop we cannot simultaneously minimize (a) and maximize (b); this is because, maximum catalytic efficiency requires that A/F be held perfectly at stoichiometry, which in turn rules out moving the cam rapidly to reduce feedgas emissions. A dynamic model of the catalytic converter efficiency could help specify a rigorous tradeoff between the two bandwidths, because, after all, the ultimate goal is to minimize tailpipe emissions. Since it is difficult to identify an accurate and simple dynamic model of the tailpipe emissions, we selected the bandwidth of the cam phasing loop based on indications taken from engine-dynamometer data and experimental vehicle tests. The tests suggest that cam transitions are to be achieved within one engine cycle (720 degrees), so that we can realize the benefits of variable cam phasing early in the transient period. This dictates the lower bound on the cam phasing bandwidth. On the other hand, we have found in the previous section that increasing the bandwidth beyond this lower bound results in unacceptable hesitation. For the above reasons we chose one engine cycle (720 degrees) to be the required time constant of the cam phasing dynamics.

4.3 Multivariable Feedback Control Design.

A multivariable controller was designed to track the desired cam phasing (value from the scheduling map) and maintain A/F at stoichiometry by controlling fuel and cam phasing command using the cam phasing position measurement, the A/F signal from the EGO sensor, and throttle position measurement. The VCT engine model does not incorporate fuel puddling dynamics. Also, there is a significant degradation of the cam phaser performance due to aging. For these two reasons the multivariable control design is based on

the LQG/LTR methodology to meet the necessary robustness properties and to meet the following performance requirements : (i) The required cam phasing dynamics are equal or faster than one engine cycle ($8\Delta T$), which, at 2000 rpm corresponds to a time constant equal or faster than 0.060 sec. (ii) Minimize A/F excursions.

We linearized the model at a throttle position equal to 9.33 degrees, cam phasing equal to 10 degrees, and engine speed equal to 2000 rpm. This operating point lies in the transition region on the cam phasing scheduling scheme shown in Fig. 4.3. The delays are represented by 1st and 2nd order Padé approximations. The linear model has 9 states and 2 integrator states. The state space representation of the linearized model is given by :

$$\begin{aligned} \dot{x}(t) &= Ax(t) + Bu(t) + B_r r(t) \\ y(t) &= Cx(t) + Du(t) \end{aligned} \tag{4.6}$$

where

$$x = \begin{bmatrix} P_m \text{ (manifold pressure)} \\ A/F \text{ (at the UEGO sensor)} \\ X \text{ (air charge estimator state)} \\ MAF \text{ (mass air flow)} \\ CAM_m \text{ (measured cam phas.)} \\ CAM_a \text{ (actual cam phas.)} \\ F_{del} \text{ (delayed fuel)} \\ A/F \text{ (at the cat. conv.)} \\ A/F \text{ (at the cylinder)} \end{bmatrix}, \quad u = \begin{bmatrix} CAM_c \text{ (cam phas. command)} \\ F_c \text{ (fuel command)} \end{bmatrix}$$

$$r = \theta \text{ throttle position, and} \quad y = \begin{bmatrix} A/F_{exh} \text{ (A/F measurement)} \\ CAM_m \text{ (cam phas. measured)} \end{bmatrix}, \text{and}$$

$$A = \begin{bmatrix} \Leftrightarrow 8.109 & 0 & 0 & 0 & 0.173 & 0 & 0 & 0 & 0 \\ 213.22 & \Leftrightarrow 14.286 & 213.221 & 3.198 & 0 & \Leftrightarrow 11.102 & \Leftrightarrow 102649 & \Leftrightarrow 44.404 & 0.056 \\ 0 & 0 & \Leftrightarrow 8.109 & 0.434 & \Leftrightarrow 0.173 & 0.422 & 0 & 0 & 0 \\ 0 & 0 & 0 & \Leftrightarrow 37.037 & 0 & 0 & 0 & 0 & 0 \\ 0 & 0 & 0 & 0 & \Leftrightarrow 26.958 & 0 & 0 & 0 & 0 \\ 0 & 0 & 0 & 0 & 109.288 & \Leftrightarrow 133.333 & 0 & 0 & 0 \\ 0 & 0 & 0.554 & 0.008 & 0.012 & \Leftrightarrow 0.029 & \Leftrightarrow 133.333 & 0 & 0 \\ 852.886 & 0 & 852.886 & 12.793 & 0 & \Leftrightarrow 44.408 & \Leftrightarrow 410595 & \Leftrightarrow 88.808 & \Leftrightarrow 40.929 \\ 0 & 0 & 0 & 0 & 0 & 0 & 0 & 64 & 0 \end{bmatrix},$$

$$B = \begin{bmatrix} \Leftrightarrow 0.000341 & 0 \\ 0 & 4 \\ 0.000341 & 0 \\ 0 & 0 \\ 4 & 0 \\ \Leftrightarrow 0.215668 & 0 \\ 0 & 0.0103 \\ 0 & 16 \\ 0 & 0 \end{bmatrix}, \quad B_r = \begin{bmatrix} 0.04010 \\ 0 \\ 0 \\ 2.6734 \\ 0 \\ 0 \\ 0 \\ 0 \\ 0 \end{bmatrix},$$

$$C = \begin{bmatrix} 0 & 3.571 & 0 & 0 & 0 & 0 & 0 & 0 & 0 \\ 0 & 0 & 0 & 0 & \Leftrightarrow 6.83 & 16.667 & 0 & 0 & 0 \end{bmatrix}, \text{ and } D = \begin{bmatrix} 0 & 0 \\ 0.0135 & 0 \end{bmatrix}.$$

During changes in throttle position, it is important to maintain A/F at stoichiometry and maintain zero tracking error in the cam timing. This is accomplished by augmenting the state vector with the integral of the error in the A/F ($\dot{q}_1 = A/F_{stoic} \Leftrightarrow A/F_{exh}$), and the integral of the error in the cam timing ($\dot{q}_2 = CAM_{des} \Leftrightarrow CAM_m$):

$$\dot{q} = y \Leftrightarrow \begin{bmatrix} A/F_{stoic} \\ CAM_{des} \end{bmatrix}. \tag{4.7}$$

We augmented the input and state vector to the VCT engine as followes :

$$\hat{r} = \begin{bmatrix} \theta \\ A/F_{stoic} \\ CAM_{des} \end{bmatrix}, \text{ and } \hat{x} = \begin{bmatrix} x \\ q \end{bmatrix}. \tag{4.8}$$

The resulting augmented system is :

$$\begin{bmatrix} \dot{x} \\ \dot{q} \end{bmatrix} = \underbrace{\begin{bmatrix} A & 0 \\ C & 0 \end{bmatrix}}_{\hat{A}} \begin{bmatrix} x \\ q \end{bmatrix} + \underbrace{\begin{bmatrix} B \\ D \end{bmatrix}}_{\hat{B}} u + \underbrace{\begin{bmatrix} B_r & 0 \\ 0 & \Leftrightarrow I \end{bmatrix}}_{\hat{B}_r} \hat{r},$$

$$y = \underbrace{\begin{bmatrix} C & 0 \end{bmatrix}}_{\hat{C}} \begin{bmatrix} x \\ q \end{bmatrix} + \underbrace{[D]}_{\hat{D}} u \tag{4.9}$$

or simpler

$$\begin{aligned} \dot{\hat{x}} &= \hat{A}\hat{x} + \hat{B}u + \hat{B}_r\hat{r} \\ \hat{y} &= \hat{C}\hat{x} + \hat{D}u\,. \end{aligned} \tag{4.10}$$

The controller feedback gain $u = \Leftrightarrow K\hat{x} = [\,-K_1\ -K_2\,]\left[\begin{smallmatrix} x \\ q \end{smallmatrix}\right]$ is found by solving the LQR problem. The weighting matrices R_{xx} and R_{uu} used in the minimization of the cost function

$J = \int_0^\infty (x' R_{xx} x + u' R_{uu} u)\, dt$ are selected so that the closed loop requirements are satisfied. Their values are :

$$\begin{aligned} R_{xx} &= diag([0.364,\ 1500,\ 0.3,\ 18,\ 1000,\ 1000,\ 0.9,\ 1500,\ 1500,\ 70000,\ 5000]) \\ R_{uu} &= diag([1,\ 1]) \end{aligned} \tag{4.11}$$

The resulting K_1 and K_2 feedback gains are :

$$K_1 = \begin{bmatrix} \Leftrightarrow 34.083 & \Leftrightarrow 8.057 & \Leftrightarrow 0.118 & \Leftrightarrow 0.0018 & 33.653 & 13.503 & 8729.56 & \Leftrightarrow 2.648 & \Leftrightarrow 8.076 \\ \Leftrightarrow 465.941 & \Leftrightarrow 60.796 & 51.999 & 0.780 & 4.443 & \Leftrightarrow 3.693 & 107225 & \Leftrightarrow 15.396 & \Leftrightarrow 54.205 \end{bmatrix}$$

$$K_2 = \begin{bmatrix} 35.096 & \Leftrightarrow 70.086 \\ 262.237 & 9.380 \end{bmatrix}. \tag{4.12}$$

The only measurements available are the CAM timing measurement, and the A/F at the EGO sensor. Perfect measurements of the throttle angle (θ) are also assumed. For the complete controller design we need to estimate the states (x) using an observer. The observer gains are derived from a Kalman filter design by minimizing the covariance between the actual and the estimated values of the state. The real symmetric positive semi-definite matrix representing the intensities of the state noises Q_{xx}, and the real symmetric positive definite matrix representing the intensities of the measurement noises Q_{yy} are assumed diagonal. The Kalman filter gain is adjusted so that the LQG controller can asymptotically approach the robustness properties of the LQR design. Loop transfer recovery in the input is employed and the final values for the covariance matrices Q_{xx}, and Q_{yy} are :

$$\begin{aligned} Q_{xx} &= diag([0.001, 0.1, 0.001, 1, 0.1, 0.1, 0.0009, 0.1, 0.1]) \\ Q_{yy} &= 1000 \cdot diag([0.1, 0.1]). \end{aligned} \tag{4.13}$$

The resulting observer gain is :

$$L = \begin{bmatrix} 1.107894e \Leftrightarrow 05 & 8.112784e \Leftrightarrow 07 \\ 5.597648e \Leftrightarrow 01 & \Leftrightarrow 6.344560e \Leftrightarrow 07 \\ \Leftrightarrow 1.197880e \Leftrightarrow 05 & 8.116791e \Leftrightarrow 07 \\ \Leftrightarrow 2.629355e \Leftrightarrow 06 & \Leftrightarrow 1.764878e \Leftrightarrow 13 \\ \Leftrightarrow 5.024201e \Leftrightarrow 07 & 8.407023e \Leftrightarrow 05 \\ \Leftrightarrow 3.418612e \Leftrightarrow 07 & 1.488718e \Leftrightarrow 04 \\ \Leftrightarrow 2.202050e \Leftrightarrow 05 & \Leftrightarrow 1.355407e \Leftrightarrow 08 \\ \Leftrightarrow 1.416589e \Leftrightarrow 01 & 5.572409e \Leftrightarrow 07 \\ 7.158249e \Leftrightarrow 02 & \Leftrightarrow 1.302364e \Leftrightarrow 05 \end{bmatrix}. \tag{4.14}$$

The combined observer and controller state-space representation is described by the

following equations:

$$\begin{aligned} \dot{x}_e &= Ax_e + Bu + B_r r_1 + L(y \Leftrightarrow y_e) \\ y_e &= Cx_e + Du + D_r r_1 \\ u &= \Leftrightarrow K_1 x_e \Leftrightarrow K_2 q \\ \dot{q} &= \Leftrightarrow y + \begin{bmatrix} r_2 \\ r_3 \end{bmatrix} \quad \text{where } x_e \text{ is the estimated state,} \end{aligned} \tag{4.15}$$

and finally

$$\begin{aligned} \frac{d}{dt}\begin{bmatrix} x_e \\ q \end{bmatrix} &= \begin{bmatrix} A \Leftrightarrow LC \Leftrightarrow BK_1 + LDK_1 & LDK_2 \Leftrightarrow BK_2 \\ 0 & 0 \end{bmatrix}\begin{bmatrix} x_e \\ q \end{bmatrix} + \begin{bmatrix} L \\ \Leftrightarrow I \end{bmatrix} y + \begin{bmatrix} B \Leftrightarrow LD_r & 0 \\ 0 & I \end{bmatrix} \hat{r} \\ u &= \begin{bmatrix} \Leftrightarrow K_1 & \Leftrightarrow K_2 \end{bmatrix}\begin{bmatrix} x_e \\ q \end{bmatrix} . \end{aligned} \tag{4.16}$$

The controller design process involved testing the performance of the linear controller when applied to the nonlinear VCT engine model. Controllers with A/F bandwidth beyond 12 rad/sec result in worse A/F response due to the deleterious effects of the delay in the A/F measurements. Figure 4.6 shows the Bode gain plots of the resulting closed loop transfer functions.

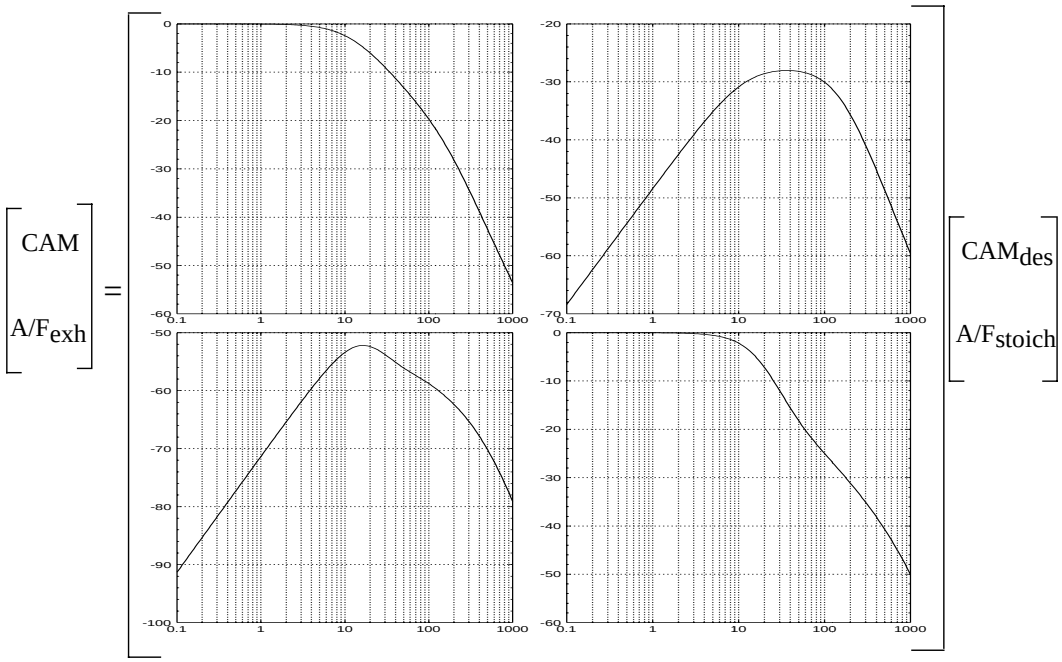

Figure 4.6: Bode gain plots of the closed loop transfer functions (frequency in rad/sec).

4.4 Nonlinear Simulation Example.

The purpose of this section is to illustrate some of the properties of the closed loop system for a conventional engine (fixed cam phasing) and the VCT engine. Figure 4.7 shows the simulated response of the conventional engine (fixed cam phasing) and the VCT engine to a square wave in commanded throttle at 2000 rpm. The sequence of throttle commands is 9.0 degrees (nominal) to 7.2 degrees to 12.0 degrees and back to 7.2 degrees and then to 9.0 degrees. The corresponding cam phasing set-points are 3 degrees to 10 degrees to 35 degrees (maximum) and back to 3 degrees and then to 10 degrees. The conventional engine scheme has fixed cam at 0 degrees.

The resulting torque response of the VCT engine is kept as responsive as the conventional engine in acceleration. During the abrupt deceleration at the 5th second of the simulation, the torque response of the VCT engine has an abrupt transient behavior which might entail drivability problems. The transient A/F response of the VCT engine is slightly worse than the A/F response of the conventional engine.

The advantage of the VCT engine over the conventional scheme is demonstrated at the feedgas NO_x and HC emissions. Using the integrated area defined by the NO_x and HC emission curves as a crude measurement of engine emissions, we can estimate a possible reduction of 10% in NO_x and 20% in HC during that period. Moreover, the engine operates in higher manifold pressure, which may reduce the pumping losses and provide an improvement in fuel economy.

4.5 PI Feedback Control Design.

In this section we investigate a simpler controller architecture for the previous feedback problem. It consists of (i) a classical, time-invariant, single-input single-output (SISO) PI controller that, based on the A/F measurement at the EGO sensor and the feedforward term (Equation 4.3), adjusts the fuel command; and (ii) a lowpass filter that regulates the cam phasing dynamic behavior. This control structure is easy to develop, implement and calibrate, and it is identical to the existing control architecture in conventional automobiles, with the addition of the cam phasing low pass filter. Investigation of simpler controller architectures is very important to the implementation stage of any controller development. Here, the motivation arises from the fact that if the simpler control structure results in satisfactory performance, then addition of the variable cam timing mechanism to a conventional automotive engine does not require completely new software development, but merely involves calibration of (i) the PI gains in the A/F loop and (ii) the time constant of the cam phasing dynamics. Figure 4.8 shows the different control architectures for the MIMO and the PI scheme.

In Sections 4.2.1 and 4.2.3 we discussed the importance of the cam transient behavior to the torque response and the A/F loop excitation. This interaction imposed bandwidth

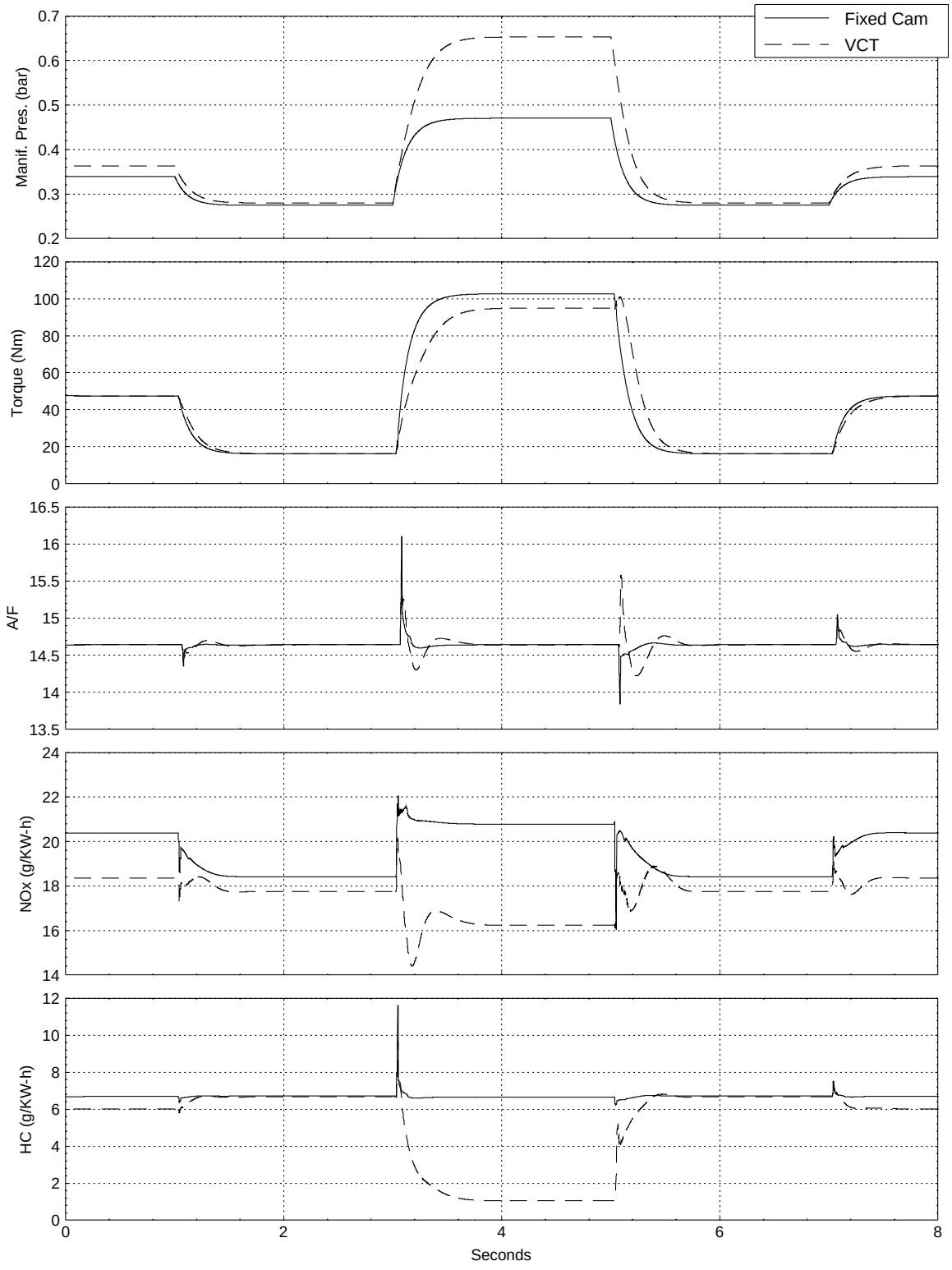

Figure 4.7: Simulation response of the conventional and the VCT engine.

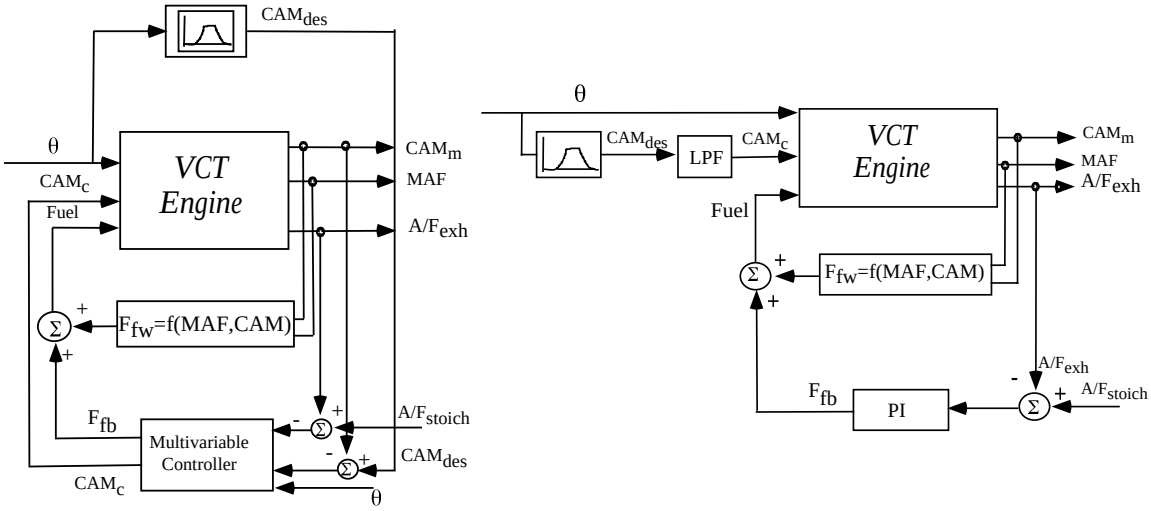

Figure 4.8: Diagrams of the MIMO control scheme, and the "PI-lowpass filter" control scheme.

limitations to the cam phasing dynamics, which corresponded to a time constant of one engine cycle. The lowpass filter designed has a time constant of 0.060 sec which corresponds to one engine cycle at 2000 rpm:

$$CAM_c = \frac{1}{0.060s + 1} CAM_{des} \ . \tag{4.17}$$

Tuning the PI gains in the A/F loop, we achieved the closed loop shown in the right plot of Fig. 4.9 (dashed line). The transfer function of the PI controller is :

$$F_c = \frac{0.57045s + 5.7045}{s} A/F_{error} \ . \tag{4.18}$$

For the comparison of the two control schemes, Figure 4.9 shows the Bode gain plots of the two resulting closed loops for the MIMO and simple PI scheme. The Bode gain plots of the closed loop transfer function between the desired and measured cam phasing for the two control schemes is shown at the left plot of Fig. 4.9. The Bode gain plot of the closed loop transfer function from the desired stoichiometric A/F (A/F_{stoic}) to the A/F at the EGO sensor (A/F_{exh}) for the two control schemes is shown at the right plot of Fig. 4.9.

Figure 4.10 compares the two schemes in a nonlinear simulation : MIMO controller versus PI controller. Similarity in the cam phasing dynamics is maintained, and the engine torque responses are almost identical. The NO_x and HC emissions in both cases are equivalent. However, the MIMO controller that coordinates the cam phasing and fuel command results in a small improvement in the nonlinear A/F simulation response. Comparison of the MIMO and the simpler controller architecture merits more investigation, since a degradation in A/F performance might cause an increase in the tailpipe emissions due to the sensitive performance of the three-way-catalytic (TWC) converter as a function of A/F. To capture the main features of the two control designs we concentrate on the linear engine

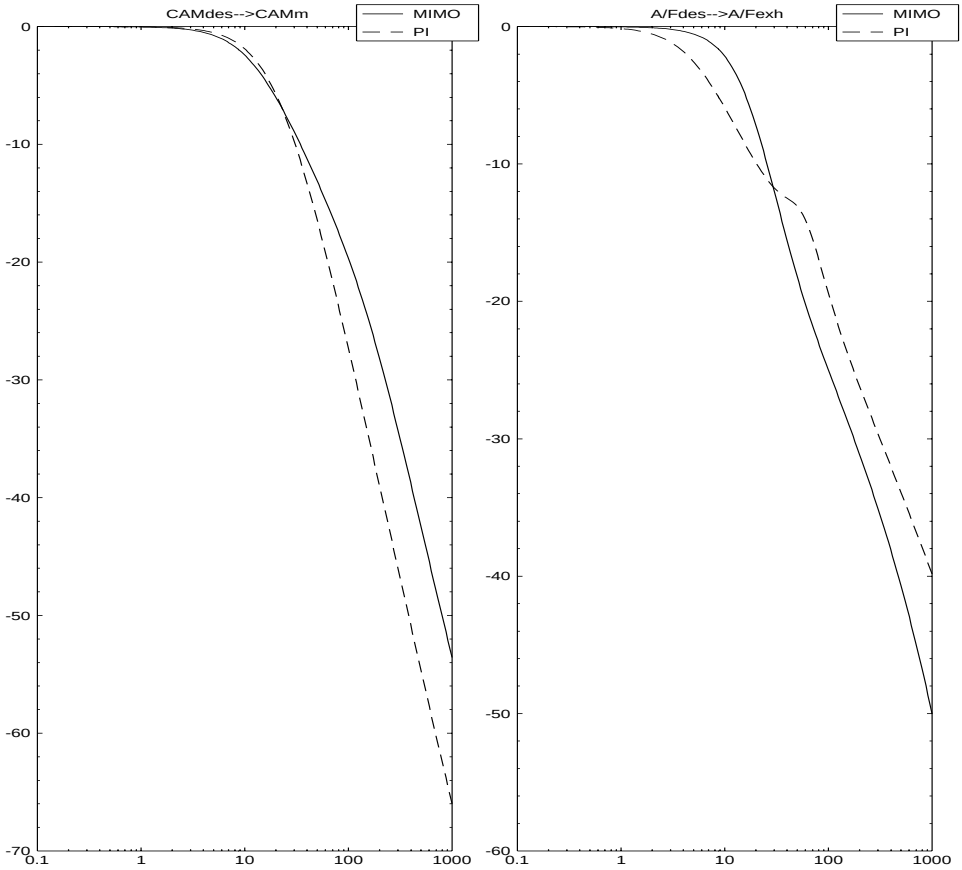

Figure 4.9: Bode gain plots of closed loop transfer functions with the MIMO and the "PI-lowpass filter" feedback controllers (frequency in rad/sec).

model and the linear closed loop response corresponding to the controller architectures. By eliminating the effects of the nonlinear engine model on the dynamic response, one can study the effects of the multivariable and the decentralized controller architecture on the dynamic response of the VCT engine.

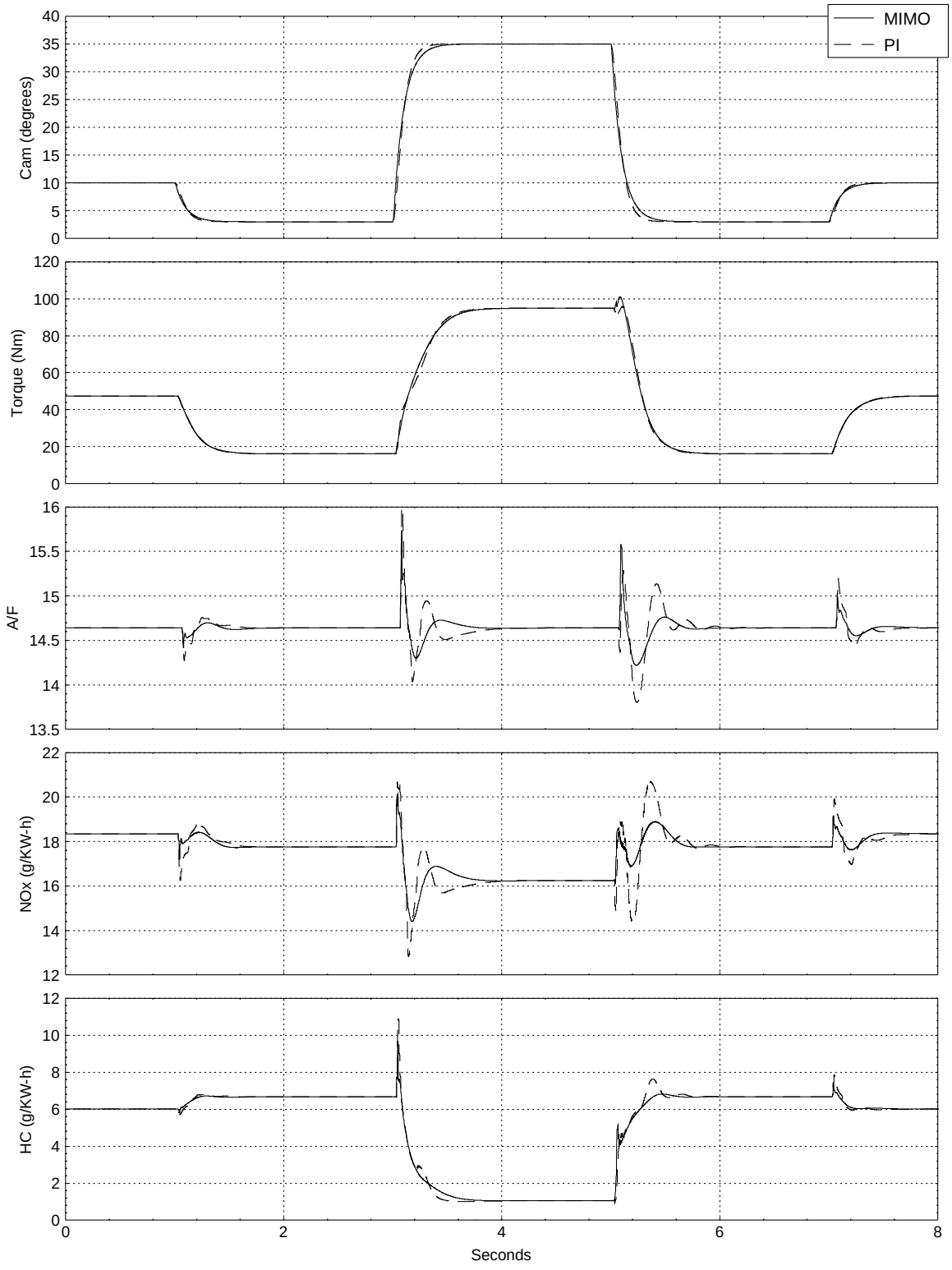

Figure 4.10: Simulation response of the multivariable and the PI control scheme.

CHAPTER 5

Consequences of Modular Controller Development for the VCT Engine.

A modular architecture refers to a software organization consisting of a collection of independent program components with well-defined interfaces specifying the information flow across module boundaries. Such an architecture has many benefits: improved productivity through module reuse, seamless integration of new features, transparent removal of obsolete features, and module sharing across powertrain platforms. Additionally, maintainability is substantially enhanced in that modules can be modified independently of other parts of the powertrain control strategy. That is, one might remove and replace the EGR or fuel control module without affecting the rest of the strategy.

Because of these advantages, modular controller architectures have largely been used in automotive industry leading to the conventional decentralized control design. Conventional control design practice has been to assume independence of the powertrain subsystems, and apply classical control techniques to individual engine and powertrain subsystems. During the calibration process the feedback gains for each control loop are tuned with the other loop in manual (open loop). Often the overall performance is unsatisfactory when the other loops are placed in automatic (closed loop) due to the interaction between the different loops, thus further calibration is required. Dynamic interactions are minimized by de-tuning or calibrating a subsystem controller to avoid the unintentional excitations. This process often results in suboptimal performance which might not be sufficient for the increasingly demanding requirements in transient engine performance. Moreover, the advanced technology engines have strongly coupled subsystems. These interactions impose performance tradeoffs and require laborious tuning process of the multiple SISO-loops (decentralized controller).

Applying modern control techniques to design a multivariable controller is the natural approach to the problem. Designing a multivariable controller, however, is a complicated task and requires the development of a complete dynamic model of the system studied. Furthermore, MIMO controllers are difficult to tune, modify, and recover after component failure. It is hard to implement MIMO controllers because they require large memory space and execution time. Due to their complexity, MIMO controllers are rare in the automotive

industry. In the next sections we show that the multivariable controller designed in the previous chapter can be simplified without detrimental consequences in the engine dynamic response.

5.1 Decentralized Control of Multivariable Plants.

The simplest approach in controlling a MIMO plant is to ignore the multivariable nature of the plant and design a set of SISO feedback systems. However, designing a set of SISO systems to satisfy individual closed loop performance (e.g. speed of response and disturbance rejection) does not imply that the whole multivariable system will inherit these properties. Closing some loops might have deleterious effects on the behavior of the remaining loops. When high loop gain is not available, the only means to reduce the interaction is to de-tune the previous loops, and therefore impose performance tradeoffs. Using decentralized controllers in MIMO plants with strong interactions imposes performance limitations that have been explored and identified as early as the 1960s in [6]. In the process control literature, there are a significant number of studies on the interactions of subprocesses in MIMO plants and their significance on the closed loop performance ([50, 70] and references therein).

One way of reducing the interaction between subsystems is to design decouplers, i.e. feedforward compensators that maximize diagonal dominance at the frequency where the subsystem interaction is strong and the loop gains are not sufficient to attenuate this interaction [38, 44]. Analysis and synthesis of robust decentralized controllers (robust decouplers and decentralized controllers) have been studied in [87], and tested through simulations in automotive control applications in [67]. Another way of reducing interactions in MIMO plants is the design of multivariable controllers. In [42] it is mentioned that multivariable design techniques reduce the interaction between subsystems even without having taken explicit steps to do so. It is also well known [50, 25] that multivariable controllers manage design tradeoffs inherent to MIMO plants more successfully than decentralized controllers.

Despite many studies in the area of multivariable feedback control, there are no well accepted guidelines in defining an acceptable tradeoff between control design complexity and system performance in highly interactive multivariable systems. Investigation of these issues in the application of the VCT engine will aid in better understanding the underlying issues of a design methodology and its portability to other systems. The VCT engine has significant interaction between the dynamics of the variable cam mechanism and those of the air-fuel ratio subsystem.

5.2 Multivariable and Decentralized Controller: Design.

In a decentralized design, one could think of controlling cam phasing to minimize feedgas emissions (cam phasing loop), and regulating fuel pulse-width duration to minimize A/F

excursions (fuel loop). This leads to two single-input single-output (SISO) control systems, which is the decentralized control approach. This approach initially ignores the interaction between cam phasing and A/F that makes the two loops (cam loop and A/F loop) dynamically coupled over a large bandwidth. Figure 5.1 shows the Bode gain plots of the plant linearized at 2000 RPM. Cam phasing is measured in degrees, A/F is dimensionless, and the fuel command is scaled so that a unit deviation in fuel causes a unit deviation in the A/F signal.

The plant has a lower triangular form because the fuel command affects the system downstream of the breathing process. Therefore, there is no interaction between the fuel command and the cam phasing loop ($p_{12}(s) = 0$). In Fig. 5.1 we can see the interaction term (p_{21}) between the cam phasing control signal and A/F measurement. Through the term (p_{21}) the cam control command acts as an output disturbance in the A/F subsystem (see Fig. 5.2).

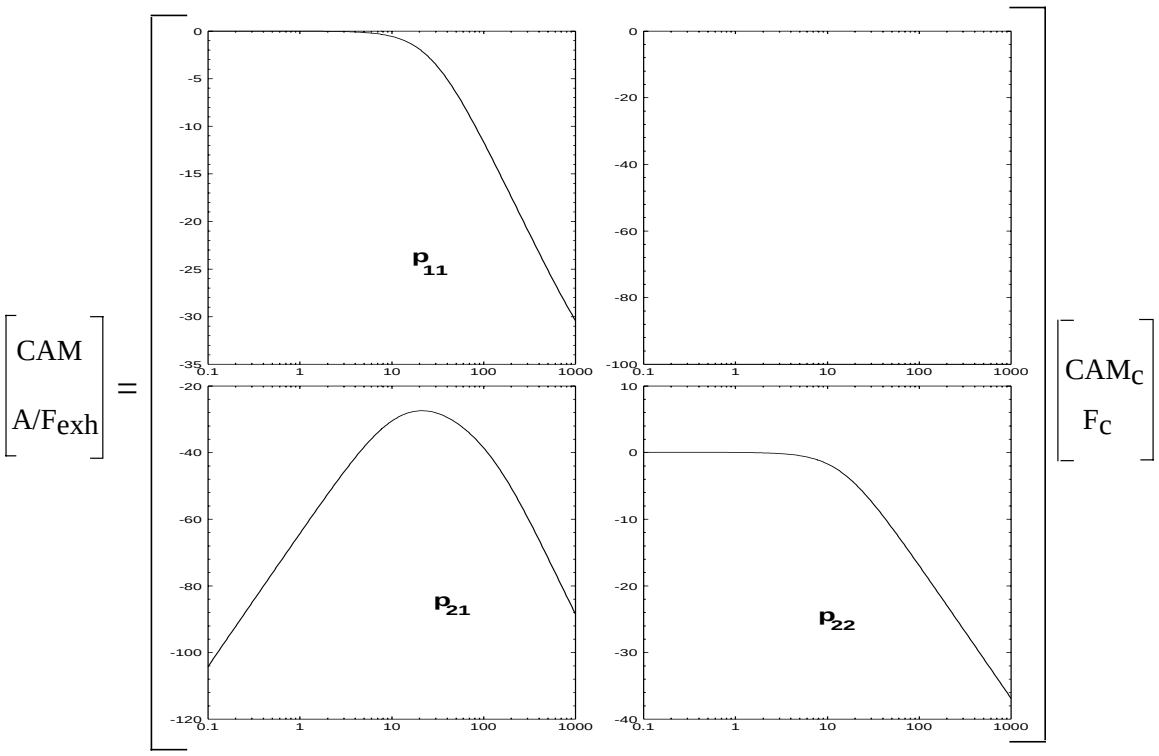

Figure 5.1: Bode gain plots of the linearized plant (frequency in rad/sec).

We repeat here the controller design considerations: (a) There is a 810 degrees of delay in the A/F process (see Fig. 5.2). At 2000 rpm, this translates into a time delay of 0.0675 sec. Due to this delay, the A/F bandwidth should not exceed 12 rad/sec (Section 4.3). (b) The required time constant for the cam phasing dynamics is 720 degrees (1 engine cycle). At 2000 rpm this corresponds to a time constant equal to 0.06 sec, which translates into a cam phasing closed loop bandwidth equal to 17 rad/sec. The peak of the interaction

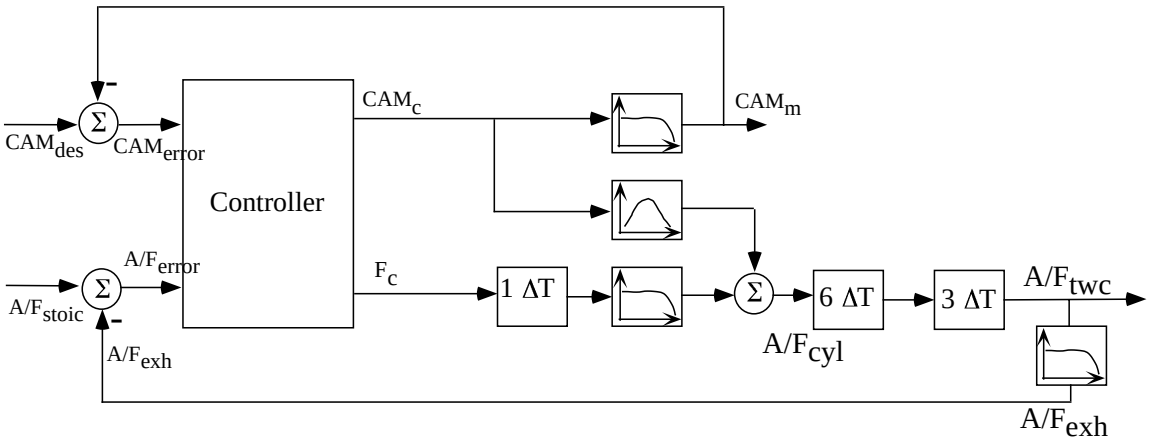

Figure 5.2: Block diagram of the linearized plant.

term (p_{21}) occurs at 20 rad/sec while we require the cam phasing activity to roll off after 17 rad/sec. Therefore, the control signal generated to force the cam phasing to track a command input will also produce a transient response in the A/F loop; in effect, the cam loop acts as a disturbance to the A/F loop. We thus see that we are faced with a difficult design problem.

The decentralized control design involves defining the two single-input single-output feedback loops that satisfy the design specifications. The transfer function describing the dynamics in the cam phasing loop (p_{11} term) is given by :

$$CAM = \underbrace{\frac{\Leftrightarrow 0.01348(s \Leftrightarrow 2000)}{s + 26.96}}_{p_{11}(s)} CAM_c \ . \tag{5.1}$$

The transfer function describing the dynamics in the A/F loop (p_{22} term) is given by :

$$A/F_{exh} = \underbrace{\frac{(s \Leftrightarrow 133.34)(s^2 \Leftrightarrow 88.8081s + 2633.67)}{(s + 14.286)(s + 133.33)(s^2 + 88.8081s + 2619.44)}}_{p_{22}(s)} F_c \ . \tag{5.2}$$

To meet the design specifications on the cam phasing loop the controller was chosen to be :

$$CAM_c = \underbrace{\frac{0.3425(s + 26.96)}{s}}_{c_{11}(s)} CAM_{error} \ . \tag{5.3}$$

A few design iterations resulted the following controller in the A/F feedback loop :

$$F_c = \underbrace{\frac{0.57(s + 10)}{s}}_{c_{22}(s)} A/F_{error} \ . \tag{5.4}$$

The Bode gain plots of the MIMO controller designed in 4.3 (solid line) and the decentralized controller (dashed line) are illustrated in Fig. 5.3. Both controller designs achieve

the bandwidth requirement in the cam phasing loop, and provide adequate speed of response in the A/F loop. The bandwidth specifications for the two loops essentially fix the band-

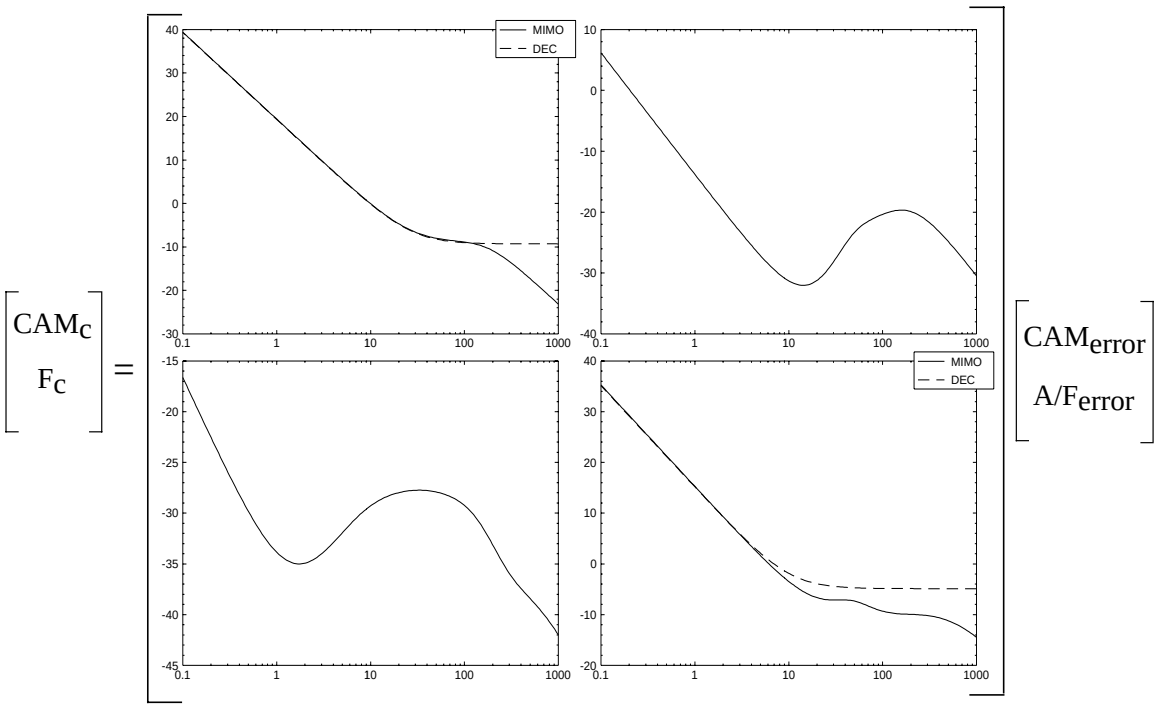

Figure 5.3: Bode gain plots of the MIMO controller and the decentralized controller (frequency in rad/sec).

widths of the diagonal elements of the controller independently of the controller structure. As a result, the diagonal elements of the two controllers are approximately identical.

Comparisons between the system response with the previously selected diagonal controller (see Fig. 5.3), and the system response with a decentralized controller consisting of the diagonal elements of the multivariable controller, showed only negligible differences. Hence, for the rest of this study, we will simply compare and discuss the decentralized controller obtained by using the diagonal elements of the multivariable controller and the fully multivariable controller.

Figure 5.3 shows linear simulations of the output and control signals during various cam phasing step commands for the two different controller architectures. The A/F deviations for the multivariable control scheme are significantly better than those corresponding to the decentralized control scheme.

Implementing the multivariable controller thus seems to be beneficial, but there are several questions we must address before we justify implementation of the multivariable strategy on a vehicle: How did the multivariable controller manage to reject the A/F disturbance faster than the decentralized controller? In which way did the multivariable controller reduce the interaction between the two loops? In the next section we identify the mechanism by which the multivariable controller achieves smaller A/F excursions during

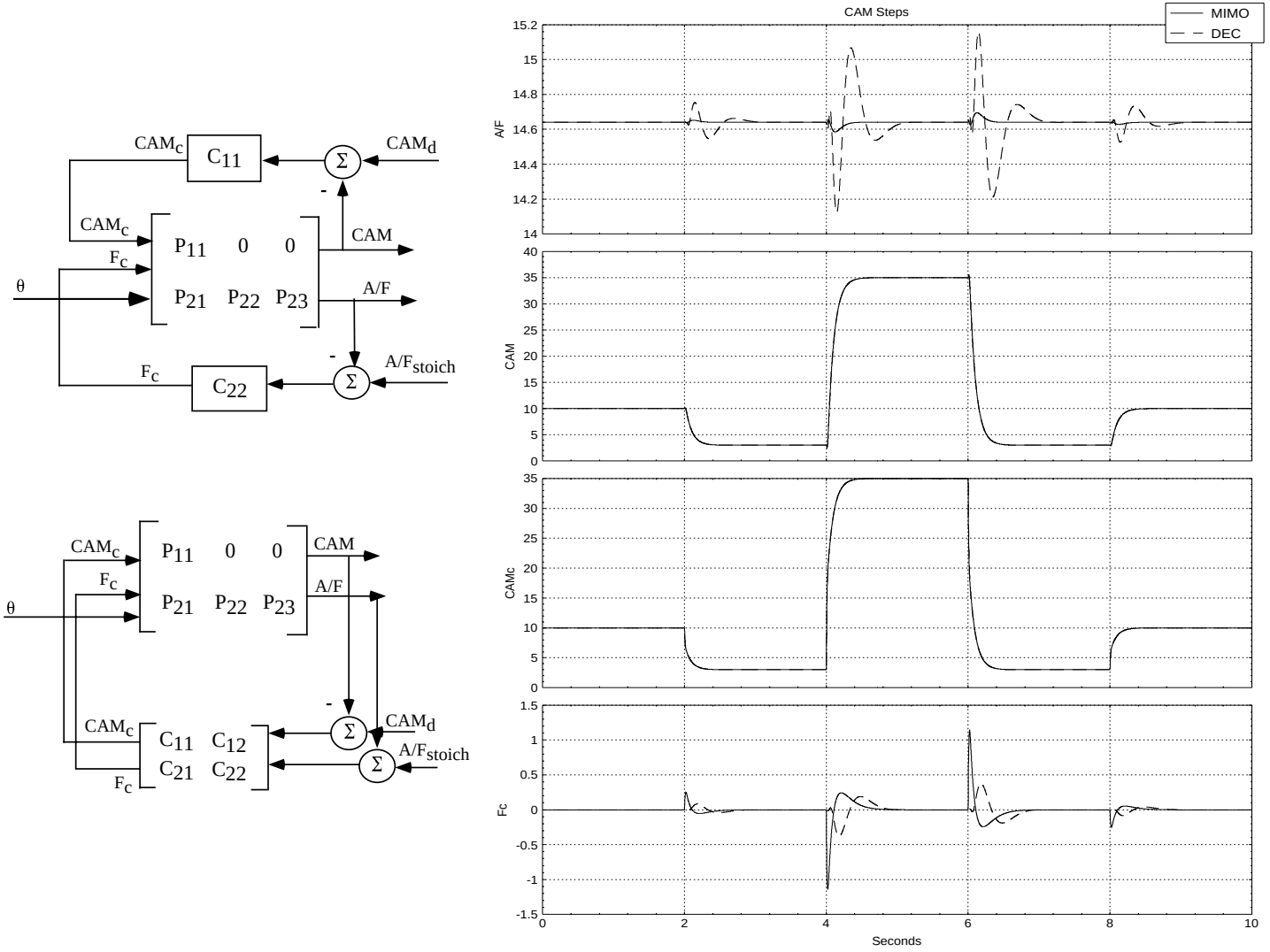

Figure 5.4: Simulation using the linearized VCT engine model during cam phasing commands.

cam phasing transients.

5.3 Multivariable and Decentralized Controller: Analysis.

We begin by describing a design limitation present with decentralized control. Consider the decentralized control system in Fig. 5.5. Topologically, the CAM loop acts as an output disturbance to the A/F loop. As noted in Section 5.2 there is no interaction from the A/F loop to the CAM loop.

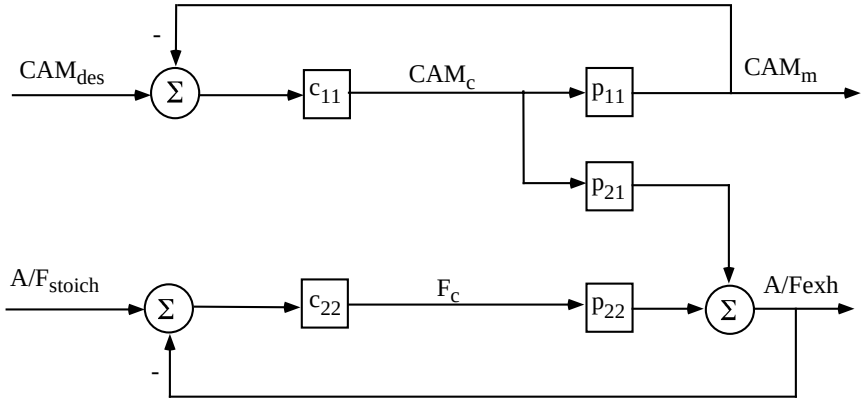

Figure 5.5: Block diagram of the decentralized control scheme.

Denote the sensitivity and complementary sensitivity functions for each loop by $s_{ii}(s) = (1 + p_{ii}(s)c_{ii}(s))^{-1}$ and $t_{ii}(s) = 1 \Leftrightarrow s_{ii}(s)$, $i = 1, 2$. Then the transfer function describing the closed loop A/F response is given by

$$A/F_{exh}(s) = t_{22}(s)A/F_{stoic}(s) + s_{22}(s)p_{21}(s)\underbrace{c_{11}(s)s_{11}(s)CAM_{des}(s)} \tag{5.5}$$

The term underlined in Equation 5.5 is equal to $CAM_c(s)$, the control signal in the CAM loop generated in response to a CAM command (CAM_{des}). As we have seen, the plant interaction (quantified by the transfer function $p_{21}(s)$), causes this signal to act as a disturbance to the A/F loop.

Suppose that this closed loop interaction results in unacceptable A/F transients. With a decentralized controller structure, there are two alternate approaches to reducing the interaction:

(i) Increase the bandwidth of the A/F loop, thus obtaining smaller sensitivity ($\mid s_{22}(j\omega) \mid \ll 1$), and greater disturbance attenuation, over a wider frequency range. This alternative is not feasible in the present problem, because of the time delay that limits the speed of response in the A/F loop (see Fig. 5.2).

(ii) Decrease the bandwidth of the CAM loop to obtain less control activity ($\mid c_{11}(j\omega)s_{11}(j\omega) \mid \ll 1$) at the frequencies of the problematic interaction. This alternative has been ruled out because it entails loss of potential benefits of the variable cam

timing engine, as argued in Section 4.2.3.

The preceding analysis implies the existence of a tradeoff between CAM and A/F responses. Specifically, to reduce the undesirable effects of interaction from CAM command to A/F response, it is necessary to either reduce the bandwidth in the CAM loop, and/or increase the bandwidth in the A/F loop. Increasing the speed of the A/F response is not feasible due to the time delay; hence, the tradeoff is resolved by sacrificing CAM performance in favor of the A/F loop.

We have seen that a decentralized controller structure imposes a tradeoff between achieving the bandwidth specifications in the two loops. Let us now consider two mechanisms by which a MIMO controller can (potentially) mitigate such a tradeoff.

(1) Let the CAM control signal depend upon errors in both cam and A/F loops (the term (c_{12}) in Fig. 5.6). Essentially, this strategy allows the controller for the CAM loop to achieve a compromise between regulating errors in the two loops and is an elegant alternative to the de-tuning practice (ii), that we mentioned above. In the present case, the delay in the A/F loop prevents this method from being useful because it is present in the response of A/F to both actuators. The significantly delayed A/F measurement cannot contribute information through the term (c_{12}) sufficient rapidly to slow the cam activity. Indeed, in Fig. 5.2 we can observe the nearly identical cam phasing control signals issued by the two controllers. We verified that the MIMO controller does not make effective use of the A/F error in computing the CAM control signal by zeroing the term (c_{12}) of the MIMO controller and noting that closed loop performance is virtually unchanged.

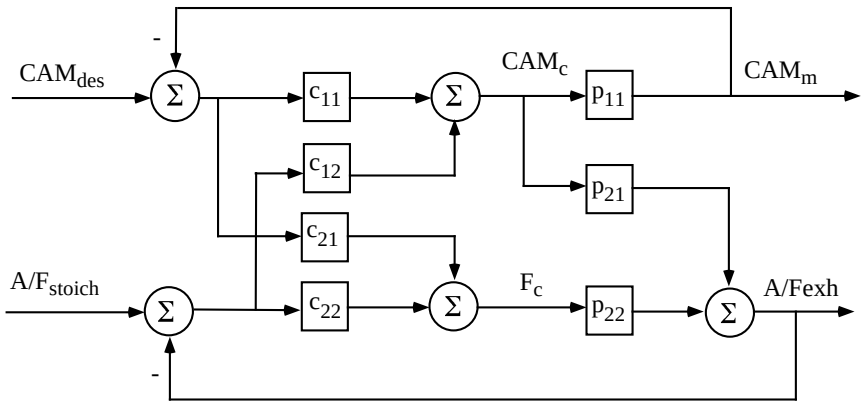

Figure 5.6: Block diagram of the fully multivariable scheme.

(2) Let the fuel signal depend upon the error in both CAM and A/F loops (the term (c_{21}) in Fig. 5.6). As depicted in Fig. 5.7, this control strategy results in a feedforward path from the cam phasing error to the fuel command used to control A/F. The feedforward term (c_{21}) sends information to the fuel command about the cam phasing error, and this allows faster response during cam phasing transients. The disturbance imposed on the A/F

loop by a command issued to cam phasing loop is shown at the following equation :

$$A/F_{exh}(s) = (p_{21}(s)c_{11}(s) + p_{22}(s)c_{21}(s))CAM_{error}(s) \tag{5.6}$$

Note here, that the same disturbance for the decentralized controller (see Fig. 5.5) is given by :

$$A/F_{exh} = p_{21}(s)c_{11}(s)CAM_{error}(s) \tag{5.7}$$

The multivariable controller can potentially reduce the coupling between the two subsystems by choosing the term (c_{21}) such that

$$\mid p_{21}(j\omega)c_{11}(j\omega) + p_{22}(j\omega)c_{21}(j\omega) \mid < \mid p_{21}(j\omega)c_{11}(j\omega) \mid \tag{5.8}$$

In Fig. 5.8, we see that MIMO control reduces the peak in the closed loop response from CAM commands to A/F measurements.

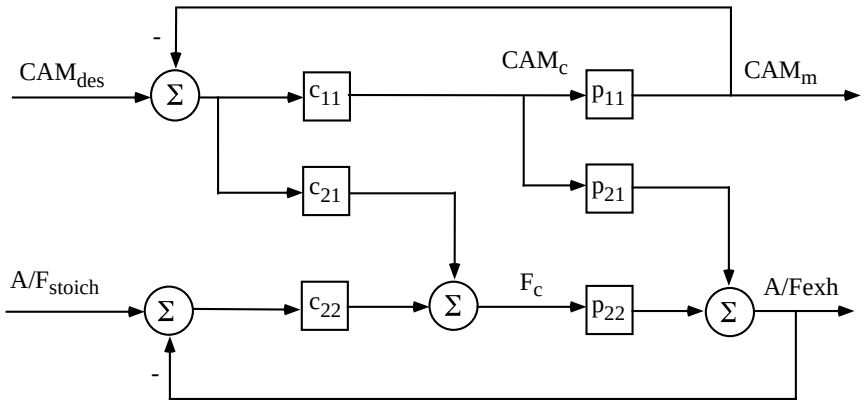

Figure 5.7: Block diagram of the simplified multivariable control scheme.

It is possible to interpret the action of the MIMO controller as partially decoupling the A/F response from the CAM loop. Indeed, setting the feedforward term equal to

$$c_{21}(s) = \frac{\Leftrightarrow c_{11}(s)p_{21}(s)}{p_{22}(s)} \tag{5.9}$$

achieves zero closed loop interaction from CAM to A/F. An alternate representation of the perfect decoupler is depicted in Fig. 5.9. With this topology, the CAM and A/F loops become completely decoupled, and the two remaining controller parameters, c_{11} and c_{22}, may be chosen independently. This controller design may be prone to robustness problems, since the term (c_{21}) is cancelling the undesired disturbance by inverting the signal along the path of the plant interaction.

In practice, there is no need to achieve perfect decoupling. Indeed, at lower frequencies, the integral action in the A/F loop achieves zero steady state error despite the interaction with the CAM loop. At higher frequencies, on the other hand, the CAM loop rolls off and thus does not produce a response in A/F.

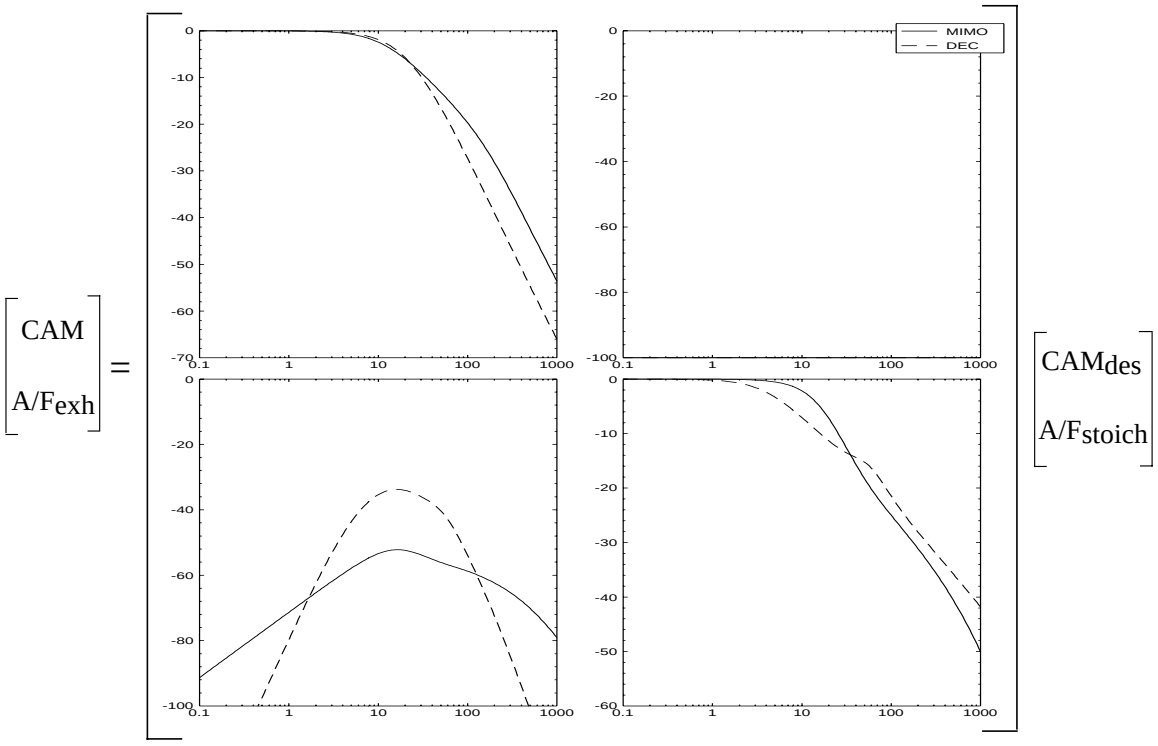

Figure 5.8: Bode gain plots of the closed loop transfer function (frequency in rad/sec).

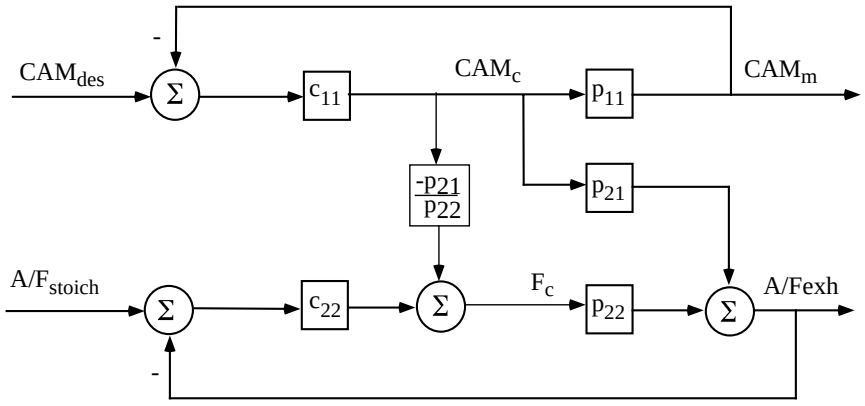

Figure 5.9: Block diagram of the decoupling controller.

As we see in Fig. 5.8, the MIMO controller merely reduces the peak due to the interaction, thus attenuating the effect of the CAM loop upon A/F without achieving total decoupling.

A potential difficulty with implementing the MIMO controller is that the feedforward term in the controller depends upon the plant; hence the performance improvements associated with MIMO control are sensitive to plant modeling errors. Indeed, the bandwidth limitation that precludes feedback from being used to reduce the effect of the CAM distur-

bance upon the A/F loop also prevents feedback from being used to reduce the effects of modeling uncertainty upon A/F.

5.4 Conclusions.

The potential benefits of multivariable control for an engine equipped with variable cam timing are demonstrated here. By designing and analyzing a multivariable controller for the cam phasing and A/F loops, we showed that coordinated control for these two loops resulted in better A/F transient performance without detuning the cam phasing loop. A complete design, including a study of robustness and scheduling, remains to be completed.

CHAPTER 6

Conclusions and Directions for Future Work.

In this dissertation we have studied control design issues for two advanced technology automotive engines. Both engine configurations were multivariable and nonlinear, thus imposing challenging control problems associated with control authority, long sensor delays, and strongly coupled subsystems. We have developed and validated dynamic engine models, studied the subsystem interactions, identified performance tradeoffs, and have applied classical and modern control techniques to improve engine performance. Moreover, we have studied the impact of modular controller architecture on the engine dynamic response, and demonstrated that even if the controller is eventually implemented in independent software modules, coordinating the design and analysis allows for a better assessment of the tradeoffs between the dynamic performance of different subsystems. In particular, the effects of subsystem interactions emerge at an earlier phase of the design process. This will reduce the calibration effort, and will result in advanced powertrain systems that can meet future performance requirements.

There are a number of directions in which the engine control applications that we have addressed in this dissertation can be extended.

Engine with secondary throttles : The control design for the engine with the secondary throttles was a preliminary assessment of the benefits of the new actuator, and there are several issues that merit further investigation. In particular, it would be valuable to experimentally validate the model of the engine with the secondary throttles. The model of the breathing process has been substantiated from the experimental data collected for the VCT engine. The secondary throttles and the variable cam timing affect the breathing process in a similar way, and it was shown that the proposed model captures the VCT engine dynamics accurately. It would be useful to extend the model to capture the nonlinear behavior of air flow through the secondary throttles and the ram air charging effects. The resulting system will provide an extremely powerful tool for the analysis and design of dynamically controlled camless engines.

We should investigate the issues arising from the assumptions made in the dissertation,

namely, the availability of good torque and throttle position measurements. Finally, it will be valuable to schedule the linear controller designed in this dissertation, and to develop an adaptive algorithm that upgrades the demand map.

Variable cam timing engine : The feedback controller designed for the VCT engine is based on a linearized engine model at one operating point. A scheduling scheme of a series of linear controllers or a completely nonlinear controller has to be designed to ensure operation over a wide range of engine speed and load conditions. This scheme has to address difficulties that arise from the event-based delays, the hybrid (continuous- and discrete-time) engine behavior, and the nonlinearities of physical processes and sensors. Furthermore, new emission mandates require emission control over an extended region (wide open throttle, cold start, etc.). Thus, modeling and control of the VCT engine, or any other conventional engine over these regions, will be imperative and challenging since no prior systematic studies in these regimes are available.

A possible way to improve the engine transient response is to coordinate the design of the feedforward (steady-state cam phasing) and the feedback terms of the variable cam timing controller. A methodology that addresses the design of feedforward and feedback controllers will assist in developing and maintaining integrated powertrain control systems.

Another significant study that remains to be completed is assessing the robustness properties of the multivariable versus the decentralized controller. The closed loop performance is affected by uncertainty in the cam actuator and/or uncertainty in the fuel puddling dynamics, and will be valuable to assess the nominal performance and the performance under uncertainty.

To address the complete powertrain control problem, it is necessary to incorporate the transmission and driveline into the existing VCT engine model. In the resulting VCT powertrain model, variable cam timing, fuel command, and gear ratio should be dynamically scheduled to improve the overall powertrain performance. A significant result of this systematic investigation will be the development of an integrated powertrain controller architecture. Implementation issues of modular controller architecture, addressed in the last chapter of this dissertation, will emerge and require a rigorous methodology of achieving a tradeoff between controller complexity and engine performance. This work is viewed as a combination of research in the area of engine modeling and multivariable control: (i) by developing dynamical models for the highly multivariable powertrain and identifying the important subsystem interactions that impose performance tradeoffs in the control design, and (ii) by translating the level of interaction in terms of design specifications for different subsystems.

It is our conclusion that the development of advanced technology powertrains requires

systematic modeling and control techniques to achieve the stringent performance requirements which are compelling their design. Moreover, there is a strong need for a systematic approach that can integrate the design phase with the implementation phase of the complete powertrain controller development on the vehicle. In this dissertation, we have demonstrated the advantages of such an integrated approach, and laid the foundations for a rigorous methodology of developing automotive powertrain control systems.

APPENDICES

APPENDIX A

Engine Mapping

The engine static mapping data, specification of the region of interest, and the set of experiments performed to obtain the nonlinear static model of the VCT engine are explained in this appendix.

A.1 Set of experiments

The goal in controlling the VCT in this dissertation is to reduce emissions and satisfy drivability, mostly in the region defined by the Federal Procedure Test (FTP) cycles, and centered in the part-throttle part-load operating regime. The static engine mapping data for the $4.6L\ V8$ experimental VCT engine spans the region between 0.15-0.65 Load (normalized torque) and 750-2000 RPM.

The independent variables for the VCT engine model are :

- Engine Speed : Experiments were performed at 750 rpm, 1000 rpm, 1500 rpm and 2000 rpm constant engine speed.
- Throttle position : The necessary throttle position (in counts=degrees*8.33) to span the region of 0.15-0.65 Load (important for the FTP cycles) was identified by cranking the engine at constant engine speed. For this reason throttle positions are different for each engine speed (see Table A1-A4).
- CAM phasing : Experiments were performed at cam phasing equal to 0, 5, 12, 19, 28, and 37 degrees for each engine speed and for each throttle position.
- A/F : Experiments were performed at A/F equal to 12.2, 13.9, 14.6, 15.2, and 16.0 for each engine speed, each throttle position, and each cam phasing.

750 rpm

		CAM phase in degrees					
Load	TPrel	0	5	12	19	28	37
0.18	18	12.2	12.2	12.2	12.2	12.2	12.2
		13.9	13.9	13.9	13.9	13.9	13.9
		14.6	14.6	14.6	14.6	14.6	14.6
		15.2	15.2	15.2	15.2	15.2	15.2
		16.0	16.0	16.0	16.0	16.0	16.0
0.20	27	12.2	12.2	12.2	12.2	12.2	12.2
		13.9	13.9	13.9	13.9	13.9	13.9
		14.6	14.6	14.6	14.6	14.6	14.6
		15.2	15.2	15.2	15.2	15.2	15.2
		16.0	16.0	16.0	16.0	16.0	16.0
0.30	49	12.2	12.2	12.2	12.2	12.2	12.2
		13.9	13.9	13.9	13.9	13.9	13.9
		14.6	14.6	14.6	14.6	14.6	14.6
		15.2	15.2	15.2	15.2	15.2	15.2
		16.0	16.0	16.0	16.0	16.0	16.0
0.40	63	12.2	12.2	12.2	12.2	12.2	12.2
		13.9	13.9	13.9	13.9	13.9	13.9
		14.6	14.6	14.6	14.6	14.6	14.6
		15.2	15.2	15.2	15.2	15.2	15.2
		16.0	16.0	16.0	16.0	16.0	16.0

Table A.1: The 120 steady-state experiments performed at 750 rpm and the associated input variables.

1000 rpm

		CAM phase in degrees					
Load	TPrel	0	5	12	19	28	37
0.15	24	12.2	12.2	12.2	12.2	12.2	12.2
		13.9	13.9	13.9	13.9	13.9	13.9
		14.6	14.6	14.6	14.6	14.6	14.6
		15.2	15.2	15.2	15.2	15.2	15.2
		16.0	16.0	16.0	16.0	16.0	16.0
0.20	41	12.2	12.2	12.2	12.2	12.2	12.2
		13.9	13.9	13.9	13.9	13.9	13.9
		14.6	14.6	14.6	14.6	14.6	14.6
		15.2	15.2	15.2	15.2	15.2	15.2
		16.0	16.0	16.0	16.0	16.0	16.0
0.30	63	12.2	12.2	12.2	12.2	12.2	12.2
		13.9	13.9	13.9	13.9	13.9	13.9
		14.6	14.6	14.6	14.6	14.6	14.6
		15.2	15.2	15.2	15.2	15.2	15.2
		16.0	16.0	16.0	16.0	16.0	16.0
0.40	77	12.2	12.2	12.2	12.2	12.2	12.2
		13.9	13.9	13.9	13.9	13.9	13.9
		14.6	14.6	14.6	14.6	14.6	14.6
		15.2	15.2	15.2	15.2	15.2	15.2
		16.0	16.0	16.0	16.0	16.0	16.0
0.50	99	12.2	12.2	12.2	12.2	12.2	12.2
		13.9	13.9	13.9	13.9	13.9	13.9
		14.6	14.6	14.6	14.6	14.6	14.6
		15.2	15.2	15.2	15.2	15.2	15.2
		16.0	16.0	16.0	16.0	16.0	16.0

Table A.2: The 150 steady-state experiments performed at 1000 rpm and the associated input variables.

1500 rpm

		CAM phase in degrees					
Load	TPrel	0	5	12	19	28	37
0.15	50	12.2	12.2	12.2	12.2	12.2	12.2
		13.9	13.9	13.9	13.9	13.9	13.9
		14.6	14.6	14.6	14.6	14.6	14.6
		15.2	15.2	15.2	15.2	15.2	15.2
		16.0	16.0	16.0	16.0	16.0	16.0
0.20	64	12.2	12.2	12.2	12.2	12.2	12.2
		13.9	13.9	13.9	13.9	13.9	13.9
		14.6	14.6	14.6	14.6	14.6	14.6
		15.2	15.2	15.2	15.2	15.2	15.2
		16.0	16.0	16.0	16.0	16.0	16.0
0.30	85	12.2	12.2	12.2	12.2	12.2	12.2
		13.9	13.9	13.9	13.9	13.9	13.9
		14.6	14.6	14.6	14.6	14.6	14.6
		15.2	15.2	15.2	15.2	15.2	15.2
		16.0	16.0	16.0	16.0	16.0	16.0
0.45	115	12.2	12.2	12.2	12.2	12.2	12.2
		13.9	13.9	13.9	13.9	13.9	13.9
		14.6	14.6	14.6	14.6	14.6	14.6
		15.2	15.2	15.2	15.2	15.2	15.2
		16.0	16.0	16.0	16.0	16.0	16.0
0.60	161	12.2	12.2	12.2	12.2	12.2	12.2
		13.9	13.9	13.9	13.9	13.9	13.9
		14.6	14.6	14.6	14.6	14.6	14.6
		15.2	15.2	15.2	15.2	15.2	15.2
		16.0	16.0	16.0	16.0	16.0	16.0

Table A.3: The 150 steady-state experiments performed at 1500 rpm and the associated input variables.

2000 rpm

		CAM phase in degrees					
Load	TPrel	0	5	12	19	28	37
0.148	63	12.2	12.2	12.2	12.2	12.2	12.2
		13.9	13.9	13.9	13.9	13.9	13.9
		14.6	14.6	14.6	14.6	14.6	14.6
		15.2	15.2	15.2	15.2	15.2	15.2
		16.0	16.0	16.0	16.0	16.0	16.0
0.20	78	12.2	12.2	12.2	12.2	12.2	12.2
		13.9	13.9	13.9	13.9	13.9	13.9
		14.6	14.6	14.6	14.6	14.6	14.6
		15.2	15.2	15.2	15.2	15.2	15.2
		16.0	16.0	16.0	16.0	16.0	16.0
0.30	104	12.2	12.2	12.2	12.2	12.2	12.2
		13.9	13.9	13.9	13.9	13.9	13.9
		14.6	14.6	14.6	14.6	14.6	14.6
		15.2	15.2	15.2	15.2	15.2	15.2
		16.0	16.0	16.0	16.0	16.0	16.0
0.40	127	12.2	12.2	12.2	12.2	12.2	12.2
		13.9	13.9	13.9	13.9	13.9	13.9
		14.6	14.6	14.6	14.6	14.6	14.6
		15.2	15.2	15.2	15.2	15.2	15.2
		16.0	16.0	16.0	16.0	16.0	16.0
0.50	152	12.2	12.2	12.2	12.2	12.2	12.2
		13.9	13.9	13.9	13.9	13.9	13.9
		14.6	14.6	14.6	14.6	14.6	14.6
		15.2	15.2	15.2	15.2	15.2	15.2
		16.0	16.0	16.0	16.0	16.0	16.0
0.65	211	12.2	12.2	12.2	12.2	12.2	12.2
		13.9	13.9	13.9	13.9	13.9	13.9
		14.6	14.6	14.6	14.6	14.6	14.6
		15.2	15.2	15.2	15.2	15.2	15.2
		16.0	16.0	16.0	16.0	16.0	16.0

Table A.4: The 180 steady-state experiments performed at 2000 rpm and the associated input variables.

A.2 Output Data Files.

The engine variables for the previously specified experiments are stored in five files at the directory `vct_dir/rawdata.dir/statdata.dir` : (i) file OUT1 contains all the necessary data for the identification of the breathing process and torque generation function, (ii) file OUT2 contains data for identification of the combustion process, (iii) file OUT3 contains additional information on the combustion process providing in-cylinder pressure information, (iv) file OUT4 contains data that address issues associated with the actual air flow through the throttle body, and the mass air flow measurement based on the hot wire anemometer, and (v) file OUT5 contains engine temperature data. Each row in files OUT1-4 represents one experiment. The first four columns in all files contain the desired inputs (independent variables) as specified in Tables A1-A4. The remaining columns contain the outputs (dependent variables). In file OUT1, the last four columns contain the actual inputs for each experiment. These inputs are slightly different from the desired inputs. The data analysis is based on the actual values of the independent variables.

OUT1: Contains the basic engine mapping information

1. Desired throttle position (TPrel in counts : degrees*8.33)
2. Desired engine speed (rpm)
3. Desired CAM phasing (degrees)
4. Desired A/F ( )
5. Torque (Nm)
6. Load ( )
7. Manifold pressure (bar)
8. Mass air flow (g/sec)
9. Mass fuel flow (g/sec)
10. MBT spark ignition timing after top dead center (TDC)
11. Actual throttle position (TPrel in counts : degrees*8.33)
12. Actual engine speed (rpm)
13. Actual CAM phasing (degrees)
14. Actual A/F

Example of **OUT1**

tpd	rpmd	camd	A/Fd	torque	load	map	maf	mff	mbt	tpa	rpma	cama	A/Fa
(cnts)	(rpm)	(deg)	( )	(Nm)	( )	(bar)	(g/s)	(mg/s)	(deg)	(deg)	(rpm)	(deg)	( )
18	750	0	12.20	34.89	0.179	0.328	5.66	516.6	33.6	16.00	748	-0.2	12.17
18	750	0	13.90	35.63	0.179	0.326	5.55	441.0	36.7	16.00	747	-0.2	14.00
18	750	0	14.60	34.67	0.179	0.325	5.62	415.8	40.0	16.00	746	-0.2	14.73
18	750	0	15.20	31.62	0.180	0.324	5.61	403.2	38.0	16.00	748	-0.2	15.38
18	750	0	16.00	26.78	0.179	0.322	5.62	378.0	38.0	16.00	748	-0.2	16.19
18	750	5	12.20	35.54	0.179	0.341	5.63	516.6	35.2	16.00	748	4.8	12.14
18	750	5	13.90	36.51	0.179	0.339	5.59	441.0	39.4	16.00	747	4.8	13.96

OUT2: Contains the data associated with the combustion process

1. Desired throttle position (TPrel in counts : degrees*8.33)
2. Desired engine speed (rpm)
3. Desired CAM phasing (degrees)
4. Desired A/F ( )
5. Break mean effective pressure, BMEP (bar)
6. Power (kW)
7. Break specific fuel consumption, BSFC (g/kW-hr)
8. Specific hydrocarbon emissions production (g/kW-hr)
9. Specific oxides of nitrogen emissions production (g/kW-hr)
10. Specific carbon monoxide emissions production (g/kW-hr)

Example of **OUT2**

TPd (cnts)	RPMd (rpm)	Camd (CA)	A/Fd ( )	BMEP (bar)	Power (kW)	BSFC (g/kW-hr)	HC (g/kW-hr)	NOx (g/kW-hr)	CO (g/kW-hr)
18	750	0	12.20	0.95	2.72	683.26	28.07	0.97	349.06
18	750	0	13.90	0.97	2.77	573.69	20.29	2.54	73.99
18	750	0	14.60	0.95	2.69	556.49	19.23	3.02	21.96
18	750	0	15.20	0.86	2.46	590.67	20.81	2.35	11.64

OUT3: contains additional information on the combustion process providing in-cylinder pressure information.

1. Desired throttle position (counts)
2. Desired engine speed (rpm)
3. Desired CAM phasing (degrees)
4. Desired A/F ( )
5. Exhaust temperature (deg. C)
6. Indicated mean effective pressure (bar)
7. Pumping mean effective pressure (bar)
8. Peak pressure (bar)
9. Peak pressure location in degrees after top dead center (DATDC)

Example of **OUT3**

TPd	RPMd	Camd	A/Fd	exh-temp	IMEP	PMEP	Peak-P	Peak-P-loc
(cnts)	(rpm)	(deg)	( )	(deg C)	(bar)	(bar)	(bar)	(DATDC)
18	750	0	12.20	299.9	1.931	-0.652	11.246	14.3
18	750	0	13.90	323.7	1.962	-0.655	10.634	15.7
18	750	0	14.60	330.7	1.937	-0.659	10.286	15.7
18	750	0	15.20	330.9	1.866	-0.664	9.059	17.0

OUT4: contains data associated with the air flow measurement.

1. Desired throttle position (counts)
2. Desired engine speed (rpm)
3. Desired CAM phasing (degrees)
4. Desired A/F ( )
5. Manifold pressure (bar)
6. Pressure on the #1 intake runner (bar)
7. Meriam up-stream pressure (bar)
8. Atmospheric pressure (bar)

Example of **OUT4**

TPd	RPMd	Camd	A/Fd	MAP	Int#1-press	Meriam-up-press	Atm-press
(cnts)	(rpm)	(deg)	( )	(bar)	(bar)	(bar)	(bar)
18	750	0	12.20	0.331	0.334	1.006	1.003
18	750	0	13.90	0.328	0.332	1.006	1.003
18	750	0	14.60	0.328	0.331	1.006	1.004
18	750	0	15.20	0.326	0.330	1.006	1.004

OUT5: contains engine temperature data.

1. Desired throttle position (counts)
2. Desired engine speed (rpm)
3. Desired CAM phasing (degrees)
4. Desired A/F ( )
5. Intake manifold temperature (deg. C)
6. Coolant temperature (deg. C)
7. Exhaust manifold temperature (deg. C)

Example of **OUT5**

TPd	RPMd	Camd	A/Fd	int-temp	H2O-temp	exh-temp
(cnts)	(rpm)	(deg)	( )	(deg C)	(deg C)	(deg C)
18	750	0	12.20	36.7	89.0	299.9
18	750	0	13.90	36.7	90.1	323.7
18	750	0	14.60	37.3	90.1	330.7
18	750	0	15.20	37.3	89.5	330.9

APPENDIX B

Nonlinear Static Maps for the VCT Engine

The identified nonlinear static maps are described in this appendix. The information in this appendix is complementary to Chapter 3. We provide all the coefficients and the exact equations that describe the nonlinear static maps used in VCT engine model.

B.1 Mass Air Flow Rate through the Throttle Body during Sonic Flow ($\dot{m}_\theta = g_2(\theta)$).

In this section we identify the nonlinear static relationship between throttle position and mass air flow through the throttle body. In Section 3.2.1 we explain this relationship based on physical laws. The mass air flow through the throttle body in sonic flow is a function of throttle position ($\dot{m}_\theta = g_2(\theta)$), whereas in subsonic flow it is a function of both manifold pressure and throttle position ($\dot{m}_\theta = g_1(P_m) \cdot g_2(\theta)$). The relationship $g_1(P_m)$ has been specified by Novak in [56] and is used to convert all the data to equivalent sonic flow data which we can use for the identification of the $g_2(\theta)$.

For simplicity, let $y =: \dot{m}_\theta$ and $x =: \theta$. In the least squares fit we used the scaled variables $\hat{y}$ and $\hat{x}$.

$$\hat{y} = \frac{y \Leftrightarrow y_{min}}{y_{max} \Leftrightarrow y_{min}} \tag{B.1}$$

where y_{min} and y_{max} is the minimum and maximum output value of the data set used.

$$\hat{x} = \frac{x \Leftrightarrow x_{min}}{x_{max} \Leftrightarrow x_{min}} \tag{B.2}$$

where x_{min} and x_{max} is the minimum and maximum input value of the data set used.

Based on the regression analysis, the function that describes the relationship between $\hat{y}$ and $\hat{x}$ is:

$$\hat{y} = 0.0062 + 0.0537\hat{x} + 1.6134\hat{x}^2 \Leftrightarrow 0.6994\hat{x}^3 \quad . \tag{B.3}$$

For the conversion from the scaled variables to the actual mass air flow and throttle position we used: $y_{min} = 4.02$, $y_{max} = 52.0558$, $x_{min} = 3.00$ and $x_{max} = 160.00$. Comparison between the identified polynomial and the experimental data is shown in Figure B.1.

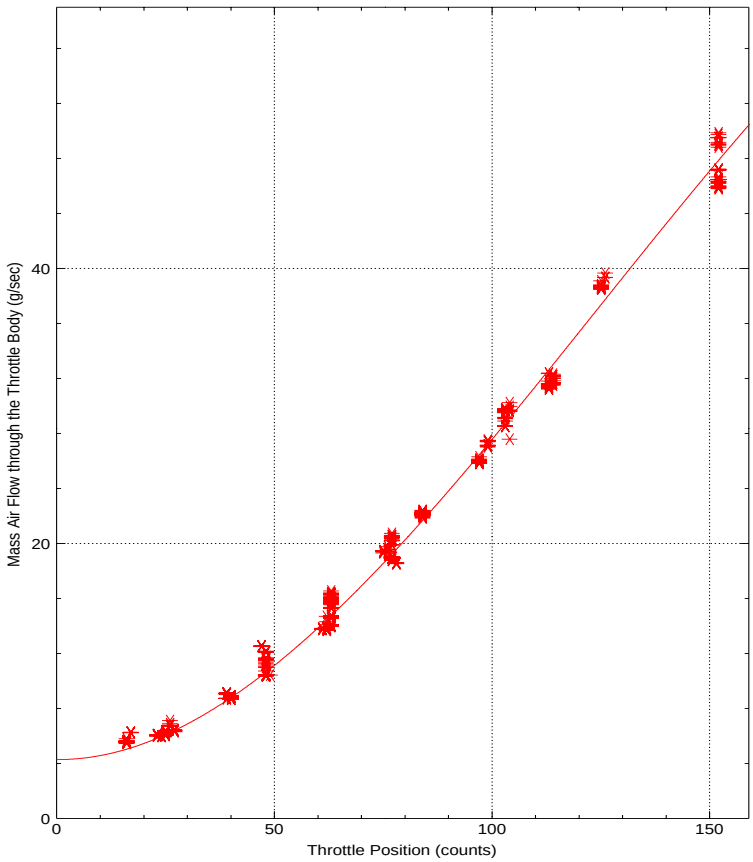

Figure B.1: Comparison between the identified polynomial $g_2(\theta)$ and the experimental data.

B.2 Engine Pumping Mass Air Flow Rate ($\dot{m}_{cyl}$)

In this section we identify the nonlinear static function that describes the engine pumping mass air flow rate. In Section 3.2.1 we described the mass air flow rate into the cylinders as a function of cam phasing (CAM), manifold pressure (P_m), and engine speed (N). The resulting polynomial is of degree three, and a third order polynomial in each individual variable:

$$\dot{m}_{cyl} = F(1, CAM, CAM^2, CAM^3, P_m, P_m^2, P_m^3, N, N^2, N^3) \quad . \tag{B.4}$$

For simplicity, let

$$y =: \dot{m}_{cyl} \text{ and } x = \begin{bmatrix} x_1 \\ x_2 \\ x_3 \end{bmatrix} =: \begin{bmatrix} CAM \\ P_m \\ N \end{bmatrix} \quad . \tag{B.5}$$

In the least squares fit we used the scaled variables $\hat{y}$ and $\hat{x}$.

$$\hat{y} = \frac{y \Leftrightarrow y_{min}}{y_{max} \Leftrightarrow y_{min}} \tag{B.6}$$

where y_{min} and y_{max} is the minimum and maximum output value of the data set used.

$$\hat{x} = \frac{x \Leftrightarrow x_{min}}{x_{max} \Leftrightarrow x_{min}} \tag{B.7}$$

where x_{min} and x_{max} is the minimum and maximum input value of the data set used.

Based on the regression analysis the function that describes the relationship between $\hat{y}$ and $\hat{x}$ is:

$$\begin{aligned}\hat{y} \;&= \Leftrightarrow 0.1231 \Leftrightarrow 0.1088\hat{x}_1 + 0.3396\hat{x}_2 \Leftrightarrow 0.1386\hat{x}_3 \\ &+0.1438\hat{x}_1\hat{x}_3 + 0.1899\hat{x}_1\hat{x}_2 + 1.4548\hat{x}_2\hat{x}_3 \\ &+0.0186\hat{x}_1^2 \Leftrightarrow 0.8495\hat{x}_2^2 \Leftrightarrow 0.0080\hat{x}_3^2 \\ &\Leftrightarrow 0.0854\hat{x}_1^2\hat{x}_3 \Leftrightarrow 0.0962\hat{x}_1^2\hat{x}_2 \Leftrightarrow 0.0992\hat{x}_3^2\hat{x}_1 + 0.1855\hat{x}_3^2\hat{x}_2 \\ &\Leftrightarrow 0.1881\hat{x}_2^2\hat{x}_1 \Leftrightarrow 0.4097\hat{x}_2^2\hat{x}_3 \\ &\Leftrightarrow 0.1900\hat{x}_1\hat{x}_2\hat{x}_3 + 0.0121\hat{x}_1^3 + 0.7603\hat{x}_2^3 + 0.0043\hat{x}_3^3\end{aligned} \tag{B.8}$$

For the conversion from the actual mass air flow into the cylinders and the actual CAM phasing, manifold pressure and engine speed to the scaled variables used in the regression analysis we used:

$$y_{min} = 3.67 \;,\; y_{max} = 54.09 \;,$$
$$x_{min} = \begin{bmatrix} x_1 \\ x_2 \\ x_3 \end{bmatrix}_{min} = \begin{bmatrix} 0 \\ 0 \\ 0 \end{bmatrix}, \text{ and } x_{max} = \begin{bmatrix} x_1 \\ x_2 \\ x_3 \end{bmatrix}_{max} = \begin{bmatrix} 35 \\ 1 \\ 2000 \end{bmatrix} . \tag{B.9}$$

Comparison between the identified polynomial and the experimental data is shown in Figure B.2.

B.3 Torque Generation (T_b).

In this section we identify the nonlinear static relationship between the brake torque (T_b) that the engine generates for specific air charge (m_a), air fuel ratio (A/F), and engine speed (N). In Section 3.2.2 we state all the assumptions associated with the uniform brake torque generation under quasi-steady conditions. We should mention here that generated torque is an implicit function of spark timing, since spark timing is scheduled at MBT for all the experiments. The modeled torque equation is a polynomial of degree three, and a third order polynomial in each individual variable :

$$T_b = F(1, m_a, {m_a}^2, {m_a}^3, A/F, A/F^2, A/F^3, N, N^2, N^3) \;\; . \tag{B.10}$$

For simplicity, let

$$y =: T_b \text{ and } x = \begin{bmatrix} x_1 \\ x_2 \\ x_3 \end{bmatrix} =: \begin{bmatrix} m_a \\ A/F \\ N \end{bmatrix} \;\; . \tag{B.11}$$

In the least squares fit we used the scaled variables $\hat{y}$ and $\hat{x}$.

$$\hat{y} = \frac{y \Leftrightarrow y_{min}}{y_{max} \Leftrightarrow y_{min}} \tag{B.12}$$

where y_{min} and y_{max} is the minimum and maximum output value of the data set used.

$$\hat{x} = \frac{x \Leftrightarrow x_{min}}{x_{max} \Leftrightarrow x_{min}} \tag{B.13}$$

where x_{min} and x_{max} is the minimum and maximum input value of the data set used.

Based on the regression analysis the function that describes the relationship between $\hat{y}$ and $\hat{x}$ is:

$$\begin{aligned}\hat{y} \;&= 0.0480 + 1.2995\hat{x}_1 \Leftrightarrow 0.0061\hat{x}_2 \Leftrightarrow 0.0814\hat{x}_3 \\ &+0.0620\hat{x}_1\hat{x}_3 + 0.2514\hat{x}_1\hat{x}_2 + 0.0218\hat{x}_2\hat{x}_3 \\ &\Leftrightarrow 0.6635\hat{x}_1^2 \Leftrightarrow 0.0835\hat{x}_2^2 + 0.0544\hat{x}_3^2 \\ &+0.2048\hat{x}_1^2\hat{x}_3 \Leftrightarrow 0.0779\hat{x}_1^2\hat{x}_2 \Leftrightarrow 0.1381\hat{x}_3^2\hat{x}_1 \Leftrightarrow 0.0179\hat{x}_3^2\hat{x}_2 \\ &\Leftrightarrow 0.2113\hat{x}_2^2\hat{x}_1 + 0.0077\hat{x}_2^2\hat{x}_3 \\ &\Leftrightarrow 0.0308\hat{x}_1\hat{x}_2\hat{x}_3 + 0.2602\hat{x}_1^3 + 0.0436\hat{x}_2^3 \Leftrightarrow 0.0153\hat{x}_3^3\end{aligned} \tag{B.14}$$

To recover the actual input-output relationship from the scaled variables the followinng constants are needed:

$$y_{min} = \Leftrightarrow 21.71\ ,\ y_{max} = 247.6\ ,$$

$$x_{min} = \begin{bmatrix} x_1 \\ x_2 \\ x_3 \end{bmatrix}_{min} = \begin{bmatrix} 0.0606 \\ 11.7 \\ 745 \end{bmatrix},\ \text{and}\ x_{max} = \begin{bmatrix} x_1 \\ x_2 \\ x_3 \end{bmatrix}_{max} = \begin{bmatrix} 0.4 \\ 16.3 \\ 2005 \end{bmatrix}. \tag{B.15}$$

Comparison between the identified polynomial and the experimental data is shown in Figure B.3.

B.4 Feedgas Emissions of Oxides of Nitrogen (NO_x)

In this section we identify the nonlinear static relationship that describes the feedgas NO_x generation based on four engine variables. In Section 3.2.3 we discuss the assumptions associated with the steady-state NO_x model as a function of engine speed (N), cam phasing (CAM), air fuel ratio (A/F), and manifold pressure (P_m). The identified polynomial is an eighth degree polynomial.

$$NO_x = f(N, CAM, A/F, P_m) \tag{B.16}$$

For simplicity, let

$$y =: NO_x \text{ and } x = \begin{bmatrix} x_1 \\ x_2 \\ x_3 \\ x_4 \end{bmatrix} =: \begin{bmatrix} N \\ CAM \\ A/F \\ P_m \end{bmatrix}. \tag{B.17}$$

In the least squares fit the scaled variables $\hat{y}$ and $\hat{x}$ are used to identify the coefficients associated with the best fit polynomial to the data.

$$\hat{y} = \frac{y \Leftrightarrow y_{min}}{y_{max} \Leftrightarrow y_{min}} \tag{B.18}$$

where y_{min} and y_{max} is the minimum and maximum output value of the data set used.

$$\hat{x} = \frac{x \Leftrightarrow x_{min}}{x_{max} \Leftrightarrow x_{min}} \tag{B.19}$$

where x_{min} and x_{max} is the minimum and maximum input value of the data set used.

Based on the regression analysis the function that describes the relationship between $\hat{y}$ and $\hat{x}$ is:

$$\begin{aligned}\hat{y} = {} & 0.0200 + 0.0529\hat{x}_1 \Leftrightarrow 0.0017\hat{x}_1^2 \Leftrightarrow 0.0266\hat{x}_2 + 0.0667\hat{x}_1\hat{x}_2 \Leftrightarrow 0.0946\hat{x}_1^2\hat{x}_2 \\ & + 0.1718\hat{x}_3 + 0.7840\hat{x}_1\hat{x}_3 + 0.1668\hat{x}_1^2\hat{x}_3 \Leftrightarrow 0.3265\hat{x}_2\hat{x}_3 + 0.0074\hat{x}_1\hat{x}_2\hat{x}_3 \Leftrightarrow 0.6932\hat{x}_1^2\hat{x}_2\hat{x}_3 \\ & \Leftrightarrow 0.5876\hat{x}_3^2 + 0.0256\hat{x}_1\hat{x}_3^2 \Leftrightarrow 0.2354\hat{x}_1^2\hat{x}_3^2 + 0.8155\hat{x}_2\hat{x}_3^2 \Leftrightarrow 1.9732\hat{x}_1\hat{x}_2\hat{x}_3^2 + 1.8512\hat{x}_1^2\hat{x}_2\hat{x}_3^2 \\ & + 0.2188\hat{x}_3^3 + 0.5549\hat{x}_1\hat{x}_3^3 \Leftrightarrow 0.7877\hat{x}_1^2\hat{x}_3^3 \Leftrightarrow 0.1859\hat{x}_2\hat{x}_3^3 + 0.0721\hat{x}_1\hat{x}_2\hat{x}_3^3 + 0.1120\hat{x}_1^2\hat{x}_2\hat{x}_3^3 \\ & + 0.2712\hat{x}_4 + 0.0067\hat{x}_1\hat{x}_4 + 0.0966\hat{x}_1^2\hat{x}_4 \Leftrightarrow 0.0932\hat{x}_2\hat{x}_4 \Leftrightarrow 0.7164\hat{x}_1\hat{x}_2\hat{x}_4 + 0.7201\hat{x}_1^2\hat{x}_2\hat{x}_4 \\ & \Leftrightarrow 0.6872\hat{x}_3\hat{x}_4 \Leftrightarrow 3.4572\hat{x}_1\hat{x}_3\hat{x}_4 + 0.5724\hat{x}_1^2\hat{x}_3\hat{x}_4 + 2.6223\hat{x}_2\hat{x}_3\hat{x}_4 \\ & + 1.5405\hat{x}_1\hat{x}_2\hat{x}_3\hat{x}_4 \Leftrightarrow 1.8901\hat{x}_1^2\hat{x}_2\hat{x}_3\hat{x}_4 + 11.2350\hat{x}_3^2\hat{x}_4 \Leftrightarrow 1.4304\hat{x}_1\hat{x}_3^2\hat{x}_4 + 4.1765\hat{x}_1^2\hat{x}_3^2\hat{x}_4 \\ & \Leftrightarrow 15.7908\hat{x}_2\hat{x}_3^2\hat{x}_4 + 8.1200\hat{x}_1\hat{x}_2\hat{x}_3^2\hat{x}_4 + 2.4157\hat{x}_1^2\hat{x}_2\hat{x}_3^2\hat{x}_4 \Leftrightarrow 7.8180\hat{x}_3^3\hat{x}_4 + 0.2633\hat{x}_1\hat{x}_3^3\hat{x}_4 \\ & \Leftrightarrow 1.3755\hat{x}_1^2\hat{x}_3^3\hat{x}_4 + 8.9838\hat{x}_2\hat{x}_3^3\hat{x}_4 + 0.6803\hat{x}_1\hat{x}_2\hat{x}_3^3\hat{x}_4 \Leftrightarrow 7.1907\hat{x}_1^2\hat{x}_2\hat{x}_3^3\hat{x}_4 \Leftrightarrow 0.1626\hat{x}_4^2 \\ & \Leftrightarrow 0.1804\hat{x}_1\hat{x}_4^2 \Leftrightarrow 0.0598\hat{x}_1^2\hat{x}_4^2 \Leftrightarrow 0.0399\hat{x}_2\hat{x}_4^2 + 1.3561\hat{x}_1\hat{x}_2\hat{x}_4^2 \Leftrightarrow 1.1440\hat{x}_1^2\hat{x}_2\hat{x}_4^2 \\ & \Leftrightarrow 1.0828\hat{x}_3\hat{x}_4^2 + 5.5225\hat{x}_1\hat{x}_3\hat{x}_4^2 \Leftrightarrow 0.4514\hat{x}_1^2\hat{x}_3\hat{x}_4^2 \Leftrightarrow 2.3212\hat{x}_2\hat{x}_3\hat{x}_4^2 \Leftrightarrow 3.8016\hat{x}_1\hat{x}_2\hat{x}_3\hat{x}_4^2 \\ & + 3.0169\hat{x}_1^2\hat{x}_2\hat{x}_3\hat{x}_4^2 \Leftrightarrow 4.3774\hat{x}_3^2\hat{x}_4^2 \Leftrightarrow 3.3992\hat{x}_1\hat{x}_3^2\hat{x}_4^2 \Leftrightarrow 6.3261\hat{x}_1^2\hat{x}_3^2\hat{x}_4^2 17.7500\hat{x}_2\hat{x}_3^2\hat{x}_4^2 \\ & \Leftrightarrow 4.3862\hat{x}_1\hat{x}_2\hat{x}_3^2\hat{x}_4^2 \Leftrightarrow 3.9039\hat{x}_1^2\hat{x}_2\hat{x}_3^2\hat{x}_4^2 + 3.1401\hat{x}_3^3\hat{x}_4^2 \\ & + 1.0739\hat{x}_1\hat{x}_3^3\hat{x}_4^2 + 4.6572\hat{x}_1^2\hat{x}_3^3\hat{x}_4^2 \Leftrightarrow 9.6303\hat{x}_2\hat{x}_3^3\hat{x}_4^2 \Leftrightarrow 3.2302\hat{x}_1\hat{x}_2\hat{x}_3^3\hat{x}_4^2 + 7.3144\hat{x}_1^2\hat{x}_2\hat{x}_3^3\hat{x}_4^2 \ . \end{aligned} \tag{B.20}$$

The minimum and maximum values that were used for the conversion from the actual variables (feedgas NO_x emissions and the actual inputs) to the scaled variables in the regression analysis are :

$$y_{min} = 3.67 \ , \ y_{max} = 54.09 \ ,$$

$$x_{min} = \begin{bmatrix} x_1 \\ x_2 \\ x_3 \\ x_4 \end{bmatrix}_{min} = \begin{bmatrix} 746 \\ \Leftrightarrow 0.2 \\ 11.7 \\ 0.148 \end{bmatrix} , \text{ and } x_{max} = \begin{bmatrix} x_1 \\ x_2 \\ x_3 \\ x_4 \end{bmatrix}_{max} = \begin{bmatrix} 2005 \\ 35.1 \\ 16.43 \\ 0.617 \end{bmatrix} . \tag{B.21}$$

Comparison between the identified polynomial and the experimental data is shown in Figure B.4.

B.5 Feedgas Emissions of Hydrocarbons (HC)

In this section we identify the nonlinear static relationship that describes the feedgas HC generation based on four engine variables. In Section 3.2.3 we discuss the assumptions associated with the steady-state HC model as a function of engine speed (N), cam phasing (CAM), air fuel ratio (A/F), and manifold pressure (P_m).

$$HC = f(N, CAM, A/F, P_m) \tag{B.22}$$

For simplicity, let

$$y =: HC \text{ and } x = \begin{bmatrix} x_1 \\ x_2 \\ x_3 \\ x_4 \end{bmatrix} =: \begin{bmatrix} N \\ CAM \\ A/F \\ P_m \end{bmatrix} \ . \tag{B.23}$$

In the least squares fit we used the scaled variables $\hat{y}$ and $\hat{x}$.

$$\hat{y} = \frac{y \Leftrightarrow y_{min}}{y_{max} \Leftrightarrow y_{min}} \tag{B.24}$$

where y_{min} and y_{max} is the minimum and maximum output value of the data set used.

$$\hat{x} = \frac{x \Leftrightarrow x_{min}}{x_{max} \Leftrightarrow x_{min}} \tag{B.25}$$

where x_{min} and x_{max} is the minimum and maximum input value of the data set used.

Based on the regression analysis the function that describes the relationship between $\hat{y}$ and $\hat{x}$ is:

$$\begin{aligned}\hat{y} \quad &= 0.0230 + 0.0350\hat{x}_3 \Leftrightarrow 0.0662\hat{x}_3^2 + (0.5933 \Leftrightarrow 1.1822\hat{x}_3 + 1.3418\hat{x}_3^2)\hat{x}_1 \\ &+(\Leftrightarrow 1.4062 + 3.0186\hat{x}_3 \Leftrightarrow 3.6013\hat{x}_3^2)\hat{x}_1^2 + (0.9045 \Leftrightarrow 2.1751\hat{x}_3 + 2.6315\hat{x}_3^2)\hat{x}_1^3 \\ &[+0.0171 \Leftrightarrow 0.0347\hat{x}_3 + 0.0405\hat{x}_3^2 + (\Leftrightarrow 0.1416 + 0.3203\hat{x}_3 \Leftrightarrow 0.3480\hat{x}_3^2)\hat{x}_1 \\ &+(0.3138 \Leftrightarrow 0.7474\hat{x}_3 + 0.7988\hat{x}_3^2)\hat{x}_1^2 + (\Leftrightarrow 0.1891 + 0.4611\hat{x}_3 \Leftrightarrow 0.4906\hat{x}_3^2)\hat{x}_1^3]\frac{1}{\hat{x}_4} \\ &\Leftrightarrow 0.6905\hat{x}_2 + 0.6338\frac{\hat{x}_2}{\hat{x}_4^{1/16}}\end{aligned} \tag{B.26}$$

The minimum and maximum values that were used for the conversion from the actual variables (feedgas HC emissions and the actual inputs) to the scaled variables in the regression analysis are :

$$y_{min} = 2.59 \ , \ y_{max} = 97.05 \ ,$$

$$x_{min} = \begin{bmatrix} x_1 \\ x_2 \\ x_3 \\ x_4 \end{bmatrix}_{min} = \begin{bmatrix} 746 \\ \Leftrightarrow 0.2 \\ 11.7 \\ 0.148 \end{bmatrix}, \text{ and } x_{max} = \begin{bmatrix} x_1 \\ x_2 \\ x_3 \\ x_4 \end{bmatrix}_{max} = \begin{bmatrix} 2005 \\ 35.1 \\ 16.43 \\ 0.617 \end{bmatrix}. \tag{B.27}$$

Comparison between the identified polynomial and the experimental data is shown in Figure B.5.

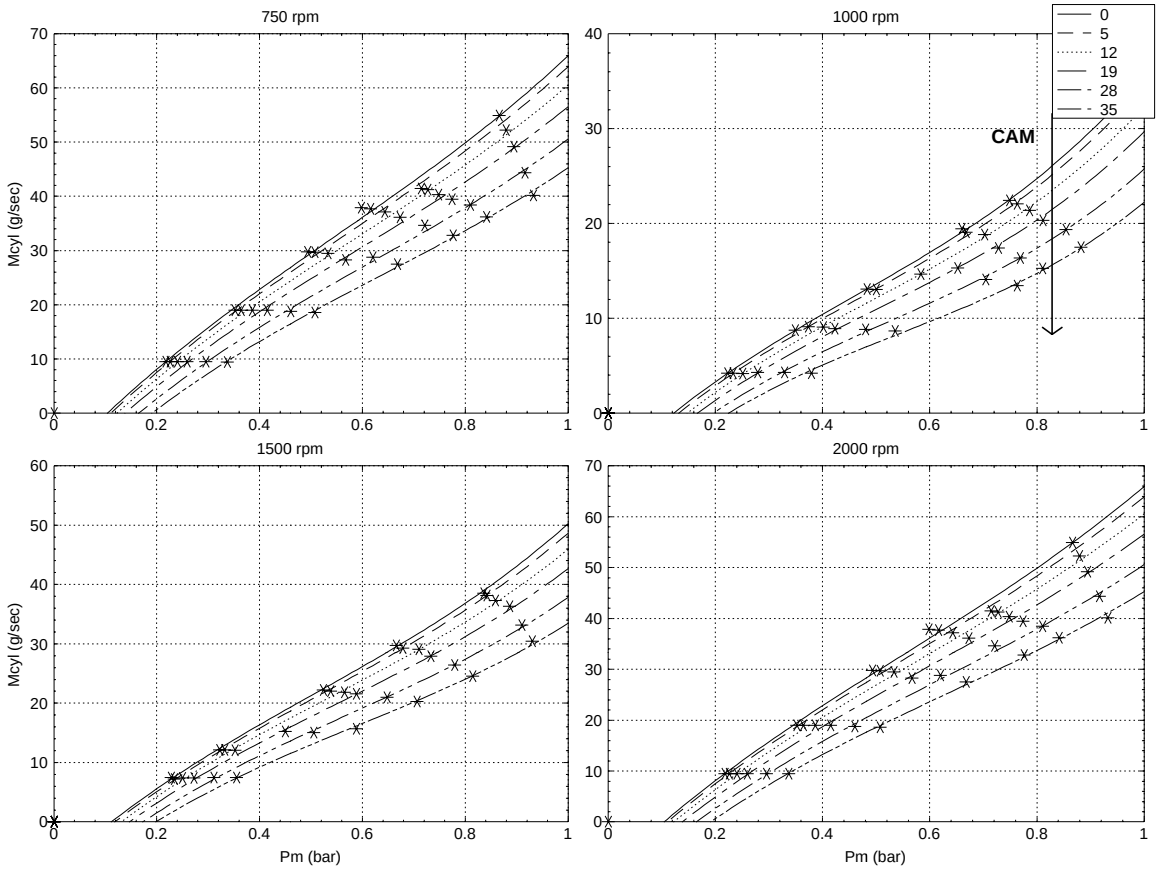

Figure B.2: Comparison between the identified polynomial $\dot{m}_{cyl}$ and the experimental data.

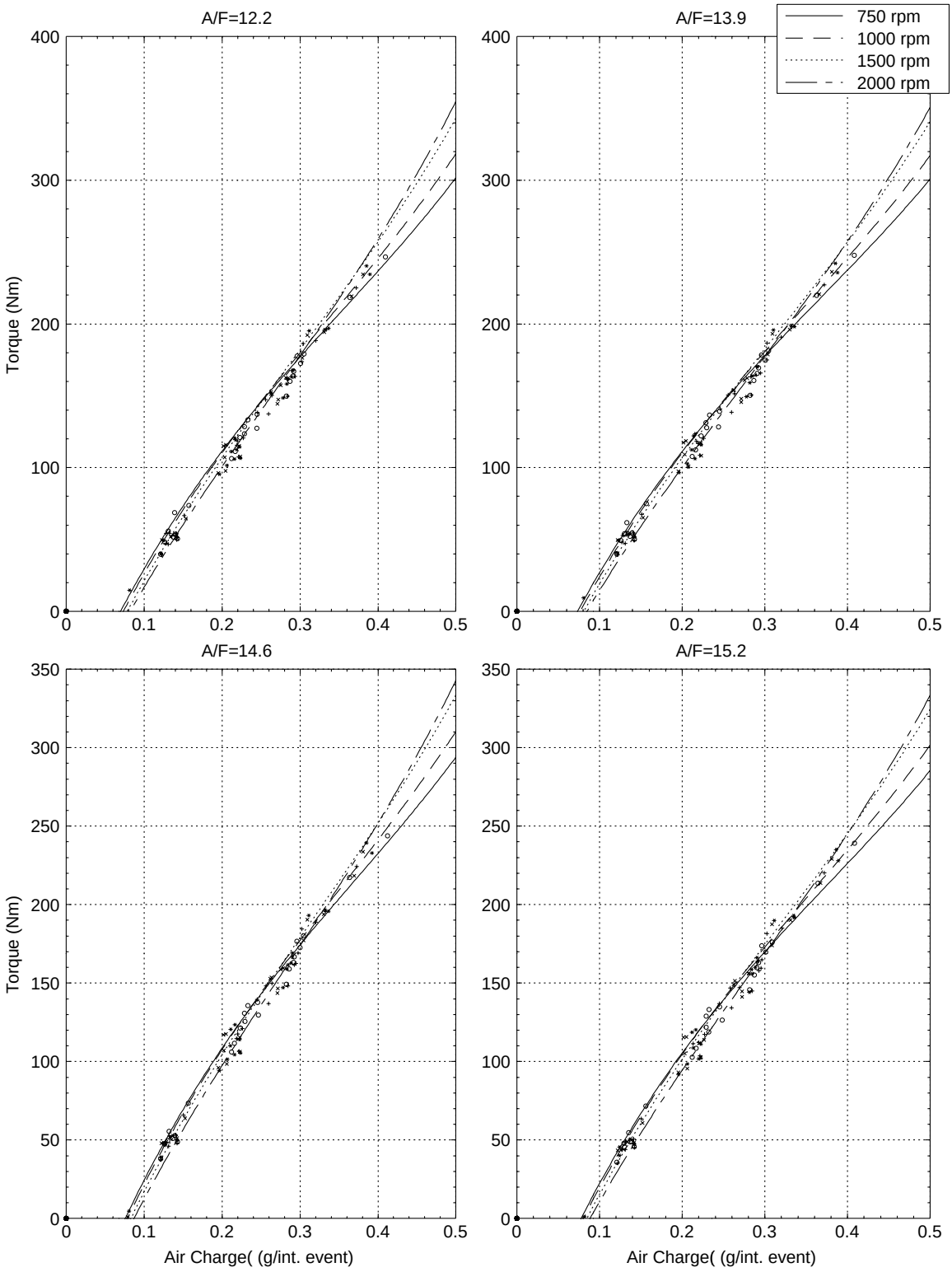

Figure B.3: Comparison between the identified polynomial T_b and the experimental data.

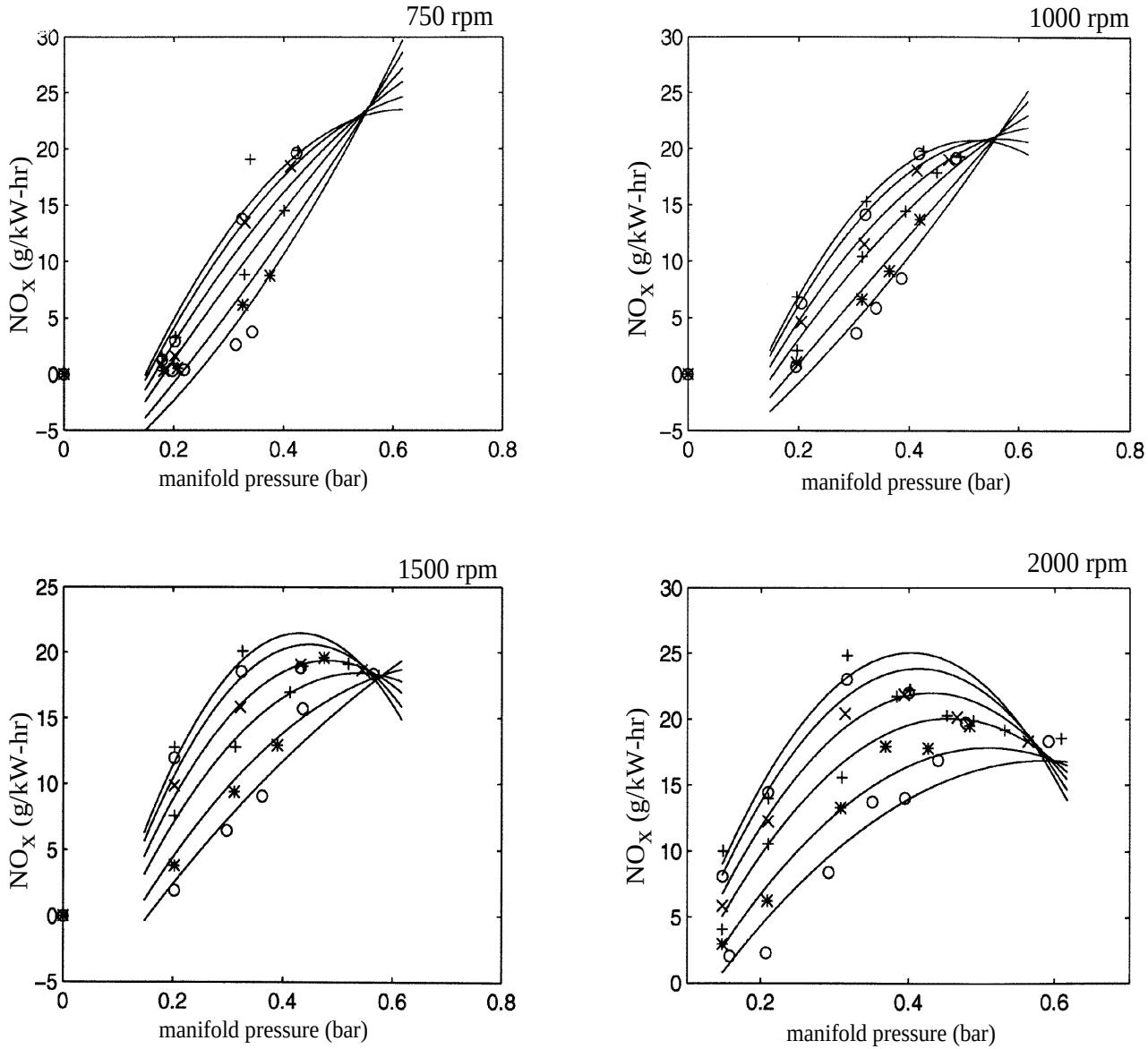

Figure B.4: Comparison between the identified feedgas NO_x and the experimental data.

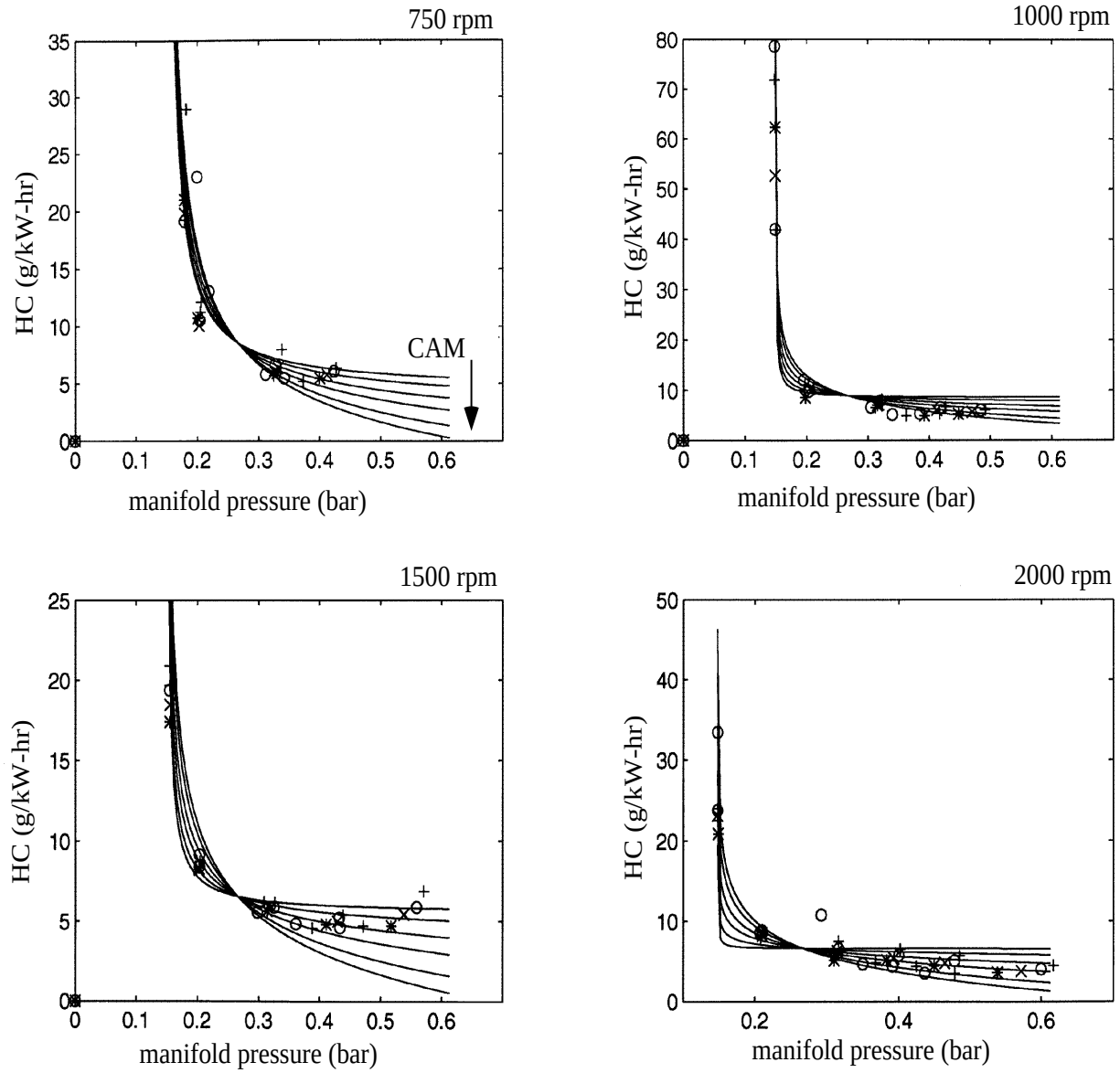

Figure B.5: Comparison between the identified feedgas HC and the experimental data.

APPENDIX C

Regression Analysis and Simulation Modeling

C.1 Overview and Organization

The programs developed for the regression analysis of the data and the resulting nonlinear static maps are described in this appendix. The information in this appendix is complementary to Chapter 3, and provides all the technical details necessary to perform a similar task. Furthermore, we provide the programming of the VCT engine model in System-Build environment. The programs to access the data in order to identify the nonlinear static relationships were written in Fortran to facilitate the 5-dimensional representation of the array that contains all the experimental static data. The input and output arrays are stored in files that can be loaded in the Matlab environment where the regression analysis is performed. The regression analysis is a least squares estimation performed using Matlab script files. Matlab was chosen at the time to be the best environment for the regression analysis due to the advanced visualization toolbox. The identification process consists of two iterative stages: (i) finding the best least squares fit to a polynomial, and (ii) altering the polynomial in order to choose the function that best approximates the shape that the data dictates. The advanced graphical interface facilitates the iteration process by allowing the plotting and evaluation of the best fit polynomial.

The identified polynomial coefficients are stored and manipulated in MatrixX script files. The script files are used in the programming of the simulation VCT engine model. The simulation model is programmed and stored in the System-Build simulation environment of MatrixX. Here, we would like to stress the need for an integrated environment that can access multi-dimensional arrays, perform the identification processes with flexibility, and synthesize the simulation model. The creation of such an integrated and flexible environment will be a useful tool for the development of powertrain control systems.

In the next section the methodology for the regression analysis is explained and the least squares problem is defined. The Fortran program used to access the experimental data is documented in Section 3. In Sections 4-8 we include all the programs and detailed explanation of the identification process of the five nonlinear static maps. Each section corresponds to one nonlinear static map and consists of two subsections. The first subsection in each of Sections 4 to 8 contains the Fortran and Matlab programs used for the regression analysis. In the second subsection of each section we illustrate the System-Build simulation model of the nonlinear static relationships.

C.2 Least Squares Estimate

The least squares approach of fitting data to a polynomial starts with the selection of the polynomial. The process of selecting the correct polynomial requires inspection of the data, and is facilitated by the knowledge of any physical laws governing the input-output relationship. Understanding the input-output relationship based on physical laws often results in a lower order polynomial that can be used in other sets of data, or even, different engine configurations and calibrations. Inspection of the data is crucial for the determination of the appropriate polynomial, because it allows the identification of inconsistent sets of data, and regions with significantly different input-output behavior.

Selecting the appropriate input-output relationship is equivalent to specifying the base functions $f_1, \ldots, f_n$, where $f_i \in \mathbb{R}^p \rightarrow \mathbb{R}$, and p is the number of input variables. We need to identify the function $F(\underline{\eta}) =: F([\eta_1, \ldots, \eta_p]')$, where $F : \mathbb{R}^p \rightarrow \mathbb{R}$ with $F = span\{f_1, \ldots, f_n\}$ or $F(\underline{\eta}) = w_1 f_1(\underline{\eta}) + \ldots + w_n f_n(\underline{\eta})$, that describes the exact input-output relationship based on the set of data $(\underline{\eta}_i, b_i)$, for $i = 1, \ldots, m$. We can write the resulting set of equations as :

$$\left.\begin{array}{lll} b_1 & = F(\underline{\eta}_1) \\ \vdots & \vdots \\ b_m & = F(\underline{\eta}_m) \end{array}\right\} \Rightarrow \begin{bmatrix} b_1 \\ \vdots \\ b_m \end{bmatrix} = \underbrace{\begin{bmatrix} f_1(\underline{\eta}_1) & \ldots & f_n(\underline{\eta}_1) \\ \vdots & & \vdots \\ f_1(\underline{\eta}_m) & \ldots & f_n(\underline{\eta}_m) \end{bmatrix}}_{G} \cdot \begin{bmatrix} w_1 \\ \vdots \\ w_m \end{bmatrix} \tag{C.1}$$

or simply

$$b = G \cdot w \tag{C.2}$$

We need to find the optimal solution w^* of the set of equations $G \cdot w = b$, where $G \in \mathbb{R}^{m \times n}$, with m: # of observations, and n : # of unknowns, with $m \geq n$.

Most probably b is not a combination of the columns of G, and this will result to an inconsistent problem. The least squares solution to an overdetermined system (regression analysis) is to project b onto the range of G, or to find a point u on the range of G ($u = G \cdot w^*$) that is closest to b (see Fig. C.1). So choose w^* such that :

$$\| Gw \Leftrightarrow b \|_{min} = \| Gw^* \Leftrightarrow b \| \tag{C.3}$$

The w^* must be the projection of b onto the column space of G, and the error vector $Gw^* \Leftrightarrow b$ must be perpendicular to that space. In other words,

$$\forall t \in \mathbb{R}^n \quad (Gw^* \Leftrightarrow b) \perp Gt \quad \Leftrightarrow \tag{C.4}$$

$$\forall t \in \mathbb{R}^n \quad (Gt)^\top (Gw^* \Leftrightarrow b) = 0 \quad \Leftrightarrow \quad t^\top (G^\top G w^* \Leftrightarrow G^\top b) = 0 \Leftrightarrow \tag{C.5}$$

$$G^\top G w^* \Leftrightarrow G^\top b = 0 \tag{C.6}$$

Which leads us to the least squares solution to an inconsistent system $Gw = b$ of m equations in n unknowns given by the normal equations: $G^\top G w^* = G^\top b$. If the columns of G are linearly independent then $G^\top G$ is invertible and the unique least squares solution is $w^* = (G^\top G)^{-1} G^\top b$.

In the above analysis we assumed that the data collected are equivalent. Sometimes we need to assign different weights on the collected data based on the confidence level associated with each pair of data. This leads to the weighted least squares solution $WGw^* = Wb$ where

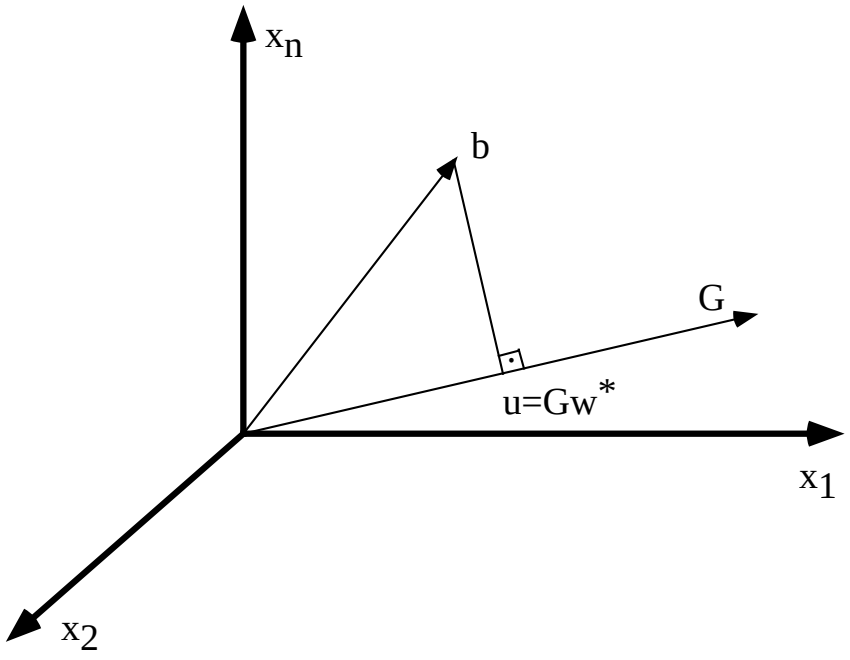

Figure C.1: The least squares solution w^* to an overdetermined system $Gw = b$.

W is a diagonal matrix containing the weights. In the following work we considered all the data equivalent ($W = I_{m \times m}$).

The least squares solution involves the inversion of the matrix $G^\top G$. It is essential to keep the condition number of the matrix $G^\top G$ as small as possible to achieve stable numerical results. For this reason it is important to scale the variables used. In the following work there is a significant variation of the data magnitude (engine speed varies from 750 rpm to 2000 rpm, and air flow varies from 0.05 g/int.event to 0.4 g/int.event), so we scaled all the variables to a uniform range from 0 to 1.

C.3 Processing the Data : Fortran Code

The collected data from the experiments is loaded in a matrix form (2-dimensional matrix), but the fact that we have 4 independent variables requires a flexible program that can extract any sequence of data and facilitate the plotting and the regression analysis. For this purpose a program was developed that accesses the data based on the required input-output relationship and its associated dependency to the independent engine variables. The program follows:

```
------------------------------------------------------
      program MAP_plot
      real out1(4,6,6,5,14),x1(6,6),x2(6,6),y(6,6)
c
c     ==========================================
c     Load the data from out1.dat
c     Indices : i_N, j_TP, k_CAM, l_A/F, m_OUTPUT
c     Creates the 5th dimensional array "out1"
c     ------------------------------------------
      open(13,file='out1.dat',status='old')
      i=1
```

```
      do 10 j=1,4
         do 10 k=1,6
            do 10 l=1,5
               read(13,*)(out1(i,j,k,l,m),m=1,14)
 10   continue
      do 20 i=2,3
         do 20 j=1,5
            do 20 k=1,6
               do 20 l=1,5
                  read(13,*)(out1(i,j,k,l,m),m=1,14)
 20   continue
      i=4
      do 30 j=1,6
          do 30 k=1,6
            do 30 l=1,5
                  read(13,*)(out1(i,j,k,l,m),m=1,14)
 30   continue
      close(13)
c     ================================================
c     table_cr(outx;y,x1,x2,ii,jj)
c     Create 3 tamplets of data but it can be expanded
c     ------------------------------------------------
      write(*,*)'Output, nout (5-10)'
      read(*,*) nout
c     The location of the output.
      write(*,*) 'Fist Coordinate, nx1 (1-14)'
      read(*,*)  nx1
c     The location of the first variable
      write(*,*) 'Second Coordinate, nx2 (1-14)'
      read(*,*) nx2
c     The location of the second variable
      write(*,*) 'First Running Index, ni1 (1-4) '
      read(*,*) ni1
c     Inspect the input-output relationship y=f(x1,x2) vs. the
c     independent variable ni1 (ex. for engine speed ni1=1)
      write(*,*) 'Second Running Index, ni2 (1-4)'
      read(*,*) ni2
c     Inspect the input-output relationship y=f(x1,x2) vs. the
c     independent variable ni2 (ex. for throttle position  ni2=2))
      write(*,*) 'First Fixed Value, nv1'
      read(*,*) nv1
c     Inspect the input-output relationship y=f(x1,x2) for fixed
c     independent variable nv1 (ex. for CAM=0 then nv1=1)
      write(*,*) 'Second Fixed Value, nv2'
      read(*,*) nv2
c     Inspect the input-output relationship y=f(x1,x2) for fixed
c     independent variable nv1 (ex. for A/F=14.64 then nv2=3)
c
      if ((ni1.eq.1).and.(ni2.eq.2)) then
         ii=4
         jj=6
         do 40 i=1,ii
            do 40 j=1,jj
               y(i,j)=out1(i,j,nv1,nv2,nout)
               x1(i,j)=out1(i,j,nv1,nv2,nx1)
               x2(i,j)=out1(i,j,nv1,nv2,nx2)
 40            continue
       endif
      if ((ni1.eq.2).and.(ni2.eq.1)) then
```

```
        ii=6
        jj=4
        do 45 i=1,ii
           do 45 j=1,jj
              y(i,j)=out1(j,i,nv1,nv2,nout)
              x1(i,j)=out1(j,i,nv1,nv2,nx1)
              x2(i,j)=out1(j,i,nv1,nv2,nx2)
45         continue
      endif
      if ((ni1.eq.1).and.(ni2.eq.3)) then
        ii=4
        jj=6
        do 50 i=1,ii
           do 50 j=1,jj
              y(i,j)=out1(i,nv1,j,nv2,nout)
              x1(i,j)=out1(i,nv1,j,nv2,nx1)
              x2(i,j)=out1(i,nv1,j,nv2,nx2)
50            continue
      endif
      if ((ni1.eq.3).and.(ni2.eq.1)) then
        write(*,*) '(3,1)'
        ii=6
        jj=4
        do 55 i=1,ii
           do 55 j=1,jj
              y(i,j)=out1(j,nv1,i,nv2,nout)
              x1(i,j)=out1(j,nv1,i,nv2,nx1)
              x2(i,j)=out1(j,nv1,i,nv2,nx2)
55         continue
      endif
      if ((ni1.eq.1).and.(ni2.eq.4)) then
        ii=4
        jj=5
        do 60 i=1,ii
           do 60 j=1,jj
              y(i,j)=out1(i,nv1,nv2,j,nout)
              x1(i,j)=out1(i,nv1,nv2,j,nx1)
              x2(i,j)=out1(i,nv1,nv2,j,nx2)
60            continue
      endif
      if ((ni1.eq.4).and.(ni2.eq.1)) then
        ii=5
        jj=4
        do 65 i=1,ii
           do 65 j=1,jj
              y(i,j)=out1(j,nv1,nv2,i,nout)
              x1(i,j)=out1(j,nv1,nv2,i,nx1)
              x2(i,j)=out1(j,nv1,nv2,i,nx2)
65         continue
      endif
      if ((ni1.eq.2).and.(ni2.eq.3)) then
        ii=6
        jj=6
        do 70 i=1,ii
           do 70 j=1,jj
              y(i,j)=out1(nv1,i,j,nv2,nout)
              x1(i,j)=out1(nv1,i,j,nv2,nx1)
              x2(i,j)=out1(nv1,i,j,nv2,nx2)
70            continue
```

```
      endif
      if ((ni1.eq.3).and.(ni2.eq.2)) then
         ii=6
         jj=6
         do 75 i=1,ii
            do 75 j=1,jj
               y(i,j)=out1(nv1,j,i,nv2,nout)
               x1(i,j)=out1(nv1,j,i,nv2,nx1)
               x2(i,j)=out1(nv1,j,i,nv2,nx2)
 75         continue
      endif
      if ((ni1.eq.2).and.(ni2.eq.4)) then
         ii=6
         jj=5
         do 80 i=1,ii
            do 80 j=1,jj
               y(i,j)=out1(nv1,i,nv2,j,nout)
               x1(i,j)=out1(nv1,i,nv2,j,nx1)
               x2(i,j)=out1(nv1,i,nv2,j,nx2)
 80         continue
      endif
      if ((ni1.eq.4).and.(ni2.eq.2)) then
         ii=5
         jj=6
         do 85 i=1,ii
            do 85 j=1,jj
               y(i,j)=out1(nv1,j,nv2,i,nout)
               x1(i,j)=out1(nv1,j,nv2,i,nx1)
               x2(i,j)=out1(nv1,j,nv2,i,nx2)
 85         continue
      endif
      if ((ni1.eq.3).and.(ni2.eq.4)) then
         ii=6
         jj=5
         do 90 i=1,ii
            do 90 j=1,jj
               y(i,j)=out1(nv1,nv2,i,j,nout)
               x1(i,j)=out1(nv1,nv2,i,j,nx1)
               x2(i,j)=out1(nv1,nv2,i,j,nx2)
 90         continue
      endif
      if ((ni1.eq.4).and.(ni2.eq.3)) then
         ii=5
         jj=6
         do 95 i=1,ii
            do 95 j=1,jj
               y(i,j)=out1(nv1,nv2,j,i,nout)
               x1(i,j)=out1(nv1,nv2,j,i,nx1)
               x2(i,j)=out1(nv1,nv2,j,i,nx2)
 95         continue
      endif
c     ============================================
c     Write the tamplets in Map.dat file
c     --------------------------------------------
      open(14,file='Map.dat',status='unknown')
      do 100 i=1,ii
         write(14,*)(y(i,j),j=1,jj)
 100     continue
      do 110 i=1,ii
```

```
          write(14,*)(x1(i,j),j=1,jj)
 110      continue
       do 120 i=1,ii
          write(14,*)(x2(i,j),j=1,jj)
 120      continue
      stop
      end
```

C.4 Mass Air Flow Rate through the Throttle Body : Code

In Section 3.2.1 we explain this relationship based on physical laws. The mass air flow through the throttle body in sonic flow is a function of throttle position ($\dot{m}_\theta = g_2(\theta)$), whereas in subsonic flow it is a function of both manifold pressure and throttle position ($\dot{m}_\theta = g_1(P_m) \cdot g_2(\theta)$). The relationship $g_1(P_m)$ has been specified by Novak in [56] and is used to convert all the data to equivalent sonic flow data which we can use for the identification of the function $g_2(\theta)$. The identification process follows in detail.

C.4.1 Script Files

The Matlab script file that is used for the identification of the nonlinear static map $g_2(\theta)$ is as follows :

```
===============vct_dir/data.dir/mth_regr.m================================
function[co_mth,y_max,y_min]=mth_regr(opt)
% Run program MAP_plot with output file mth_data and the following inputs:
%      nout=8 MAF (f/sec)
%      nx1=13 CAM_actual (degrees)
%      nx2=7 MAP (bar)
%      nx3=12 N_actual (rpm)
%      ni1=1 first index: engine speed (N)
%      ni2=2 second index :throttle position (TP)
%      nv2=3 fixed index : A/F
%out(8-->mth
%     7-->pm
%    11-->tp
%     2-->itp
%     1-->iN
%     2-->CAM
%     3-->A/F=14.64)
load mth_data.dat
mth=mth_data(1:6,:);
pm=mth_data(7:12,:);
tp=mth_data(13:18,:);

[i,j]=find(pm>0);
N=length(i);
for k=1:N
y(k,3)=mth(i(k),j(k));...
y(k,2)=pm(i(k),j(k));...
y(k,1)=tp(i(k),j(k));...
end
N=length(y(:,2));
```

```
% Find the correction coefficient for the subsonic flow.
for k=1:N
    if y(k,2)>0.5;
       cf(k)=2*sqrt(y(k,2)-y(k,2)^2);
    else
       cf(k)=1;
    end
end
% Corrected air flow for subsonic flow (only)
y(:,3)=y(:,3)./cf';
%
% Scale the variables for the least squares estimation
for i=1:2:3
y_max(i)=max(y(:,i));...
y_min(i)=min(y(:,i));...
sc_y(:,i)=(y(:,i)-y_min(i))./(y_max(i)-y_min(i));...
end
%------------
%mth_a provides the structure of the regressing polynomial : mth=P(theta)
%The overdetermined set of equations you solve is :  A*co_MTH=sc_Y,
%where co_MTH are the coefficients to be determined.
%The solution in Least Squares sense is co_MTH=pinv(A)*sc_Y.
%
a=mth_a(sc_y(:,1));
co_mth=a\sc_y(:,3);
%------------
%Statistical measures for the regression analusis
% It doesn't mean much if you don't look at the plots
% of estimated and actual data.
%
sc_yh=a*co_mth;
yh(:)=sc_yh(:)*(y_max(3)-y_min(3))+y_min(3);
res=yh-y(:,3);
res=res'*res;
res=sqrt(res)/N;
%------------
% Plot the identified funtion with the actual data
% Introduce the estimated polynomial and evaluate at a dense interval.
%
if opt==1
sc_ye(:,1)=[0:0.01:1]';
ae=mth_a(sc_ye(:,1));
sc_ye(:,3)=ae*co_mth;
for i=1:2:3
ye(:,i)=sc_ye(:,i)*(y_max(i)-y_min(i))+y_min(i);
end
% Plot true-estimated values.
plot(y(:,1),y(:,3),'b*',ye(:,1),ye(:,3));
end
=========End of vct_dir/data.dir/mth_regr.m=========================
============vct_dir/data.dir/mth_a.m================================
function a=mth_a(x)
%Calculates the matrix of coefficients for mth=P(theta)
a=[ones(size(x)) x x.^2 x.^3];
========End of vct_dir/data.dir/mth_a.m=============================
```

C.4.2 Simulation of $\dot{m}_\theta$ in System-Build

To construct the simulation model of the mass air flow through the throttle body during sonic flow (i.e. to program the $\dot{m}_\theta = g_2(\theta)$ relationship) shown in Figure C.2 we used the following MatrixX script commands in the file `vct_dir/vct_model.dir/vct_polyn.ms`.

```
=================vct_dir/vmodel.dir/vct_polyn.ms=========================
%Build  the mth_func (Mass air flow through the THrottle body FUNCtion)]
%------------------  -                        --           ----
%Take the data from the mth_regr.m files located in ../data.dir
%and paste them here. Here actually you are loading the regression
%analysis data (made in MATLAB) environment to the MATRIXx environment.
%
v_mth_co=[ 0.0062 ; 0.0537 ; 1.6134 ; -0.6994];
v_mth_max=[160.0000 ; 52.0558];
v_mth_min=[3.0000  ;  4.0200];
%Build the variables as they appear in vct_tablet.bl (the simulation
%model in System-Build).
%
%Input scaling
v_mthxsp=1/(v_mth_max(1)-v_mth_min(1));
v_mthx1sp=-v_mth_min(1)/(v_mth_max(1)-v_mth_min(1));
%The polynomial coefficients
v_mthcosp=v_mth_co';
%Output scaling
v_mthysp=(v_mth_max(2)-v_mth_min(2));
v_mthyysp=v_mth_min(2);
===========End of vct_dir/vmodel.dir/vct_polyn.ms============================
```

C.5 Engine Pumping Mass Air Flow Rate : Codes

In Section 3.2.1 we described the mass air flow rate into the cylinders as a function of cam phasing (CAM), manifold pressure (P_m), and engine speed (N). The resulting polynomial is of degree three, and a third order polynomial in each individual variable:

$$\dot{m}_{cyl} = F(1, CAM, CAM^2, CAM^3, P_m, P_m^2, P_m^3, N, N^2, N^3) \quad . \tag{C.7}$$

The identification algorithm follows in detail.

C.5.1 Script Files

The following fortran program is a modification of the program `MAP_plot`; it is used to access all the necessary sequences of data for the $\dot{m}_{cyl}$ identification.

```
=============vct_dir/data.dir/mcyl_plot.f=============================
      program mcyl_plot
      real out1(4,6,6,5,14),x1(24,6),x2(24,6),x3(24,6),y(24,6)
c
c     ==========================================
c     Load the data from out1.dat
c     Indices : i_N, j_TP, k_CAM, l_A/F, m_OUTPUT
c     Create the 5th dimensional array "out1"
c     ------------------------------------------
      open(13,file='out1.dat',status='old')
      i=1
```

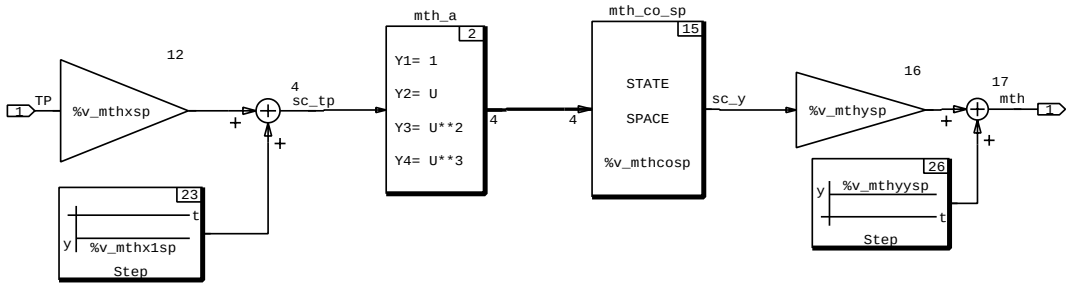

Figure C.2: Simulation model of the mass air flow through the throttle body during sonic flow programmed in the System-Build environment.

```
      do 10 j=1,4
         do 10 k=1,6
            do 10 l=1,5
               read(13,*)(out1(i,j,k,l,m),m=1,14)
  10   continue
      do 20 i=2,3
         do 20 j=1,5
            do 20 k=1,6
               do 20 l=1,5
                  read(13,*)(out1(i,j,k,l,m),m=1,14)
 20   continue
      i=4
      do 30 j=1,6
          do 30 k=1,6
            do 30 l=1,5
                  read(13,*)(out1(i,j,k,l,m),m=1,14)
 30   continue
      close(13)
c     ============================================
c     table_cr(outx;y,x1,x2,ii,jj)
c     Create 6 tablets of data
c     --------------------------------------------
      nout=8 c MAF (g/sec)
      nx1=13 c CAM_actual (degrees)
      nx2=7 c MAP (bar)
      nx3=12 c N_actual (rpm)
      ni1=1 c first index: engine speed (N)
```

```
      ni2=2 c second index :throttle position (TP)
      nv2=3 c fixed index : A/F
         nn=1
         ii=4
         jj=6
         do 40 k=1,6
         do 38 i=1,ii
            do 35 j=1,jj
               y(nn,j)=out1(i,j,k,nv2,nout)
               x1(nn,j)=out1(i,j,k,nv2,nx1)
               x2(nn,j)=out1(i,j,k,nv2,nx2)
               x3(nn,j)=out1(i,j,k,nv2,nx3)
 35            continue
               nn=nn+1
 38            continue
 40            continue
c     ============================================
c     Write the tablets in mcyl_map.dat file
c     --------------------------------------------
       open(14,file='mcyl_map.dat',status='unknown')
       do 100 i=1,24
          write(14,*)(y(i,j),j=1,jj)
 100      continue
       do 110 i=1,24
          write(14,*)(x1(i,j),j=1,jj)
 110      continue
       do 120 i=1,24
          write(14,*)(x2(i,j),j=1,jj)
 120      continue
       do 130 i=1,24
          write(14,*)(x3(i,j),j=1,jj)
 130      continue
      stop
      end
=========End of vct_dir/data.dir/mcyl_plot.f==========================
```

The following Matlab script files are used for the identification of the nonlinear static map $\dot{m}_{cyl} = F(1, CAM, CAM^2, CAM^3, P_m, P_m^2, P_m^3, N, N^2, N^3)$. Furthermore, the last part of the following Matlab script file is used for the evaluation of the model goodness based on plotting the best fit polynomial versus the actual data.

```
==============vct_dir/data.dir/mcyl_regr.m============================
function[co_mcyl,y_max,y_min,res,R,N]=mcyl_regr(opt)
load mcyl_map.dat;
mcyl=mcyl_map(1:24,:);
ca=mcyl_map(25:48,:);
pm=mcyl_map(49:72,:);
rpm=mcyl_map(73:96,:);
[i,j]=find(pm>0);
N=length(i);
for k=1:N
y(k,4)=mcyl(i(k),j(k));...
y(k,3)=rpm(i(k),j(k));...
y(k,2)=pm(i(k),j(k));...
y(k,1)=ca(i(k),j(k));...
end
% Scale the variables for the least squares estimation
y_max=[35,1,2000,max(y(:,4))]';
y_min=[0,0,0,min(y(:,4))]';
```

```
for i=1:4
sc_y(:,i)=(y(:,i)-y_min(i))/(y_max(i)-y_min(i));
end
%-----------
%mcyl_a provides the structure of the regressing polynomial : mcyl=P(CAM,Pm,N)
%The overdetermined set of equations you solve is :  A*co_MCYL=sc_Y,
%where co_CYL are the coefficients to be determined.
%The solution in Least Squares sense is co_MTH=pinv(A)*sc_Y.
%
a=mcyl_a(sc_y(:,1),sc_y(:,2),sc_y(:,3));
co_mcyl=a\sc_y(:,4);
%-----------
%Calculate the residual
%
sc_yh=a*co_mcyl;
yh(:)=sc_yh(:)*(y_max(4)-y_min(4))+y_min(4);
res=yh-y(:,4);
R=max(res);
res=res'*res;
res=sqrt(res)/N;
%----------
if opt==1
% Introduce the estimated polynomial
% evaluated at a dense interval.
CAMprime=[0 5 12 19 28 35]'; %CAM values
ye(:,2)=[0:0.01:1]'; %2nd variable :Man. Pres.
sc_ye(:,2)=ye(:,2); %No need to scale Manif. Pres.
ye(:,3)=2000*ones(size(ye(:,2)));%Engine speed (N=2000 rpm)
sc_ye(:,3)=ye(:,3)/2000; %Scale the 3rd variable (engine speed)
for k=1:6
    ye(:,1)=CAMprime(k)*ones(size(ye(:,2)));... %1st variable: cam phasing
    sc_ye(:,1)=ye(:,1)/35;...  %Scale the 1st variable
    ae=mcyl_a(sc_ye(:,1),sc_ye(:,2),sc_ye(:,3));...
    sc_ye(:,4)=ae*co_mcyl;...
    ye(:,4)=sc_ye(:,4)*(y_max(4)-y_min(4))+y_min(4);...
    comp_y(:,k)=ye(:,4); %Values of the identified function
end
%Create the array of data to be plotted versus
% estimated data.
%N=750 , 1000 , 1500 , 2000 RPM
%k=1   ,  2   ,   3  ,   4
k=4;
l=1;
for n=1:6
    nn=4*l-(4-k);...
    pm_plot(:,l)=pm(nn,:)';...
    mcyl_plot(:,l)=mcyl(nn,:)';...
    l=l+1;...
end
plot(ye(:,2),comp_y,pm_plot,mcyl_plot,'b*');
end
==========End of vct_dir/data.dir/mcyl_regr.m======================
=================vct_dir/data.dir/mcyl_a.m=========================
function a=mcyl_a(x1,x2,x3)
%Calculates the matrix of coefficients for mcyl
a=[ones(size(x1)) x1 x2 x3 ...
x1.*x3 x1.*x2 x2.*x3 ...
x1.^2 x2.^2 x3.^2 ...
x1.^2.*x3 x1.^2.*x2 x3.^2.*x1 x3.^2.*x2 x2.^2.*x1 x2.^2.*x3 ....
```

```
x1.*x2.*x3 x1.^3 x2.^3 x3.^3];
==========End of vct_dir/data.dir/mcyl_a.m=======================
```

C.5.2 Simulation of $\dot{m}_{cyl}$ in System-Build

To construct the simulation model of the engine pumping mass air flow shown in Figure C.3 (i.e. to program the $\dot{m}_{cyl} = F(1, CAM, CAM^2, CAM^3, P_m, P_m^2, P_m^3, N, N^2, N^3)$ relationship) we used the following MatrixX script commands in the file `vct_dir/vct_model.dir/vct_polyn.ms`.

```
==================vct_dir/vmodel.dir/vct_polyn.ms==============================
%Build the \dot{m}_{cyl}$ (Mass air flow into the CYLinders)
%------------------------  -                       ---
%Take the data from the mcyl_regr.m files located in ../data.dir
%and paste them here. Here actually you are loading the regression
%analysis data (made in MATLAB) environment to the MATRIXx environment.
%
v_mcyl_co=[-0.1231;-0.1088;0.3396;-0.1386;0.1438;0.1899;1.4548;0.0186;-0.8495;
-0.0080;-0.0854;-0.0962;-0.0992;0.1855;-0.1881;-0.4097;-0.1900;0.0121;0.7600;0.0043];
v_mcyl_max=1.0e+03 *[0.0350;0.0010;2.0000;0.0549];
v_mcyl_min=[0;0;0;3.6700];
%
%Build the variables as they appear in vct_tablet.bl (the simulation
%model in System-Build).
%
%Input scaling
v_mcylx1=1/(v_mcyl_max(1)-v_mcyl_min(1));
v_mcylx2=1/(v_mcyl_max(2)-v_mcyl_min(2));
v_mcylx3=1/(v_mcyl_max(3)-v_mcyl_min(3));
v_mcylxsp=[v_mcylx1 0 0;0 v_mcylx2 0; 0 0 v_mcylx3];
v_mcylx1sp=-v_mcyl_min(1)/(v_mcyl_max(1)-v_mcyl_min(1));
v_mcylx2sp=-v_mcyl_min(2)/(v_mcyl_max(2)-v_mcyl_min(2));
v_mcylx3sp=-v_mcyl_min(3)/(v_mcyl_max(3)-v_mcyl_min(3));
%
%The polynomial coefficients
v_mcylcosp=v_mcyl_co';
%
%Output scaling
v_mcylysp=(v_mcyl_max(4)-v_mcyl_min(4));
v_mcylyysp=v_mcyl_min(4);
==========End of vct_dir/vmodel.dir/vct_polyn.ms==============================
```

C.6 Torque Generation : Codes

In Section 3.2.2 we state all the assumptions associated with the uniform brake torque generation under quasi-steady conditions. We should mention here that generated torque is an implicit function of spark timing, since spark timing is scheduled at MBT for all the experiments. The modeled torque equation is a polynomial of degree three, and a third order polynomial in each individual variable :

$$T_b = F(1, m_a, {m_a}^2, {m_a}^3, A/F, A/F^2, A/F^3, N, N^2, N^3) \quad . \tag{C.8}$$

The identification algorithm follows in detail.

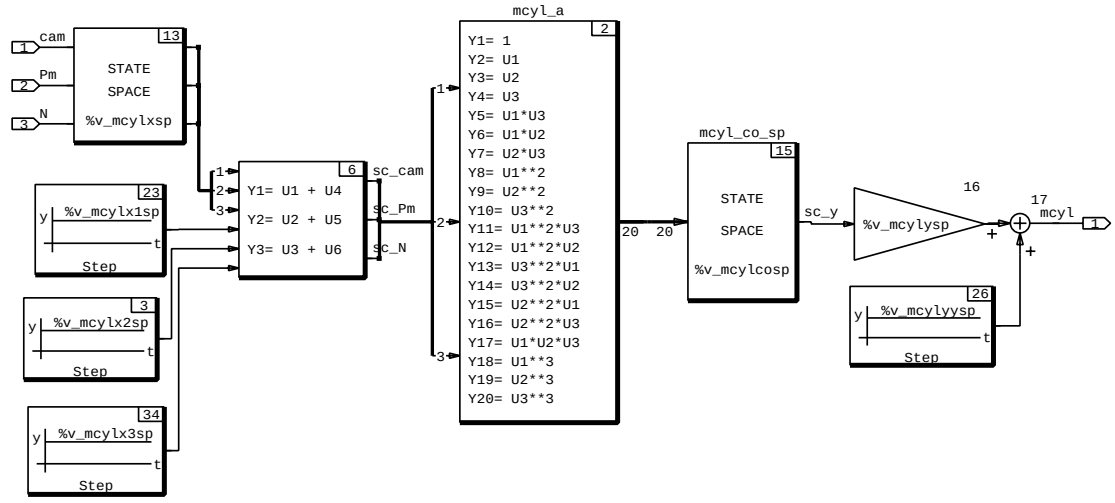

Figure C.3: Simulation model of the engine pumping mass air flow rate programmed in the System-Build environment.

C.6.1 Script Files

The following fortran program is a modification of the program `MAP_plot` shown in Appendix B, and is used to access all the necessary sequences of data for the identification of the torque generation model.

```
==============vct_dir/data.dir/tq_plot.f=================================
      program tq_plot
      real x1(6,6),x2(6,6),x3(6,6),x4(6,6)
      real y(6,6),out1(4,6,6,5,14)
c     ------------------------------------------
c     Load the data from out1.dat
c     ------------------------------------------
      open(13,file='out1.dat',status='old')
      i=1
      do 10 j=1,4
         do 10 k=1,6
            do 10 l=1,5
               read(13,*)(out1(i,j,k,l,m),m=1,14)
 10   continue
      do 20 i=2,3
         do 20 j=1,5
            do 20 k=1,6
               do 20 l=1,5
                  read(13,*)(out1(i,j,k,l,m),m=1,14)
 20   continue
      i=4
      do 30 j=1,6
```

```
          do 30 k=1,6
            do 30 l=1,5
                  read(13,*)(out1(i,j,k,l,m),m=1,14)
 30   continue
      close(13)
c     -----------------------------------------
c     table_cr(outx;y,x1,x2,x3,x4,ii,jj)
c     Create 4 tamplets of data
c     -----------------------------------------
      nout=5
      nx1=13
      nx2=8
      nx3=14
      nx4=12
      open(14,file='tq_tq.dat',status='unknown')
      open(15,file='tq_ca.dat',status='unknown')
      open(16,file='tq_m.dat',status='unknown')
      open(17,file='tq_af.dat',status='unknown')
      open(18,file='tq_n.dat',status='unknown')
      ii=6
      jj=6
      do 200 naf=1,5
         do 200 nn=1,4
            do 70 i=1,ii
               do 70 j=1,jj
                  y(i,j)=out1(nn,i,j,naf,nout)
                  x1(i,j)=out1(nn,i,j,naf,nx1)
                  x2(i,j)=out1(nn,i,j,naf,nx2)
                  x3(i,j)=out1(nn,i,j,naf,nx3)
                  x4(i,j)=out1(nn,i,j,naf,nx4)
 70         continue
c     -----------------------------------------
c     Write the tamplets in tq_*.dat file
c     -----------------------------------------
            do 100 i=1,ii
               write(14,*)(y(i,j),j=1,jj)
 100        continue
            do 110 i=1,ii
               write(15,*)(x1(i,j),j=1,jj)
 110        continue
            do 120 i=1,ii
               write(16,*)(x2(i,j),j=1,jj)
 120        continue
            do 130 i=1,ii
               write(17,*)(x3(i,j),j=1,jj)
c               write(*,*) (x3(i,j),j=1,jj)
 130        continue
            do 140 i=1,ii
               write(18,*)(x4(i,j),j=1,jj)
 140        continue
 200   continue
       close(14)
       close(15)
       close(16)
       close(17)
       close(18)
      stop
      end
==========End of vct_dir/data.dir/tq_plot.f=========================
```

The following Matlab script file (`tq_regr.m`) is used for the identification of the nonlinear static map $T_b = F(1, A, A^2, A^3, A/F, A/F^2, A/F^3, N, N^2, N^3)$. The second Matlab script file (`tq_a.m`) contains the structure of the polynomial that is used for the multivariable polynomial curve fitting. The third Matlab script file (`tq_pram.m`) is used for the evaluation of the goodness of the model based on plotting the best fit polynomial versus the actual data.

```
=============vct_dir/data.dir/tq_regr.m============================
function[co_tq,y_max,y_min,res]=tq_regr(opt)
%Torque fiting polynomial, choose opt=1 to plot
%Run first the tq_plot.x to get the data points.
%have fun :-)
load tq_tq.dat
load tq_ca.dat
load tq_m.dat
load tq_af.dat
load tq_n.dat
%---------------------
% Calculate the air charge from the air flow
[m,n]=size(tq_m);
tq_m=tq_m(:);
tq_n=tq_n(:);
N=length(tq_n);
for i=1:N
  if tq_n(i)>0
  tq_m(i)=tq_m(i)*15./tq_n(i);
  end
end
tq_m=reshape(tq_m,m,n);
tq_n=reshape(tq_n,m,n);
%
[i,j]=find(tq_n>0);
N=length(i);
for k=1:N
y(k,5)=tq_tq(i(k),j(k));...
y(k,1)=tq_ca(i(k),j(k));...
y(k,2)=tq_m(i(k),j(k));...
y(k,3)=tq_af(i(k),j(k));...
y(k,4)=tq_n(i(k),j(k));...
end
%---------------------
%Scale the DATA
y_max=[max(y(:,1)),max(y(:,2)),max(y(:,3)),max(y(:,4)),max(y(:,5))]';
y_min=[min(y(:,1)),min(y(:,2)),min(y(:,3)),min(y(:,4)),min(y(:,5))]';
for i=2:5
sc_y(:,i)=(y(:,i)-y_min(i))/(y_max(i)-y_min(i));
end
%---------------------
%Least Squares Estimate
a=tq_a(sc_y(:,2),sc_y(:,3),sc_y(:,4));
co_tq=a\sc_y(:,5);
%---------------------
%Calculate the residual
sc_yh=a*co_tq;
yh(:)=sc_yh(:)*(y_max(5)-y_min(5))+y_min(5);
res=yh-y(:,5);
res=res'*res;
res=sqrt(res)/N;
```

```
%_____________________
%Evaluation of the best fit polynomial
if opt==1
% Introduce the estimated polynomial
% ----------------------------------
% evaluated at a dense interval of the mass air flow.
sc_ye(:,2)=[0:0.01:1]';
ye(:,2)=sc_ye(:,2)*(y_max(2)-y_min(2))+y_min(2);
%
% Change the A/F (outer loop)
ye(:,3)=12.2*ones(size(ye(:,2)));
sc_ye(:,3)=(ye(:,3)-y_min(3))/(y_max(3)-y_min(3));
%
% Change the N (inner loop)
prime=[750 1000 1500 2000]';
for k=1:4
    ye(:,4)=prime(k)*ones(size(ye(:,2)));...
    sc_ye(:,4)=(ye(:,4)-y_min(4))/(y_max(4)-y_min(4));...
    ae=tq_a(sc_ye(:,2),sc_ye(:,3),sc_ye(:,4));...
    sc_ye(:,5)=ae*co_tq;...
    ye(:,5)=sc_ye(:,5)*(y_max(5)-y_min(5))+y_min(5);...
    comp_y(:,k)=ye(:,5);
end
%--------------------------
%Create the array of data to be plotted versus
% estimated data.
%A/F=12.2 , 13.9 , 14.6 , 15.2 , 16.0
%naf= 1   ,  2   ,   3  ,  4   ,  5
naf=1;
nca=1;
%%
for i=1:4
nbeg=24*(naf-1)+1+6*(i-1);
nfin=24*(naf-1)+6+6*(i-1);
y_plot(:,i)=tq_tq(nbeg:nfin,nca);
x_plot(:,i)=tq_m(nbeg:nfin,nca);
end
plot(ye(:,2),comp_y,x_plot,y_plot,'*');
end
============End of vct_dir/data.dir/tq_regr.m===============
====================vct_dir/data.dir/tq_a.m==================
function a=tq_a(x1,x2,x3)
%Calculates the matrix of coefficients for tq
a=[ones(size(x1)) x1 x2 x3 ...
x1.*x3 x1.*x2 x2.*x3 ...
x1.^2 x2.^2 x3.^2 ...
x1.^2.*x3 x1.^2.*x2 x3.^2.*x1 x3.^2.*x2 x2.^2.*x1 x2.^2.*x3 ....
x1.*x2.*x3 x1.^3 x2.^3 x3.^3];
==============End of vct_dir/data.dir/tq_a.m===============
==================vct_dir/data.dir/tq_param.m==================
load tq_coef
%
% Introduce the estimated polynomial
% ----------------------------------
sc_ye(:,4)=[0:0.01:1]';
ye(:,4)=sc_ye(:,4)*(y_max(4)-y_min(4))+y_min(4);
%
ye(:,2)=25*ones(size(ye(:,4)));
sc_ye(:,2)=(ye(:,2)-y_min(2))/(y_max(2)-y_min(2));
```

```
%
ye(:,1)=19*ones(size(ye(:,4)));
sc_ye(:,1)=(ye(:,1)-y_min(1))/(y_max(1)-y_min(1));
%
%
prime=[12.2 13.0 13.9 14.3 14.6];
%
for k=1:5
    ye(:,3)=prime(k)*ones(size(ye(:,4)));...
    sc_ye(:,3)=(ye(:,3)-y_min(3))/(y_max(3)-y_min(3));...
    ae=tq_a(sc_ye(:,1),sc_ye(:,2),sc_ye(:,3),sc_ye(:,4));...
    sc_ye(:,5)=ae*co_tq;...
    ye(:,5)=sc_ye(:,5)*(y_max(5)-y_min(5))+y_min(5);...
    comp_y(:,k)=ye(:,5);
end
plot(ye(:,4),comp_y);
==============End of vct_dir/data.dir/tq_param.m ===============
```

C.6.2 Simulation of the brake torque (T_b) simulation model in System-Build.

To construct the simulation model of the brake torque shown in Figure C.4 (i.e. to program the $T_b = F(1, A, A^2, A^3, A/F, A/F^2, A/F^3, N, N^2, N^3)$ relationship) we used the following MatrixX script commands from the file `vct_dir/vct_model.dir/vct_polyn.ms`.

```
-----------------------------------------------------------------------
%Build the $T_b$ model (Brake Torque)
%---------------        -     -
%Take the data from the tq_regr.m files located in ../data.dir
%and paste them here. Here actually you are loading the regression
%analysis data (made in MATLAB environment) to the MATRIXx
%environment.
%
v_tq_co=[0.0480;1.2995;-0.0061;-0.0814;0.0620;0.2514;0.0218;-0.6635;
-0.0835;0.0544;0.2048;-0.0779;-0.1381;-0.0179;-0.2113;0.0077;
        -0.0308;0.2602;0.0436;-0.0153];

v_tq_max=1.0e+03 *[0.0004;0.0163;2.0050;0.2476];

v_tq_min=[0.0606;11.7000;745.0000;-21.7100];
%----------------------
%Build the variables as they appear in vct_tablet.bl (the simulation
%model in System-Build).
%
%Input scaling
v_tqx1=1/(v_tq_max(1)-v_tq_min(1));
v_tqx2=1/(v_tq_max(2)-v_tq_min(2));
v_tqx3=1/(v_tq_max(3)-v_tq_min(3));
v_tqxsp=[v_tqx1 0 0;0 v_tqx2 0; 0 0 v_tqx3];
v_tqx1sp=-v_tq_min(1)/(v_tq_max(1)-v_tq_min(1));
v_tqx2sp=-v_tq_min(2)/(v_tq_max(2)-v_tq_min(2));
v_tqx3sp=-v_tq_min(3)/(v_tq_max(3)-v_tq_min(3));
%The polynomial coefficients
v_tqcosp=v_tq_co';
%Output scaling
v_tqysp=(v_tq_max(4)-v_tq_min(4));
v_tqyysp=v_tq_min(4);
```

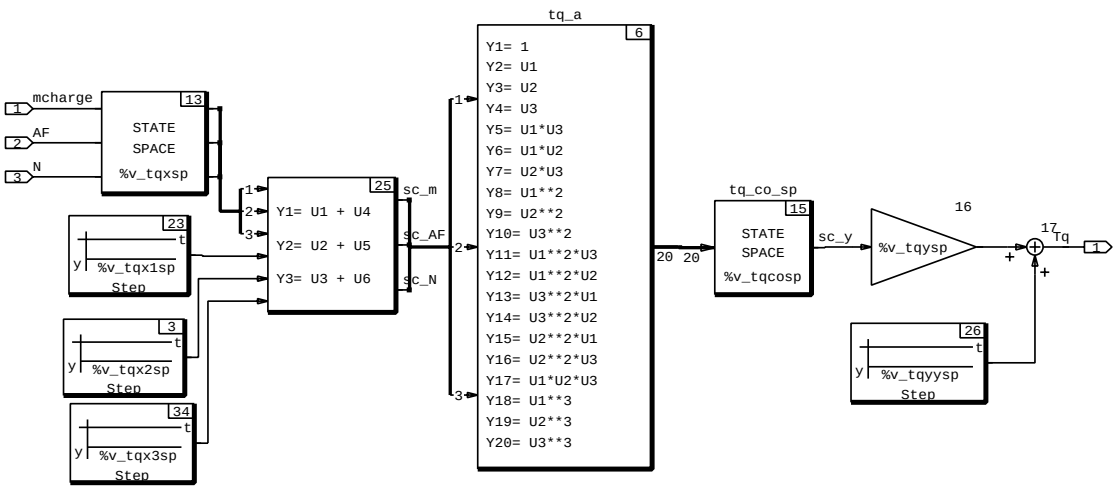

Figure C.4: Simulation model of the brake torque programmed in the System-Build environment.

C.7 Feedgas Emissions of Oxides of Nitrogen : Codes

In Section 3.2.3 we discuss the assumptions associated with the steady-state NO_x model as a function of engine speed (N), cam phasing (CAM), air fuel ratio (A/F), and manifold pressure (P_m). The identified polynomial is an eighth degree polynomial :

$$NO_x = f(N, CAM, A/F, P_m) \; . \tag{C.9}$$

The identification algorithm follows in detail.

C.7.1 Script Files

The following fortran program is a modification of the program `MAP_plot`, and is used to access all the necessary sequence of data for the NO_x identification.

```
==================vct_dir/data.dir/nox_plot.f=====================
      program nox_plot
      real x1(6,6),x2(6,6),x3(6,6),x4(6,6)
      real y(6,6),out1(4,6,6,5,14),out2(4,6,6,5,10)
c     -----------------------------------------
c     Load the data from out1.dat
c     -----------------------------------------
      open(13,file='out1.dat',status='old')
      i=1
      do 10 j=1,4
         do 10 k=1,6
            do 10 l=1,5
```

```
               read(13,*)(out1(i,j,k,l,m),m=1,14)
 10    continue
       do 20 i=2,3
          do 20 j=1,5
             do 20 k=1,6
                do 20 l=1,5
                   read(13,*)(out1(i,j,k,l,m),m=1,14)
 20    continue
       i=4
       do 30 j=1,6
           do 30 k=1,6
             do 30 l=1,5
                   read(13,*)(out1(i,j,k,l,m),m=1,14)
 30    continue
       close(13)
c      -----------------------------------------
c       Load the data from out2.dat
c      -----------------------------------------
       open(14,file='out2.dat',status='old')
       i=1
       do 40 j=1,4
          do 40 k=1,6
             do 40 l=1,5
                read(14,*)(out2(i,j,k,l,m),m=1,10)
 40    continue
       do 41 i=2,3
          do 41 j=1,5
             do 41 k=1,6
                do 41 l=1,5
                 read(14,*)(out2(i,j,k,l,m),m=1,10)
 41    continue
       i=4
       do 42 j=1,6
           do 42 k=1,6
             do 42 l=1,5
                read(14,*)(out2(i,j,k,l,m),m=1,10)
 42    continue
       close(14)
c      -----------------------------------------
c      table_cr(outx;y,x1,x2,x3,x4,ii,jj)
c      Creat 4 tamplets of data
c      -----------------------------------------
       nout=9
       nx1=12
       nx2=13
       nx3=14
       nx4=6
       open(15,file='nox_nox.dat',status='unknown')
       open(16,file='nox_n.dat',status='unknown')
       open(17,file='nox_cam.dat',status='unknown')
       open(18,file='nox_af.dat',status='unknown')
       open(19,file='nox_pm.dat',status='unknown')
       ii=6
       jj=6
       do 200 naf=1,5
          do 200 nn=1,4
             do 70 i=1,ii
                do 70 j=1,jj
                   y(i,j)=out2(nn,i,j,naf,nout)
```

```
                  x1(i,j)=out1(nn,i,j,naf,nx1)
                  x2(i,j)=out1(nn,i,j,naf,nx2)
                  x3(i,j)=out1(nn,i,j,naf,nx3)
                  x4(i,j)=out1(nn,i,j,naf,nx4)
 70         continue
c     ------------------------------------------
c     Write the tamplets in nox_*.dat file
c     ------------------------------------------
            do 100 i=1,ii
               write(15,*)(y(i,j),j=1,jj)
 100        continue
            do 110 i=1,ii
               write(16,*)(x1(i,j),j=1,jj)
 110        continue
            do 120 i=1,ii
               write(17,*)(x2(i,j),j=1,jj)
 120        continue
            do 130 i=1,ii
               write(18,*)(x3(i,j),j=1,jj)
c               write(*,*) (x3(i,j),j=1,jj)
 130        continue
            do 140 i=1,ii
               write(19,*)(x4(i,j),j=1,jj)
 140        continue
 200   continue
       close(15)
       close(16)
       close(17)
       close(18)
       close(19)
      stop
      end
==========End of vct_dir/data.dir/nox_plot.f======================
```

The following Matlab script file (`nox_regr.m`) is used for the identification of the nonlinear static map $NO_x = f(N, CAM, A/F, P_m)$. The second Matlab script file (`nox_a4444.m`) contains the structure of the polynomial that is used for the multivariable polynomial curve fitting. The third Matlab script file (`nox_param.m`) is used for the evaluation of the goodness of the model based on plotting the best fit polynomial versus the actual data.

```
====================vct_dir/data.dir/nox_regr.m===================
load nox_nox.dat
load nox_cam.dat
load nox_pm.dat
load nox_af.dat
load nox_n.dat
[i,j]=find(nox_n>0);
N=length(i);
for k=1:N
y(k,5)=nox_nox(i(k),j(k));...
y(k,1)=nox_n(i(k),j(k));...
y(k,2)=nox_cam(i(k),j(k));...
y(k,3)=nox_af(i(k),j(k));...
y(k,4)=nox_pm(i(k),j(k));...
end
% Scale the variables for the least squares estimation
y_max=[max(y(:,1)),max(y(:,2)),max(y(:,3)),max(y(:,4)),max(y(:,5))]';
y_min=[min(y(:,1)),min(y(:,2)),min(y(:,3)),min(y(:,4)),min(y(:,5))]';
```

```
for i=1:5
sc_y(:,i)=(y(:,i)-y_min(i))/(y_max(i)-y_min(i));
end
%-----------
%nox_a provides the structure of the regressing polynomial :
% NOx=P(N,CAM,AF,Pm)
%The overdetermined set of equations you solve is :  A*co_NOx=sc_Y,
%where co_CYL are the coefficients to be determined.
%The solution in Least Squares sense is co_NOx=pinv(A)*sc_Y.
%
a=nox_a(sc_y(:,1),sc_y(:,2),sc_y(:,3),sc_y(:,4));
co_nox=a\sc_y(:,5);
%--------------------
%Calculate the residual
sc_yh=a*co_nox;
yh(:)=sc_yh(:)*(y_max(5)-y_min(5))+y_min(5);
res=yh-y(:,5);
R=max(res);
res=res'*res;
res=sqrt(res)/N;
===========End of vct_dir/data.dir/nox_regr.m======================
============vct_dir/data.dir/nox_a4444.m==========================
function a=nox_a(x1,x2,x3,x4)
%Calculates the matrix of coefficients for nox
%Very difficult and tedious procedure, I almost chose to split
%the function to 4 air-to-fuel ratio regions.
%
%NOx as function of sc_N (up to second order).
%Results in a 3 terms polynomial
a=[ones(size(x1)) x1 x1.^2];
%---------------------------------------------
%Use a nested polynomial to represent NOx as a function
% of the other variables.
%Start with adding the NOx dependancy on CAM (almost linear).
qo=a;
[n,m]=size(qo);
for i=1:m
    q1(:,i)=qo(:,i).*x2;
end
%---------------------------------------------
%NOx as function of sc_N (up to second order) and sc_CAM (linear).
%Results in a 6 terms polynomial.
a=[qo q1];
%---------------------------------------------
%Add the NOx dependancy on A/F (it is cubic!).
qo=a;
[n,m]=size(qo);
for i=1:m
    q1(:,i)=qo(:,i).*x3;
    q2(:,i)=qo(:,i).*x3.^2;
    q3(:,i)=qo(:,i).*x3.^3;
end
%---------------------------------------------
%NOx as function of sc_N (up to second order), sc_CAM (linear)
% and sc_AF (cubic).
%Results in a 24 terms polynomial (!!)
a=[qo q1 q2 q3];
%---------------------------------------------
%Add the NOx dependancy on Pm (it is quadratic).
```

```
qo=a;
[n,m]=size(qo);
for i=1:m
    q1(:,i)=qo(:,i).*x4;
    q2(:,i)=qo(:,i).*x4.^2;
end
%NOx as function of sc_N (up to second order), sc_CAM (linear)
% sc_AF (cubic), and sc_Pm (quadratic).
%Results in a 72 terms polynomial (!!!!)
a=[qo q1 q2];
========End of vct_dir/data.dir/nox_a4444.m====================
===============vct_dir/data.dir/nox_param.m====================
% Introduce the estimated polynomial
% ----------------------------------
% evaluated at a dense interval of Torque.
sc_ye(:,4)=[0:0.01:1]';
ye(:,4)=sc_ye(:,4)*(y_max(4)-y_min(4))+y_min(4);
%
% Change the N (outer loop)
ye(:,1)=750*ones(size(ye(:,4)));
nn=1;
naf=4;
sc_ye(:,1)=(ye(:,1)-y_min(1))/(y_max(1)-y_min(1));
%
% Change the A/F (inner loop)
ye(:,3)=15.2*ones(size(ye(:,4)));
sc_ye(:,3)=(ye(:,3)-y_min(3))/(y_max(3)-y_min(3));
%
CAprime=[0 5 12 19 28 35]';
for k=1:6
    ye(:,2)=CAprime(k)*ones(size(ye(:,4)));...
    sc_ye(:,2)=(ye(:,2)-y_min(2))/(y_max(2)-y_min(2));...
    ae=nox_a444(sc_ye(:,1),sc_ye(:,2),sc_ye(:,3),sc_ye(:,4));...
    sc_ye(:,5)=ae*co_nox;...
    ye(:,5)=sc_ye(:,5)*(y_max(5)-y_min(5))+y_min(5);...
    comp_y(:,k)=ye(:,5);...
end
comp_x=ye(:,4);
%---------------
%Create the array of data to be plotted versus
% estimated data.
%N=750 , 1000 , 1500 , 2000 RPM
%nn=1   ,  2   ,   3  ,   4
%A/F=12.2 , 13.9 , 14.6 , 15.2 , 16.0
%naf= 1   ,  2   ,   3  ,  4   ,  5
nbeg=24*(naf-1)+6*(nn-1)+1;
nfin=24*(naf-1)+6*(nn-1)+6;
plot(comp_x,comp_y(:,1),nox_pm(nbeg:nfin,1),nox_nox(nbeg:nfin,1),'y+');
hold
plot(comp_x,comp_y(:,2),'m',nox_pm(nbeg:nfin,2),nox_nox(nbeg:nfin,2),'mo');
plot(comp_x,comp_y(:,3),'c',nox_pm(nbeg:nfin,3),nox_nox(nbeg:nfin,3),'cx');
plot(comp_x,comp_y(:,4),'r',nox_pm(nbeg:nfin,4),nox_nox(nbeg:nfin,4),'r+');
plot(comp_x,comp_y(:,5),'g',nox_pm(nbeg:nfin,5),nox_nox(nbeg:nfin,5),'g*');
plot(comp_x,comp_y(:,6),'b',nox_pm(nbeg:nfin,6),nox_nox(nbeg:nfin,6),'bo');
===========End of vct_dir/data.dir/nox_param.m==================================
```

C.7.2 Simulation of NO_x in System-Build

To construct the simulation model of the feedgas NO_x emissions shown in Figure C.5 we used the following MatrixX script commands from the file `vct_dir/vct_model.dir/vct_polyn.ms`.

```
=====================================================================
%Build the feedgas $NO_x$ emissions model
%---------------------------------------
%Take the data from the nox_regr.m files located in ../data.dir
%and paste them here. Here actually you are loading the regression
%analysis data (made in MATLAB environment) to the MATRIXx environment.
%
v_nox_co=[0.0200 0.0529 -0.0017 -0.0266 0.0667 -0.0946 0.1718 0.7840
    0.1668 -0.3265 0.0074 -0.6932 -0.5876 0.0256 -0.2354 0.8155
    -1.9732 1.8512 0.2188 0.5549 -0.7877 -0.1859 0.0721 0.1120 0.2712
    0.0067 0.0966 -0.0932 -0.7164 0.7201 -0.6872 -3.4572 0.5724 2.6223
    1.5405 -1.8901 11.2350 -1.4304 4.1765 -15.7908 8.1200 2.4157
    -7.8180 0.2633 -1.3755 8.9838 0.6803 -7.1907 -0.1626 -0.1804
    -0.0598 -0.0399 1.3561 -1.1440 -1.0828 5.5225 -0.4514 -2.3212
    -3.8016 3.0169 -4.3774 -3.3992 -6.3261 17.7500 -4.3862 -3.9039
    3.1401 1.0739 4.6572 -9.6303 -3.2302 7.3144]';
v_nox_max=[2005 35.1000 16.4300 0.6170 24.8400]';
v_nox_min=[746 -0.2000 11.7000 0.1480 -0.2200]';
%Build the variables as they appear in vct_tablet.bl (the simulation
%model in System-Build).
%
%Input scaling
v_noxx1=1/(v_nox_max(1)-v_nox_min(1));
v_noxx2=1/(v_nox_max(2)-v_nox_min(2));
v_noxx3=1/(v_nox_max(3)-v_nox_min(3));
v_noxx4=1/(v_nox_max(4)-v_nox_min(4));
v_noxxsp=[v_noxx1 0 0 0
          0 v_noxx2 0 0
          0 0 v_noxx3 0
          0 0 0 v_noxx4];
v_noxx1sp=-v_nox_min(1)/(v_nox_max(1)-v_nox_min(1));
v_noxx2sp=-v_nox_min(2)/(v_nox_max(2)-v_nox_min(2));
v_noxx3sp=-v_nox_min(3)/(v_nox_max(3)-v_nox_min(3));
v_noxx4sp=-v_nox_min(4)/(v_nox_max(4)-v_nox_min(4));
%The polynomial coefficients
v_noxcosp=v_nox_co';
%Output scaling
v_noxysp=(v_nox_max(5)-v_nox_min(5));
v_noxyysp=v_nox_min(5);
=====================================================================
```

C.8 Feedgas Emissions of Hydrocarbons : Codes

In Section 3.2.3 we discuss the assumptions associated with the steady-state HC model as a function of engine speed (N), cam phasing (CAM), air fuel ratio (A/F), and manifold pressure (P_m):

$$HC = f(N, CAM, A/F, P_m) \; . \tag{C.10}$$

The identification algorithm follows in detail.

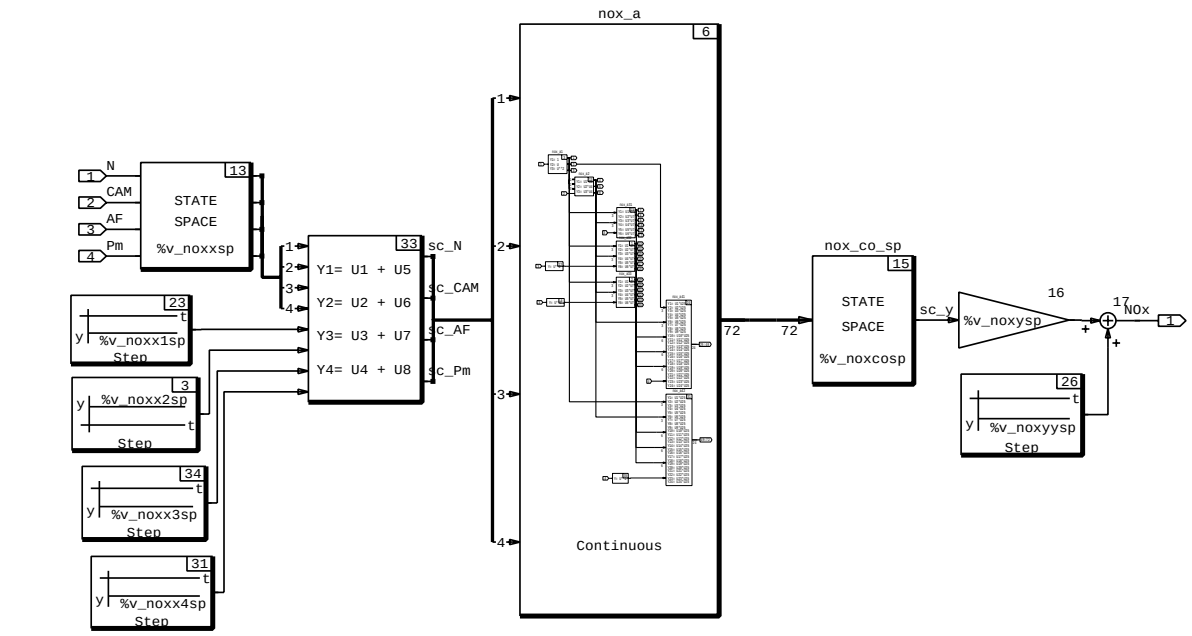

Figure C.5: Simulation model of the feedgas NO_x emissions model programmed in the System-Build environment.

C.8.1 Script Files

The following fortran program is a modification of the program `MAP_plot` shown in Appendix B, and is used to access all the necessary sequences of data for the HC identification.

```
==================vct_dir/data.dir/hc_plot.f=====================
      program hc_plot
      real x1(6,6),x2(6,6),x3(6,6),x4(6,6)
      real y(6,6),out1(4,6,6,5,14),out2(4,6,6,5,10)
c     ------------------------------------------
c     Load the data from out1.dat
c     ------------------------------------------
      open(13,file='out1.dat',status='old')
      i=1
      do 10 j=1,4
         do 10 k=1,6
            do 10 l=1,5
               read(13,*)(out1(i,j,k,l,m),m=1,14)
 10   continue
      do 20 i=2,3
         do 20 j=1,5
            do 20 k=1,6
               do 20 l=1,5
                  read(13,*)(out1(i,j,k,l,m),m=1,14)
 20   continue
      i=4
      do 30 j=1,6
          do 30 k=1,6
```

```
            do 30 l=1,5
                  read(13,*)(out1(i,j,k,l,m),m=1,14)
 30   continue
      close(13)
c     ------------------------------------------
c      Load the data from out2.dat
c     ------------------------------------------
      open(14,file='out2.dat',status='old')
      i=1
      do 40 j=1,4
         do 40 k=1,6
            do 40 l=1,5
               read(14,*)(out2(i,j,k,l,m),m=1,10)
 40   continue
      do 41 i=2,3
         do 41 j=1,5
            do 41 k=1,6
               do 41 l=1,5
                read(14,*)(out2(i,j,k,l,m),m=1,10)
 41   continue
      i=4
      do 42 j=1,6
          do 42 k=1,6
            do 42 l=1,5
               read(14,*)(out2(i,j,k,l,m),m=1,10)
 42   continue
      close(14)
c     ------------------------------------------
c     table_cr(outx;y,x1,x2,x3,x4,ii,jj)
c     Creat 4 tamplets of data
c     ------------------------------------------
      nout=8
      nx1=12
      nx2=13
      nx3=14
      nx4=6
      open(15,file='hc_hc.dat',status='unknown')
      open(16,file='hc_n.dat',status='unknown')
      open(17,file='hc_cam.dat',status='unknown')
      open(18,file='hc_af.dat',status='unknown')
      open(19,file='hc_pm.dat',status='unknown')
      ii=6
      jj=6
      do 200 naf=1,5
         do 200 nn=1,4
            do 70 i=1,ii
               do 70 j=1,jj
                  y(i,j)=out2(nn,i,j,naf,nout)
                  x1(i,j)=out1(nn,i,j,naf,nx1)
                  x2(i,j)=out1(nn,i,j,naf,nx2)
                  x3(i,j)=out1(nn,i,j,naf,nx3)
                  x4(i,j)=out1(nn,i,j,naf,nx4)
 70         continue
c     ==========================================
c     Write the tamplets in tq_*.dat file
c     ------------------------------------------
            do 100 i=1,ii
               write(15,*)(y(i,j),j=1,jj)
 100        continue
```

```
            do 110 i=1,ii
               write(16,*)(x1(i,j),j=1,jj)
 110        continue
            do 120 i=1,ii
               write(17,*)(x2(i,j),j=1,jj)
 120        continue
            do 130 i=1,ii
               write(18,*)(x3(i,j),j=1,jj)
 130        continue
            do 140 i=1,ii
               write(19,*)(x4(i,j),j=1,jj)
 140        continue
 200   continue
       close(15)
       close(16)
       close(17)
       close(18)
       close(19)
      stop
      end
==============End of vct_dir/data.dir/hc_plot.f==========================
```

The following Matlab script file (`hc_regr.m`) is used for the identification of the nonlinear static map $HC = f(N, CAM, A/F, P_m)$. The second Matlab script file (`hc_a.m`) contains the structure of the polynomial that is used for the multivariable polynomial curve fitting. The third Matlab script file (`hc_param.m`) is used for the evaluation of the goodness of the model based on plotting the best fit polynomial versus the actual data.

```
====================vct_dir/data.dir/hc_regr.m====================
%function[co_hc,y_max,y_min,res]=hc_regr(opt)
if opt==1
load hc_hc.dat
load hc_cam.dat
load hc_pm.dat
load hc_af.dat
load hc_n.dat
[i,j]=find(hc_pm>0.05);
N=length(i);
for l=1:N
k=l;
y(k,5)=hc_hc(i(l),j(l));...
y(k,1)=hc_n(i(l),j(l));...
y(k,2)=hc_cam(i(l),j(l));...
y(k,3)=hc_af(i(l),j(l));...
y(k,4)=hc_pm(i(l),j(l));...
end
y_max=[max(y(:,1)),max(y(:,2)),max(y(:,3)),max(y(:,4)),max(y(:,5))]';
y_min=[min(y(:,1)),min(y(:,2)),min(y(:,3)),min(y(:,4)),min(y(:,5))]';
y_min(4)=y_min(4)-0.001;
for i=1:5
sc_y(:,i)=(y(:,i)-y_min(i))/(y_max(i)-y_min(i));
end
a=hc_a(sc_y(:,1),sc_y(:,2),sc_y(:,3),sc_y(:,4));
co_hc=a\sc_y(:,5);
%
%Calculate the residual
sc_yh=a*co_hc;
yh(:)=sc_yh(:)*(y_max(5)-y_min(5))+y_min(5);
```

```
yh(:)=yh(:);
res=yh-y(:,5);
R=max(res);
res=res'*res;
res=sqrt(res)/N;
end
=====================End of vct_dir/data.dir/hc_regr.m===================
====================vct_dir/data.dir/hc_a.m==============================
function a=try_a(x1,x2,x3,x4)
%Calculates the matrix of coefficients for the crazy HC
%HC as function of sc_AF (up to second order).
%Results in a 3 terms polynomial
a=[ones(size(x1)) x3 x3.^2];
%-----------------------------------------------
%Use a nested polynomial to represent HC as a function
% of the other variables.
%Start with adding the HC dependancy on N (cubic).
qo=a;
[n,m]=size(qo);
for i=1:m
    q1(:,i)=qo(:,i).*x1;
    q2(:,i)=qo(:,i).*x1.^2;
    q3(:,i)=qo(:,i).*x1.^3;
end
%-----------------------------------------------
%NOx as function of sc_AF (up to second order) and sc_N (cubic).
%Results in a 12 terms polynomial.
a=[qo q1 q2 q3];
%-----------------------------------------------
%Add the NOx dependancy on P_m (it is very difficult to find the exact order)
qo=a;
[n,m]=size(qo);
for i=1:m
    q1(:,i)=qo(:,i)./x4;
end
a=[qo q1];
%results in a 24 terms polynomial
%-----------------------------------------------
%Add the NOx dependancy on CAM (linear) and the slight twist that
%manifold pressure introduces in the HC data.
qo=a;
a=[qo x2 x2./(x4).^(1/16)];
%Results a 26 terms polynomial (!)
=================End of vct_dir/data.dir/hc_a.m==============================
==================vct_dir/data.dir/hc_param.m================================
%function[comp_x,comp_y,nbeg,nfin]=hc_paramet(hc_pm,hc_hc,co_hc,kaf,naf,kn,nn)
% Introduce the estimated polynomial
% ----------------------------------
% evaluated at a dense interval of Torque.
sc_ye(:,4)=[0.001:0.01:1]';
ye(:,4)=sc_ye(:,4)*(y_max(4)-y_min(4))+y_min(4);
%
% Change the N (outer loop)
ye(:,1)=2000*ones(size(ye(:,4)));
nn=4;
naf=2;
sc_ye(:,1)=(ye(:,1)-y_min(1))/(y_max(1)-y_min(1));
%
% Change the A/F (inner loop)
```

```
ye(:,3)=13.9*ones(size(ye(:,4)));
sc_ye(:,3)=(ye(:,3)-y_min(3))/(y_max(3)-y_min(3));
%
%
CAprime=[0 5 12 19 28 35]';
for k=1:6
    ye(:,2)=CAprime(k)*ones(size(ye(:,4)));...
    sc_ye(:,2)=(ye(:,2)-y_min(2))/(y_max(2)-y_min(2));...
    ae=hc_a(sc_ye(:,1),sc_ye(:,2),sc_ye(:,3),sc_ye(:,4));...
    sc_ye(:,5)=ae*co_hc;...
    ye(:,5)=sc_ye(:,5)*(y_max(5)-y_min(5))+y_min(5);...
    comp_y(:,k)=ye(:,5);
end
comp_x=ye(:,4);
%Create the array of data to be plotted versus
% estimated data.
%N=750 , 1000 , 1500 , 2000 RPM
%nn=1   ,  2   ,   3  ,   4
%
%A/F=12.2 , 13.9 , 14.6 , 15.2 , 16.0
%naf= 1   ,  2   ,   3  ,  4   ,  5
nbeg=24*(naf-1)+6*(nn-1)+1;
nfin=24*(naf-1)+6*(nn-1)+6;
plot(comp_x,comp_y(:,1),hc_pm(nbeg:nfin,1),hc_hc(nbeg:nfin,1),'y+');
hold
plot(comp_x,comp_y(:,2),'m',hc_pm(nbeg:nfin,2),hc_hc(nbeg:nfin,2),'mo');
plot(comp_x,comp_y(:,3),'c',hc_pm(nbeg:nfin,3),hc_hc(nbeg:nfin,3),'cx');
plot(comp_x,comp_y(:,4),'r',hc_pm(nbeg:nfin,4),hc_hc(nbeg:nfin,4),'r*');
plot(comp_x,comp_y(:,5),'g',hc_pm(nbeg:nfin,5),hc_hc(nbeg:nfin,5),'g+');
plot(comp_x,comp_y(:,6),'b',hc_pm(nbeg:nfin,6),hc_hc(nbeg:nfin,6),'bo');
=================End of vct_dir/data.dir/hc_param.dir====================
```

C.8.2 Simulation of HC in System-Build

To construct the simulation model of the feedgas HC emissions shown in Figure C.6 we used the following MatrixX script commands from the file `vct_dir/vct_model.dir/vct_polyn.ms`.

```
=========================================================================
%Build the feedgas $HC$ emissions model
%---------------------------------------
%Take the data from the hc_regr.m files located in ../data.dir
%and paste them here. Here actually you are loading the regression
%analysis data (made in MATLAB environment) to the MATRIXx environment.
%
v_hc_co=[0.0230 0.0350 -0.0662 0.5933 -1.1822 1.3418 -1.4062 3.0186
    -3.6013 0.9045 -2.1751 2.6315 0.0171 -0.0347 0.0405 -0.1416 0.3203
    -0.3480 0.3138 -0.7474 0.7988 -0.1891 0.4611 -0.4906 -0.6905 0.6338]';
v_hc_max=[ 2005 35.1000 16.4300 0.6170 97.0500]';
v_hc_min=[746 -0.2000 11.7000 0.1470 2.5900]';
v_hcx4min=v_hc_min(4)+0.001;
%Build the variables as they appear in vct_tablet.bl (the simulation
%model in System-Build).
%
%Input scaling
v_hcx1=1/(v_hc_max(1)-v_hc_min(1));
v_hcx2=1/(v_hc_max(2)-v_hc_min(2));
```

```
v_hcx3=1/(v_hc_max(3)-v_hc_min(3));
v_hcx4=1/(v_hc_max(4)-v_hc_min(4));
v_hcxsp=[v_hcx1 0 0 0
         0 v_hcx2 0 0
         0 0 v_hcx3 0
         0 0 0 v_hcx4];
v_hcx1sp=-v_hc_min(1)/(v_hc_max(1)-v_hc_min(1));
v_hcx2sp=-v_hc_min(2)/(v_hc_max(2)-v_hc_min(2));
v_hcx3sp=-v_hc_min(3)/(v_hc_max(3)-v_hc_min(3));
v_hcx4sp=-v_hc_min(4)/(v_hc_max(4)-v_hc_min(4));
%The polynomial coefficients
v_hccosp=v_hc_co';
%Output scaling
v_hcysp=(v_hc_max(5)-v_hc_min(5));
v_hcyysp=v_hc_min(5);
================================================================================
```

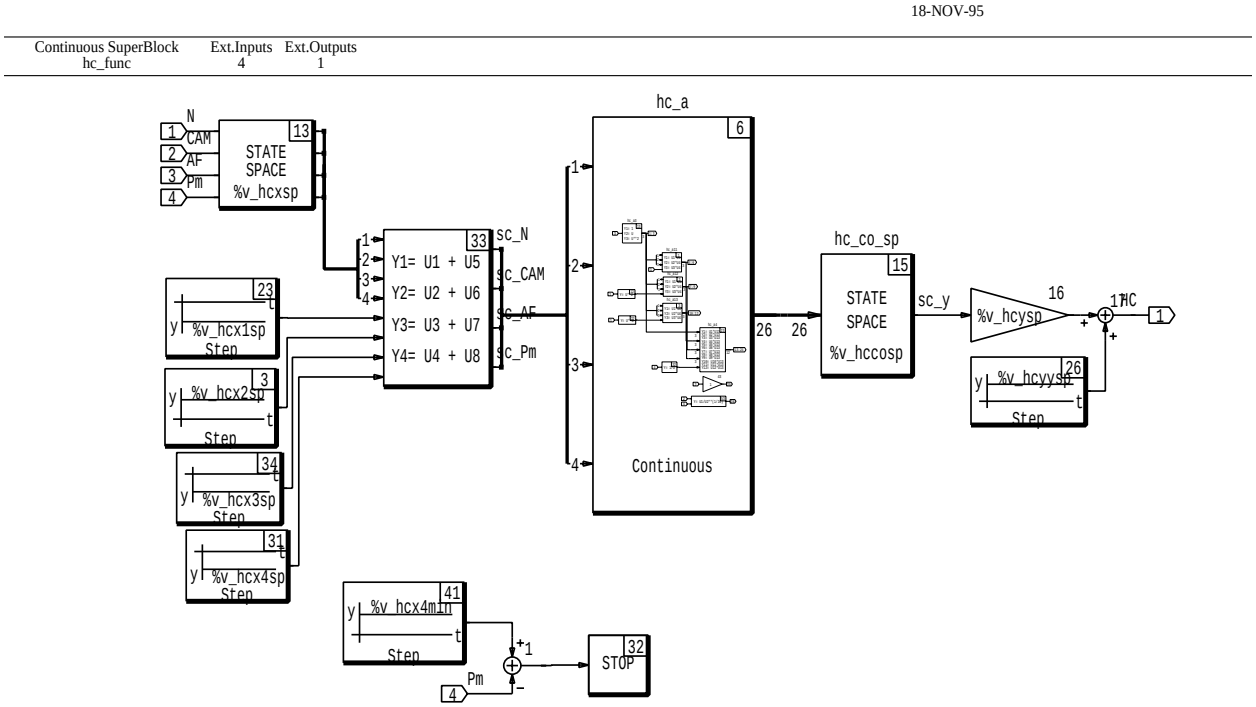

Figure C.6: Simulation model of the feedgas HC emissions model programmed in the System-Build environment.

BIBLIOGRAPHY

[1] C. F. Aquino, "Transient A/F Control Characteristics of the 5 Liter Central Injection Engine," SAE Paper No. 810494, 1981.

[2] B. D. O. Anderson and J. B. Moore, *Optimal Control: Linear Quadratic Methods,* Prentice Hall, Englewood Cliffs, NJ. 1990.

[3] O. Arici, R. J. Tabaczynski, and V. S. Arpaci, "A Model for the Lean Misfire Limit in S.I. Engines," Combustion Science and Technology, vol. 30, pp. 31-45, 1983.

[4] M. Athans, "A Tutorial on the LQG/LTR Method," Proc. 1986 Conf. Amer. Contr. Conf., Vol 2 ,pp. 1289-1296, June 1986.

[5] P. Bidan, S. Boverie, and V. Chaumerliac, "Nonlinear Control of a Spark Ignition Engine," IEEE Trans. Control Systems Technology, Vol. 3, No. 1, pp. 4-13, March 1993.

[6] E. H. Bristol, "On a New Measure of Interaction for Multivariable Process Control," IEEE Trans. Automatic Control, Vol. AC-11, No. 1, pp. 133-134, 1966.

[7] J. F. Cassidy, W. H. Lee, and M. Athans, "On the Design of Electronic Automotive Engine Controls Using Linear Quadratic Control Theory," Proc. IEEE Conference on Decision and Control, San Diego, Jan. 1979.

[8] C.-F. Chang, N. P. Fakete and J. D. Powell, "Engine Air-Fuel Ratio Control Using an Event-Based Observer", SAE Paper No. 930766, 1993.

[9] B. M. Chen, A. Saberi and P. Sannuti, "A New Stable Compensator Design for Exact and Approximate Loop Transfer Recovery", Automatica, Vol.27, no. 2, pp. 257–280, 1991

[10] D. Cho and J. K. Hedrick, "A Nonlinear Controller Design Method for Fuel-Injected Automotive Engines", Journal of Engineering for Gas Turbines and Power, Vol 110, pp. 313-320, July 1988.

[11] D. Cho and J. K. Hedrick, "Automotive Powertrain Modeling for Control", Transactions of ASME Vol. 111, pp. 568-576, Dec. 1989.

[12] S. B. Choi and J. K. Hedrick, "Sliding control of automotive engines: Theory and experiment," Dynamic Systems and Control Division DSC v44. Publ. by ASME, pp. 281-291, New York,1992

[13] J. A. Cook and B. K. Powell, "Discrete Simplified External Linearization and Analytical Comparison of IC Engine Families," in Proc. of Amer. Contr. Conf., Minneapolis, pp. 325-333, June 1987, .

[14] J. A. Cook, J. W. Grizzle and J. Sun, "Engine Control", *The Control Handbook*, Electrical Engineering Handbook Series, CRC Press, 1995.

[15] J. A. Cook, W. J. Johnson, "Automotive Powertrain Control: Emission Regulation to Advanced Onboard Control Systems", Proceedings of the American Control Conference, Seattle, pp. 2571-2575, June 1995.

[16] P. R. Crossley and J. A. Cook, "A Nonlinear Model for Drivetrain System Development," IEE Conference 'Control 91', Edinburgh, U.K., March 1991, IEE Conference Publication 332 Vol. 2, pp. 921-925.

[17] R. G. Delosh, K. J. Brewer, L. H. Bush, T. F. Ferguson, and W. E. Tobler, "Dynamic Computer Simulation of a Vehicle with Electronic Engine Control," SAE Paper No. 810447, 1981.

[18] D. J. Dobner, "A Mathematical Engine Model for Development of Dynamic Engine Control", SAE Paper No. 800054, 1980.

[19] J. C. Doyle and G. Stein, "Robustness with Observers", IEEE Trans. on Automatic Control, Vol. 24, No. 4, pp. 607-611, Aug. 1979.

[20] J. C. Doyle and G. Stein, "Multivariable Feedback Design: Concepts for a Classical/Modern Synthesis", IEEE Trans. Automat. Contr., Vol. AC-26, No. 1, pp. 4-16, 1981.

[21] A. C. Elrod and M. T. Nelson, "Development of a Variable Valve Timing Engine to Eliminate the Pumping Losses Associated with Throttled Operation," SAE Paper No. 860537, 1986.

[22] A. L. Emtage, P. A. Lawson, M. A. Passmore, G. G. Lucas and P. L. Adcock, "The Development of an Automotive Drive-By-Wire Throttle System as a Research Tool", SAE Paper No. 910081, 1991.

[23] A. M. Foss, R. P. G. Heath and P. Heyworth, Cambridge Control, Ltd., and J. A. Cook and J. McLean, Ford Motor Co., "Thermodynamic Simulation of a Turbocharged Spark Ignition Engine for Electronic Control Development", Proc. of the Inst. Mech. Eng. Seventh International Conference on Automotive Electronics, London, U.K., C391/044 pp. 195-202, October, 1989

[24] J. S. Freudenberg and D. P. Looze, "Right Half Plane Poles and Zeros and Design Tradeoffs in Feedback Systems," IEEE Transactions of Automatic Control, Vol. AC-30, No. 6, pp. 555-556, June 1985.

[25] J. S. Freudenberg, J. W. Grizzle and B. A. Rashap, "A Feedback Limitation of Decentralized Controllers for TITO Systems, with Application to a Reactive Ion Etcher," Proc. 1994 Conference on Decision and Control, pp. 2312-2317, Orlando, 1994.

[26] C. Gray, "A Review of Variable Engine Valve Timing," SAE Paper No. 880386, 1988.

[27] J. W. Grizzle, J. A. Cook and W. P. Milam, "Improved Transient Air-Fuel Ratio Control using Air Charge Estimator," Proc. 1994 Amer. Contr. Conf., Vol. 2, pp. 1568-1572, June 1994.

[28] J. W. Grizzle, K. L. Dobbins and J. A. Cook, "Individual Cylinder Air-Fuel Control with a Single EGO Sensor," IEEE Trans. on Vehicular Technology, Vol 40, No. 1, pp. 280-286, Feb.1991.

[29] D. R. Hamburg and J. E. Hyland, "A Vaporized Fuel Metering System for Internal Combustion Engines," SAE Paper No. 760288, 1976.

[30] D. R. Hamburg, and M. J. Throop, "A Comparison Between Predicted and Measured Feedgas Emissions for Dynamic Engine Operation", SAE Paper No. 841256, 1984.

[31] S. Hara, Y. Nakajima and S. Nagumo, "Effects of Intake-Valve Closing Timing on Spark-Ignition Engine Combustion," SAE Paper No. 850074, 1985.

[32] P. A. Hazel and J. O. Flower, "Sampled Data Theory Applied to the Modeling and Control Analysis of Compression Ignition Engines-Part I," Int. J. Contr., vol. 13, No. 3, pp. 549-562, 1971.

[33] P. A. Hazel and J. O. Flower, "Sampled Data Theory Applied to the Modeling and Control Analysis of Compression Ignition Engines-Part II," Int. J. Contr., vol. 13, No. 4, pp. 609-623, 1971.

[34] P. A. Hazel and J. O. Flower, "Discrete Modeling of Spark Ignition Engines for Control Purposes," Int. J. Contr., vol. 13, No. 4, 1971.

[35] E. Hendricks and S. C. Sorenson, "Mean Value Modeling of Spark Ignition Engines," SAE Paper No. 900616, 1990.

[36] E. Hendricks, M. Jensen, P. Kaidatzis, P. Rasmussen and T. Vesterholm, "Transient A/F Ratio Error in Conventional SI Engines Controllers", SAE Paper No. 930856, 1993.

[37] J. B. Heywood, *Internal Combustion Engine Fundamentals,* McGraw-Hill, 1988.

[38] Liu Chen Hui, *General decoupling theory of multivariable process control systems,* Springer-Verlag, 1983.

[39] V. K. Jones, B. A. Ault, G. F. Franklin and J. D. Powell, "Identification and Air-Fuel Ratio Control of a Spark Ignition Engine," IEEE Trans. Control Systems Technology, Vol. 3, No. 1, pp. 14-21, March 1993.

[40] H. P. Lenz, K. Wichart, and D. Gruden, "Effects of Variable Engine Valve Timing on Fuel Economy," SAE Paper No. 880390, 1988.

[41] T. H. Ma, "Effects of Variable Engine Valve Timing on Fuel Economy," SAE Paper No. 880390, 1988.

[42] J. M. Maciejowski, *Multivariable Feedback Control*, Addison-Wesley Publishing Company, 1989.

[43] P.-W. Manz, "Influence of a Rapid Throttle Opening on the Transient Behavior of an Otto Engine,", SAE Paper No. 922234, 1992.

[44] T. J. McAvoy, *Interaction Analysis : Principles and Applications,* Research Triangle Park, NC : Instrument Society of America, 1983.

[45] G.-B. Meacham, "Variable Cam Timing as an Emission Control Tool," SAE Paper No. 700645, 1970.

[46] D. Milot, "Steady-State Wide-Range Air-Fuel Ratio Control," SAE Paper No. 922172, 1992.

[47] P. E. Moraal, J. W. Grizzle and J. A. Cook, "An Observer for Single-Sensor Individual Cylinder Pressure Control," Proc 1993 Conf. on Decision and Control, Vol. 3, pp. 2955-2961, San Antonio, Dec. 1993.

[48] P. E. Moraal, J. A. Cook, and J. W. Grizzle, "Modeling the induction process of an automobile engine," *Control problems in industry,* I. Lasiecka and B. Morton, Ed., Birkhauser, pp. 253-270, 1995.

[49] P. E. Moraal, "Adaptive Compensation of Fuel Dynamics in an SI Engine using a Switching EGO Sensor," Proc. 1995 Conf. on Decision and Control, pp. 661-667, New Orleans, 1995.

[50] M. Morari and E. Zafiriou, *Robust Process Control,* Prentice Hall, 1990.

[51] J. J. Moskwa and J. K. Hedrick, "Automotive Engine Modeling for Real Time Control Application," Proc. 1987 Amer. Contr. Conf., Vol 1, pp. 341-346, June 1987.

[52] J. J. Moskwa and J. K. Hedrick, "Modeling and validation of automotive engines for control algorithm development," ASME J. Dynamic Systems, Meas., and Contr., Vol. 114, pp. 278-285, 1992.

[53] P. Myers, "The Art of Choosing a Model," SAE Paper No. 850341, 1985.

[54] C. Nesbit and J. K. Hedrick, "Adaptive Engine Control", Proc. 1991 Amer. Contr. Conf., Boston, pp. 2072-2076, 1991.

[55] R. Nishiyama, S. Okhubo and S. Washino, "An Analysis of Controlled Factors Improving Transient A/F Ratio Control Characteristics," SAE Paper No. 890761, 1989.

[56] J. M. Novak, "Simulation of the Breathing Process and Air-Fuel Ratio Distribution Characteristics of Three-Valve, Stratified Charge Engines," SAE Paper No. 770881, 1977.

[57] C. H. Onder and H. P. Geering, "Model-Based Multivariable Multivariable Speed and Air-to-Fuel Ratio Control of an SI Engine," SAE Paper No. 930857, 1993.

[58] B. K. Powell, "A Simulation Model of an Internal Combustion Engine-Dynamometer System," Proceedings of the 18th IEEE Conference on Decision and Control, pp. 120-126, 1979.

[59] B. K. Powell, J. A. Cook and J. W. Grizzle, "Modeling and Analysis of an Inherently Multi-Rate Sampling Fuel-Injected Engine Idle Speed Control Loop," Journal of Dynamic Systems, Measurements and Control, Vol. 109, pp. 405-410, Dec. 1987.

[60] B. K. Powell and J. A. Cook, "Nonlinear Low Frequency Phenomenological Engine Modeling and Analysis," Proc. 1987 Amer. Contr. Conf., Vol. 1, pp. 332-340, June 1987.

[61] B. K. Powell, "Applied mathematics and systematic automotive powertrain synthesis," *Control Problems in Industry,*, I.Lasiecka and B.Morton (Editors), pp. 271-300, Birkhauser, 1995.

[62] J. D. Powell, "A Review of IC Engine Models for Control System Design," International Federation of Automatic Control, Munich, pp. 233-238, Germany, July 1987.

[63] J. D. Powell, and M. Hubbard, "Closed Loop Control for Internal Combustion Engine Exhaust Emissions," Technical Report for: Department of Transportation, Office of Systems Engr., University Res. Prog., Feb. 1974.

[64] J. D. Powell; "Engine Control Using Cylinder Pressure: Past, Present and Future," Journal of Dynamic Systems, Measurements and Control, June 1993, Vol. 115, pp. 343-350.

[65] R. Prabhakar, *Optimal and Suboptimal Control of Automotive Engine Efficiency and Emissions*, Ph.D. Thesis, Purdue University, West Lafayette, IN, 1975.

[66] R. Prabhakar, S. J. Citron and R. E. Goodson, "Optimization of Automobile Engine Fuel Economy and Emissions," ASME Paper 75-WA/Aut-19, Dec. 1975.

[67] A. Raftari, *Robust Control of Interconnected Systems with Applications to Automotive Control: Optimal Decoupling and Decentralized Control*, Ph.D. Thesis, Wayne State University, Detroit, MI., 1995.

[68] W. B. Ribbens, *Understanding Automotive Electronics*, Fourth Edition, SAMS, 1992.

[69] R. G. Rivard, "Closed Loop Electronic Fuel Injection Control of I.C. Engine," SAE Paper No. 730005, International Automotive Engineering Congress, Detroit, Jan. 1973.

[70] F. G. Shinskey, *Process Control Systems,* John Wiley & Sons,1989.

[71] S. Shiraishi, S. L. Ipri and D.-I. D.Cho, "CMAC Neural Network Controller for Fuel-Injection Systems," IEEE Trans. Control Systems Technology, Vol. 3, No. 1, pp. 23-32, March 1993.

[72] Per Søgaard-Andersen, "Loop Transfer Recovery with Minimal-Order Observers", Proc 1987 on Decision and Control, Vol. 2, pp. 933-938, Dec. 1987.

[73] R. A. Spilski and W. D. Creps, "Closed Loop Carburetor Emission Control System," SAE Paper No. 750371, International Automotive Engineering Congress, Detroit, 1975.

[74] K. Srinivasan, G. Rizzoni, M. Trigui and G.-C. Luh, "On Line Estimation of net Engine Torque from Crankshaft Angular Velocity Measurements Using Repetitive Estimators," Proc. 1992 Amer. Contr. Conf., Vol. 1 ,pp. 516-520, June 1992.

[75] D. L. Stivender, "Engine Air Control-Basis of a Vehicular Systems Control Hierarchy," SAE Paper No, 780346, 1978.

[76] A. G. Stefanopoulou, J. W. Grizzle and J. S. Freudenberg, "Engine Air-Fuel Ratio and Torque Control using Secondary Throttles," Proc.1994 Conf. on Decision and Control, pp. 2748-2753, Orlando, 1994.

[77] A. G. Stefanopoulou, J. A. Cook, J. S. Freudenberg, J. W. Grizzle, M. Haghgooie and P. S. Szpak, "Modeling and Control of a Spark Ignition Engine with Variable Cam Timing," Proc. 1995 Amer. Contr. Conf., pp. 2576-2581, Seattle, 1995.

[78] A. G. Stefanopoulou, K. R. Butts, J. A. Cook, J. S. Freudenberg and J. W. Grizzle, "Consequences of Modular Controller Development for Automotive Powertrains: A Case Study," Proc. 1995 Conf. on Decision and Control, pp. 768-773, New Orleans, 1995.

[79] R. A. Stein, K. M. Galietti and T. G. Leone, "Dual Equal VCT- A Variable Camshaft Timing Strategy for Improved Fuel Economy and Emissions," SAE Paper No. 950975, 1995.

[80] M. J. Throop, J. A. Cook and D. R. Hamburg, "The Effect of EGR System Response Time on NO_x feedgas Emissions during Engine Transients," SAE Paper No. 850133, 1985.

[81] R. Turin and H. P. Geering, "On Line Identification of Air-Fuel Ratio Dynamics in a Sequential Injected SI Engine," SAE Paper No. 930857, 1993.

[82] R. Turin and H. P. Geering, "Model-based Adaptive Fuel Control in an SI Engine," SAE Paper 940374.

[83] J. H. Tuttl, "Controlling Engine Load by Means of Late Intake-Valve Closing," SAE Paper No. 800794, 1980.

[84] T. Vesterholm, E. Hendricks, N. Houbak, "High Order Continuous SI Engine Observer," Proc. 1992 Amer. Contr. Conf., Vol. 1, pp. 510-515, Chicago, June 1992.

[85] H. Wu, "A Computer Model for a Centrally-Located, Closed Loop, Automotive Fuel Metering System," ASME International Computer Technology Conference, pp. 98-104, San Francisco, Aug. 1980.

[86] W. W. Yuen, and H. Servati, "A Mathematical Engine Model Including the Effect of Engine Emission," SAE Paper No. 840036, 1984.

[87] G. Zames, and D. Bensoussan, "Multivariable Feedback, Sensitivity, and Decentralized Control," IEEE Trans. Automatic Control, Vol. AC-28, pp. 1030-1035, 1983.

[88] R. Zechnall, G. Bauman and H. Eisele, "Closed Loop Exhaust Emission Control System with Electronic Fuel Injector," SAE Paper No. 730566, National Automotive Engineering Meeting, Detroit, May 1973.

[89] Z. Zhang and J. S. Freudenberg, "Loop Transfer Recovery for Nonminimum Phase Plants," IEEE Trans. on Automatic Control, Vol. 35, No. 5, pp. 547-553, May 1990.